Late Holocene Mongolian climate and environment reconstructions from brGDGTs, NPPs and pollen transfer functions for Lake Ayrag: Paleoclimate implications for Arid Central Asia

Lucas Dugerdil, Guillemette Ménot, Odile Peyron, Isabelle Jouffroy-Bapicot, Salomé Ansanay-Alex, Ingrid Antheaume, Hermann Behling, Bazartseren Boldgiv, Anne-Lise Develle, Vincent Grossi, et al.

Late Holocene Mongolian climate and environment reconstructions from brGDGTs, NPPs and pollen transfer functions for Lake Ayrag: paleoclimate implications for Arid Central Asia

Lucas Dugerdil[a,b,*,1], Guillemette Ménot[a], Odile Peyron[b], Isabelle Jouffroy-Bapicot[c], Salomé Ansanay-Alex[a], Ingrid Antheaume[a], Hermann Behling[d], Bazartseren Boldgiv[e], Anne-Lise Develle[f], Vincent Grossi[a], Jérôme Magail[g], Matthew Makou[a], Mary Robles[b], Julia Unkelbach[d], Boris Vannière[c] and Sébastien Joannin[b]

[a] *Univ. Lyon, ENS de Lyon, Université Lyon 1, CNRS, UMR 5276 LGL-TPE, F-69364, Lyon, France*
[b] *Université de Montpellier, CNRS, IRD, EPHE, UMR 5554 ISEM, Montpellier, France*
[c] *Université Bourgogne Franche Comté, CNRS UMR 6249 Laboratoire Chrono-environnement, F-25030, Besançon, France*
[d] *University of Goettingenn Department of Palynology and Climate Dynamics, Albrecht-von-Haller-Institute for Plant Sciences, Germany*
[e] *National University of Mongolia, Ecology Group, Department of Biology, School of Arts and Sciences, Ulaanbaatar 14201, Mongolia*
[f] *Université de Savoie, CNRS UMR 5204 EDYTEM, 73376 Le Bourget-du-Lac, France*
[g] *Musée d'anthropologie préhistorique de Monaco, 56, boulevard du Jardin exotique, 98000 MC, Monaco*

ARTICLE INFO

Keywords:
Climate reconstruction
Arid Central Asia
Dryland
Pollen transfer function
brGDGTs
Stable isotope geochemistry
Non-Pollen Palynomorphs
Algae
micro-XRF
Magnetic susceptibility

ABSTRACT

A coupled pollen-brGDGT paleoclimate reconstruction approach has been tested to provide independent and robust estimates of Holocene climate and environment changes in the extremely arid environment of the mountainous areas ranging from northern Arid Central Asia (ACA) to the Mongolian Plateau. The two proxies were calibrated for both global and local modern data sets (NMSDB). This multi-proxy approach was then applied to a sediment core collected from Lake Ayrag, Arkhangai, covering the Late Holocene. In addition to brGDGTs and pollen, we also performed magnetic susceptibility, micro-XRF, elemental and isotopic bulk chemistry, and Non-Pollen Palynomorph (NPP) analyses on the Lake Ayrag sediments in order to better understand the lake system and human impact dynamics. While the globally calibrated record (both for pollen and brGDGTs) displayed a slight millennial-scale cooling, the locally calibrated results exhibit centennial-scale climate oscillations such as the 4.2 and 3.5 kyr events, the Roman Warm Period (RWP), Dark Ages Cold Period (DACP), Medieval Warm Period (MWP) and Little Ice Age (LIA). These climate oscillations and vegetation changes are discussed with regard to the main Mongolian human historical occupation events documented by pastoralism proxies, especially the Xiongnu, Mongol Empire, Mandchou and Soviet periods. The climate systems currently dominating the Mongolian Plateau are difficult to resolve because inter-annual climate variability is pronounced. However, precipitation mainly occurs in summer (easterly monsoon driven) when the winter Westerlies lead the air mass movement. In the past, both pollen and biomarkers exhibited anti-correlated trends with annual precipitation and temperature: over the last 4,000 kcal yr BP, the warm periods (MWP, RWP) were dry and the cold periods (LIA, DACP, 3.5 kyrs) were humid. Thus, the East Asian Summer Monsoon (i.e., warm and wet conditions dominant during summer) seems not to have influenced central Mongolian climate during the Late Holocene, which could have remained dominated by the Westerlies / Siberian High cells conflict. A comparison between the Ayrag record and other paleoclimate records from the Baikal area (Dulikha), Mongolian Plateau (D3L6, D1L1, NRX, ATM), and continental China (Kesang, Baluk and Tonnel caves, XRD section) to the Loess Plateau (Huangye and Xianglong caves) suggests that the monsoon front has oscillated since the Early Holocene. A climate synthesis following strictly the same approach (locally calibrated brGDGTs vs. pollen-inferred climate) for all the ACA records available for the Late Holocene helps us to resolve the climate systems paced by centennial to millennial-scale oscillations and their consequences for human societies.

Abbreviations: Arid Central Asia (**ACA**); Arboreal Pollen (**AP**); Advanced Space-borne Thermal Emission and Reflection Radiometer (**ASTER**); Branched vs. Isoprenoid Tetraether (**BIT**); Before Present (**BP**); Boosted Regression Trees (**BRT**); Cyclisation of Branched Tetraether (**CBT**); Dark Ages Cold Period (**DACP**); East Asian Summer Monsoon (**EASM**); glycerol dialkyl glycerol tetraethers (**GDGTs**); Inter-Tropical Convergence Zone (**ITCZ**); Little Ice Age (**LIA**); Mean Annual Air Temperature (**MAAT**); Mean Annual Precipitation (**MAP**); Methylation of Branched Tetraether (**MBT**); Mongolian Plateau (**MP**); Magnetic Susceptibility (**MS**); Medieval Warm Period (**MWP**); Non Arboreal Pollen (**NAP**); New Mongolian-Siberian Surface Data Base (**NMSDB**); Non-Pollen Palynomorphs (**NPPs**); Organic matter (**OM**); Roman Warm Period (**RWP**); Sedimentary Accumulation Rate (**SAR**); Siberian High (**SH**); Total Inorganic Carbon (**TIC**); Total Organic Carbon (**TOC**). Weighted Averaging Partial Least Squares (**WAPLS**); Westerlies-Dominated Climatic Regime (**WDCR**); micro X-Ray Fluorescence (micro-**XRF**).

*Corresponding author
lucas.dugerdil@ens-lyon.fr (L. Dugerdil)
ORCID(s): 0000-0003-0266-564X (L. Dugerdil)

1. Introduction

Since conservation ecology (the study of biodiversity management and protection) represents a major solution for reducing human impacts on climate change and ecosystem degradation (Dinerstein et al., 2017), a historical approach towards the dynamic comprehension of human, ecologic and climatic systems is necessary and helpful (Barnosky et al., 2017; Carter et al., 2018). Moreover, ecosystem services are directly linked to climatic conditions (Hao and Yu, 2018). Paleoclimatic and paleoecological contexts will help us to better understand the ecosystem-climate relationship in human constrained systems (Barnosky et al., 2017). Notably, the Late Holocene period marks the rise of both human impacts on ecosystems (Miehe et al., 2007, 2014) and climate changes on human societies (e.g., Roberts et al., 2011; Berger et al., 2016; deMenocal and Stringer, 2016; Magny, 2019). One of the main consequences of climate change is global aridification, especially within large continental land masses (Sherwood and Fu, 2014; Huang et al., 2016; Park et al., 2018). More particularly, studying arid environment dynamics in an over-grazing context is essential since the climate forecast for European grasslands (Vozhehova et al., 2020) to Arid Central Asian (ACA) steppes suggests a strong and fast desertification associated with a loss in biodiversity and regional economic instability (Li et al., 2019; Nunez et al., 2020).

The reconstruction of paleoclimatic parameters in arid environments is a challenging issue since the best sedimentary archives often appear in wetlands such as lakes and peats, rarely in arid environments. However, arid environments can be investigated notably through the use of loess and paleosoil sequences (An, 2000; Kehl, 2009; Sun et al., 2019; Hou et al., 2020), or peat-lands and lakes from surrounding mountainous areas (Rudaya et al., 2008; Sun et al., 2011; Felauer et al., 2012; Murad, 2012; Rudaya and Li, 2013; Huang et al., 2018b; Unkelbach et al., 2019, 2020). Within a large range of proxies deposited and conserved in these sedimentary archives, it is common to use pollen assemblages as a vegetation change indicator, following the recent studies from the Tian Shan (Li et al., 2020c), Tibetan Plateau (Miehe et al., 2014; Li et al., 2020b), Alashan Plateau (Herzschuh et al., 2004), Qilian Shan (Huang et al., 2018a), Altai mountains (Huang et al., 2018b; Unkelbach et al., 2020) and Mongolian Plateau (Ma et al., 2008; Feng et al., 2013). Pollen transfer functions (Wen et al., 2013; Peyron et al., 2017; Chevalier et al., 2020) are one of the most reliable methods for paleoclimate reconstruction of continental Mean Annual Air Temperature (MAAT) and Mean Annual Precipitation (MAP) while other methods are preferred for the reconstruction of vegetation as past biomes (i.e. *biomization*, Prentice, 1985; Prentice et al., 1996). Pollen assemblage analysis also gives an overview of human impacts on the environment (Miehe et al., 2014; Tian et al., 2014; Djamali et al., 2016; Ghosh et al., 2017) and is commonly coupled with Non-Pollen Palynomorph (NPP) studies, especially with algal and fungal remains (Van Geel and Aptroot, 2006; Cugny et al., 2010; Baker et al., 2013; Gauthier and Jouffroy-Bapicot, 2021). The NPPs–human impact approach is especially interesting for investigating the history of nomadic societies where archaeological remains are rare, such as in Mongolia (Murad, 2012; Tian et al., 2014; Unkelbach et al., 2019, 2020). Since the 1980's, the use of a new generation of organic geochemical proxies has been developed for continental paleo-studies. Among them, glycerol dialkyl glycerol tetraethers (GDGTs) are relevant for temperature reconstruction (Sun et al., 2011; Naafs et al., 2017a, 2018) and organic matter tracing (Hopmans et al., 2004), although this approach is hampered by effects from vegetation change and human impacts (Davtian et al., 2016; Martin et al., 2019). Finally, a better comprehension of lake systems at the local scale is provided by micro-fossil algae counting (Van Geel, 1978; Jankovská and Komárek, 2000; Last et al., 2001; Stivrins et al., 2018) and elemental analyses (XRF, TOC, etc., Löwemark et al., 2011; Rudaya and Li, 2013; Croudace and Rothwell, 2015). Because these proxies are still biased (e.g., algae *taxa* are often identified at the family level, which remains ubiquist, and the core-scanning micro-XRF is considered as semi-quantitative, Jankovská and Komárek, 2000; Croudace et al., 2006; Liu et al., 2013), all the interpretations and reconstructions resulting from them need to be considered with regard to other surrounding archives and archeological sites in order to place the local historical interpretation within a global context (Gupta, 2004; d'Alpoim Guedes and Bocinsky, 2018; Li et al., 2020c).

Within this framework emerges the importance of diversifying studied sedimentary archive sites in arid regions, and especially in poorly documented areas. For example, Arid Central Asia (ACA) and especially its northern part, from the Mongolian Plateau (MP) to southern Siberia, require more detailed studies. The works of An et al. (2008) and Klinge and Sauer (2019) review all the previous paleoclimate investigations in Mongolia; the majority of them are based on pollen, diatoms, and sedimentological studies from the western (Altai Mountains) and northern parts (Sayan Mountains) of the country. The central drier and warmer part of the country has attracted researchers' attentions over the last two decades both for paleo-pollen studies (Gaillard et al., 1992; Herzschuh, 2006; Wang et al., 2011; Felauer et al., 2012; Murad, 2012; Wang and Feng, 2013; Lehmkuhl et al., 2011, 2018) and to calibrate proxy-climate relationships (Weng et al., 2006; Ma et al., 2008; Cao et al., 2014; Dugerdil et al., 2021). An increasing number of biomarker studies, in particular using brGDGTs, have focused on calibrations (Xie et al., 2012; Yang et al., 2014; Ding et al., 2015; Zang et al., 2018; Dugerdil et al., 2021) and Holocene climate reconstructions in arid and semi-arid areas (Cao et al., 2017; Zheng et al., 2018; Sun et al., 2019; He et al., 2020; Wu et al., 2020). All of these efforts to better constrain northern ACA Holocene climatic change are necessary to understand the past influence and extent of Westerlies-Dominated Climatic Regime

(WDCR, Chen et al., 2019), East Asian Summer Monsoon (EASM, Chen et al., 2009) and East Asian Winter Monsoon (EAWM, Wang and Feng, 2013) variations throughout the Holocene (Zheng et al., 2004; Klinge and Sauer, 2019), and in particular during Late Holocene climatic events such as the 3.5 kyr event, Roman Warm Period, Dark Ages Cold Period, Medieval Warm Period and Little Ice Age (respectively 3.5 kyr, RWP, DACP, MWP and LIA; Zhang et al., 2008; Chen et al., 2015b; Aichner et al., 2019).

These calibrations and reconstructions reach beyond an understanding the global climate system solely. With regard to its particular geographical features, the Mongolian plateau is delimited by several high-elevation mountain ranges (Altai, Sayan, Khangai and Khentii, Fig. 1.A and B, Klinge et al., 2018) and defines a biogeographical transition between the Siberian taiga on the north and the Gobi desert on its southern edge (Gunin et al., 1999; Ma et al., 2008). This plateau, culminating at around 1,500 m a.s.l., hosts diverse open land vegetation such as, following a gradient of aridity, steppe-deserts, steppes, mountain grasslands, and forest-steppes (Wesche et al., 2016; Pfeiffer et al., 2018). In this context, Mongolia represents a case study for the whole paleartic grassland and our understanding of treeline settlement and dynamics (Klinge et al., 2018), climate change impact on high-altitude permafrost (Sharkhuu, 2003; Sharkhuu et al., 2007), the grassland vulnerability assessment (Tian et al., 2014), and the link between grasslands and pastoralism of nomadic societies (Fernández-Giménez, 1999, 2006). Of note, the question of our archaeological knowledge of steppe populations since the Bronze Age is determinant (Honeychurch and Amartuvshin, 2007; Honeychurch, 2010; Esin et al., 2017).

Despite the statistical efficiency of using global calibration studies (Cao et al., 2014; Naafs et al., 2017a; Dearing Crampton-Flood et al., 2020; Davis et al., 2020), it is often necessary to conduct an accurate local survey to best address the regional specificity of vegetation, soil and bacterial communities (Herzschuh et al., 2010; Lu et al., 2011; Yang et al., 2014; Rudaya et al., 2020; Wang et al., 2020) and thus improve climate reconstruction fidelity (Sun et al., 2020). In this context, our study is a continuation of the calibration work conducted along a cold-arid bioclimatic gradient from southern Siberia (Lake Baikal) to the Mongolian Gobi desert Dugerdil et al. (2021). This regional approach involves (1) collecting surface data (pollen, NPPs and GDGTs); (2) examining the correlations between this data set and associated climatic parameters; and finally, (3) testing and validating these calibrations in light of interdisciplinary knowledge on ecology and ecophysiology in order to detect potential biases.

The present study focuses on a sedimentary sequence from Lake Ayrag, a shallow lake in Arkhangai, center-Mongolia. This area (within the transition zone between the Westerlies and the EASM influence, Chen et al., 2019) is especially poorly studied. Lake Ayrag represents the first coupled pollen-brGDGT study in ACA, and is accompanied here by NPP and sediment geochemical characterizations. The principal goals of this investigaiton are the following:

1. Reconstruct Lake Ayrag ecosystems and dynamics (for example, algal growth, watershed fluxes, and in-situ organic mater production).
2. Discuss influences on the sedimentary record from the development and spreading of steppe nomadic societies.
3. Infer temperature and precipitation variations from specific proxies and test the potential of local, regional, and global calibrations (Herzschuh et al., 2010; Lu et al., 2011; Cao et al., 2014; De Jonge et al., 2014b,a; Yang et al., 2014; Zheng et al., 2014; Ding et al., 2015; Naafs et al., 2017a; Davis et al., 2020; Dearing Crampton-Flood et al., 2020; Dugerdil et al., 2021; Rudaya et al., 2020; Wang et al., 2020) to provide the most reliable climate reconstruction.
4. Map the variations in front of the EASM line during Late-Holocene oscillations by recalibrating existing pollen paleorecords such as Dulikha (Bezrukova et al., 2005; Binney, 2017), D1L1 and D3L6 (Unkelbach et al., 2019, 2020), as well as brGDGT paleorecords such as NRX (Rao et al., 2020), ATM (Wu et al., 2020), and XRD (Sun et al., 2019).

2. Mongolian study area and historical context

2.1. The Mongolian Plateau, on the ACA margin

In the northern part of Arid Central Asia, the Khangai mountain range is located in the center-north part of the Mongolian Plateau (MP, Fig. 1.A; Windley and Allen, 1993) and overlaps two Mongolian districts: Arkhangai in the north and Ovorkhangai in the south. Among the Mongolian mountain ranges, the Khangai is surrounded by Altai on the west (Fig. 1.B), Sayan on the north, Gobi-Altai on the south, and Khentii on the east. The Khangai mountains (Fig. 1.C), culminating at 4,000 m a.s.l, originated in the Central Asian orogenic belt, resulting in one of the largest granitic batholiths in the world (from the Late Paleozoic to Early Mesozoic, Yarmolyuk et al., 2019). The regional geology is also marked by volcanic rocks with younger origins (Late Cenozoic, Yarmolyuk et al., 2008), especially on the upper part of the Khanuii rivershed.

2.2. The Mongolian Plateau and ACA climate systems

Unraveling MP climate dynamics is complicated since the area is located at a convergence of several climate systems, themselves teleconnected with other oscillating systems (Fig. 1.D). The complex climate system interconnections include the Siberian High (SH) reaction to Atlantic (NAO) and Pacific (WPO) variations (Aizen et al., 2001; Gong and Ho, 2002; Labban et al., 2021),

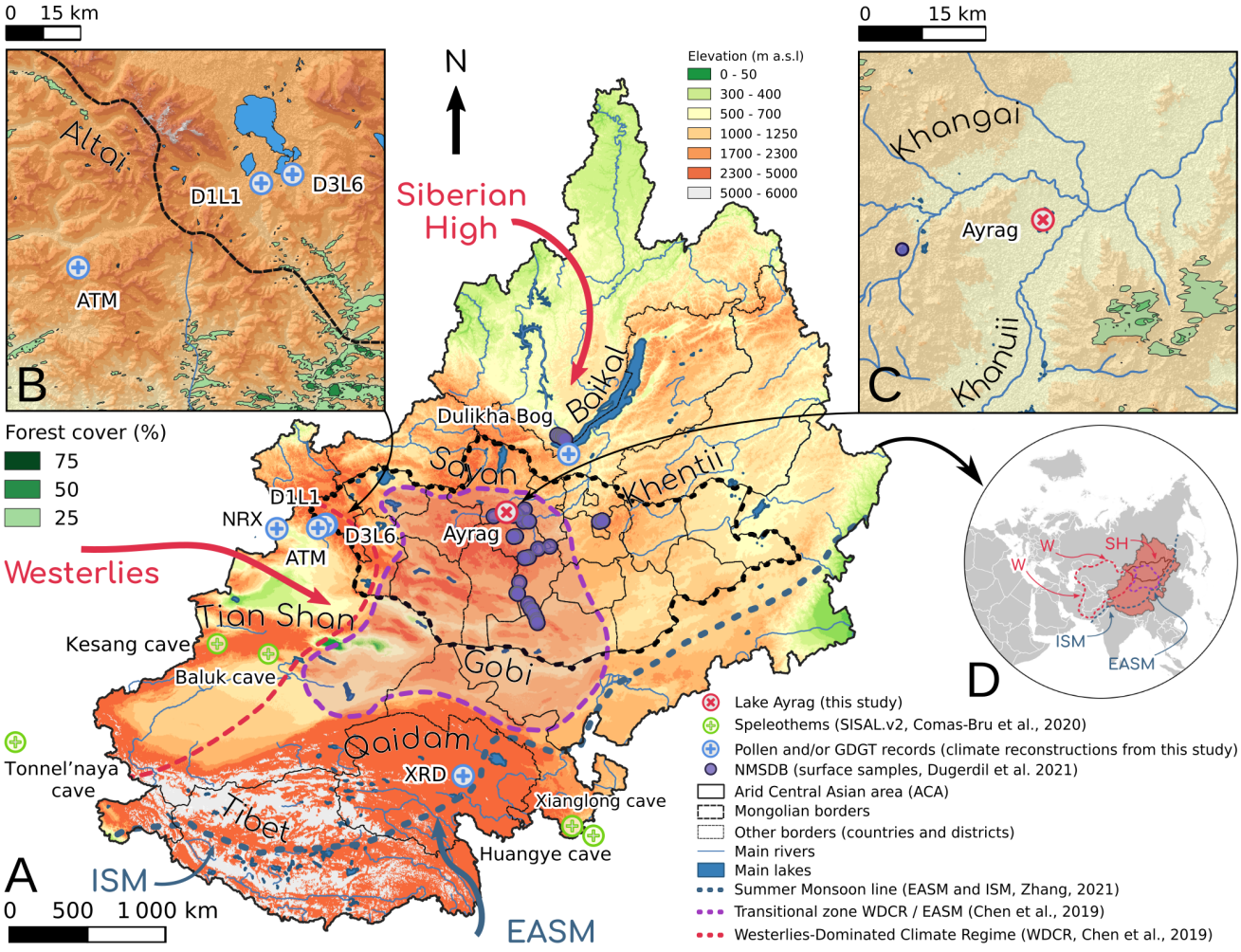

Figure 1: **A**: Topographic map of Arid Central Asia (from Advanced Space-borne Thermal Emission and Reflection Radiometer (ASTER) data, JPL, 2014) with the surface samples (Dugerdil et al., 2021), cores, and main geographical areas labeled; **B**: Insert panel of the Altai Mountains showing the D1L1, D3L6 (Unkelbach et al., 2019, 2020) and ATM cores (Wu et al., 2020); **C**: Insert panel of the Ayrag Nuur core (this study), which is compared with a pollen sequence from Dulikha Bog (Bezrukova et al., 2005; Binney, 2017), a brGDGT sequence from the XRD section (Sun et al., 2019), NRX Bog (Rao et al., 2020), and the cave speleothem database (SISAL.v2, Comas-Bru et al., 2020). **D**: Current climate system interactions in Eurasia. The forest cover data were extracted from the MOD44B database (Dimiceli et al., 2015) and the lakes from the Global Forest Cover Change–Water Cover database (GFCC Townshend, 2016). Both have been vectorized in QGIS (Free et al., 2015). The East Asian Summer Monsoon (EASM) line was recreated from Chen et al. (2009) and Zhang (2021)

as well as the Westerlies and EASM reactions to changes in the Inter-Tropical Convergence Zone (ITCZ) and El Niño Southern Oscillation (ENSO, An et al., 2008). The Westerlies themselves are influenced by the EASM (Chen et al., 2008; Mathis et al., 2014) and SH (Wolff et al., 2017). Finally, the Arctic Oscillation (AO) impacts the SH and the EAWM (Gong et al., 2001; Wu and Wang, 2002). These complex interconnections lead to inter-annual variability in regional climate patterns, complicating modern climate data analysis (Aizen et al., 2001; Chen et al., 2008; Wolff et al., 2017). The alternating domination of seasonal cells is also a parameter to take into account (Warner, 2004). For example, the climate in southern Siberia around the Baikal area is kept locked by SH during winter. In the summer when most of the rainfall occurs, the water vapor is delivered by the northernmost part of the EASM system (Shukurov and Mokhov, 2017).

2.3. Mongolian vegetation and bioclimate

Around Lake Ayrag, the vegetation is fully open and marked by Poaceae, Cyperaceae and *Artemisia* spp. steppe, only interrupted by some sub-shrub patches of *Stellera*

chamaejasme. At a larger scale within the Khanuii River basin, the mountain grassland is mixed with wetlands (*Potentilla ansulina*, *Iris lactea*, *Bistorta* spp., etc.) close to the meander banks. These periodically immersed wetlands are locally called *Namak*. There are rupicolous short vegetation communities on the most sloping flank of the watershed. On the flattest flank, especially on the northwestern slope, the taiga-steppe vegetation consists of a mix between mountain grassland and light forest largely dominated by *Larix sibirica*. Among the other major tree types, some *Betula* spp., *Pinus sibirica*, *Pinus sylvestris* and *Picea sylvestris* are also found. These communities occur on the ecotone between steppes and the forest-steppe vegetation ensemble (Ma et al., 2008; Klinge and Sauer, 2019).

This ecotone is mainly maintained by climatic conditions (Schlütz et al., 2008; Cheng et al., 2020) and sun exposition (Klinge and Sauer, 2019), more so than anthropic pressure, even if human impacts are currently threatening the Eurasian forest-steppe (Erdos et al., 2018). In terms of climate nodes, the extreme continental cold-dry climate of Mongolia issues from the Westerlies to EASM transition zone (Chang, 2004; Chen et al., 2019). The impact of the SH is strong across the whole mid-latitudes of Asia (Gong and Ho, 2002), up to the ACA (Aizen et al., 2001) and even the Middle East (Labban et al., 2021). The SH affects the MP especially during winter (high pressure cold air masses, Ahrens and Henson, 2021) and is also connected with the Arctic Oscillation (AO, Gong et al., 2001; Wu and Wang, 2002). This transition zone between the different climate cells complicates interpretation of MP paleoclimates (Chen et al., 2019). EASM front variations have been used to simplify modeling of climate oscillations through time (Herzschuh, 2006; Haoran and Weihong, 2007; Chen et al., 2009, 2010; Wang et al., 2010; Li et al., 2018; Chen et al., 2019; Sun et al., 2019; Wang et al., 2019). Among the ways to define the EASM influence zone, Zhang (2021) introduce the MAP = 400 mm.yr^{-1} isoline as the EASM threshold. Changing EASM influence over time is linked to Holocene climate events.

2.4. ACA paleoclimate system variations

An increasing number of studies highlight the complex teleconnections between climatic cells as documented by paleoclimate reconstructions. Some hypotheses have been advanced regarding Mongolian summer precipitation occurrence. First, winter precipitation may not have been recorded by the weather stations (Rudaya et al., 2020). Second, despite their low moisture content, the summer westerlies may be responsible for the Mongolian P_{sum} (Wang et al., 2009; Tian et al., 2013). Finally, Piao et al. (2018) suggest an influence of locally evaporated water recycling on the Mongolian MAP amount. However, this argument is denied by Zhang (2021) for ACA based on the δ^{18}O of water vapor. In their study, they suggest an incursion of EASM rainfall into ACA and the southern MP depending on monsoon strength; the weaker the monsoon, the further it goes into the WDCR/EASM transitional zone (Chen et al., 2019; Zhang, 2021), following the current Baikal climate system dominated by the EASM.

According to Chen et al. (2019), the climatic variations affecting the whole of central Asia (from Turkmenistan to the MP) are numerous throughout the Late-Holocene period. This period is marked by two initial centennial-scale oscillations: the 3.5 kyr event (Yao et al., 2017; Aichner et al., 2019; Lu et al., 2019). Some studies also link warm and dry conditions from 2.5 to 1.9 kyr BP with the European Roman Warm Period (RWP), and colder conditions to the Dark Ages Cold Period (DACP, Zhang et al., 2008). Nevertheless, the timing of the DACP in central Asia is less constrained, lasting from 1.8–1.6 kyr BP in the Karakul Lake region (Aichner et al., 2019), and from 2.1–1.8 kyr BP at Qinghai Lake (Ji et al., 2005; Liu et al., 2006). Finally, the Medieval Warm Period (MWP, 950–650 cal yr BP), Little Ice Age (LIA, 550–50 cal yr BP, Chen et al., 2015b) and Current Warm Period (CWP, Zhang et al., 2008) are all well observed in ACA.

2.5. Human occupation of the Mongolian Plateau from the Bronze Age to the present day

Mongolian cultural history is very rich for the Late-Holocene (Xiongnu, Ruanruan, Körtürk, Uighur, Kirghiz and Mongol occupations, Honeychurch and Amartuvshin, 2007; Savelyev and Jeong, 2020) and has intermixed relationships with vegetation and land use. Despite the unwelcoming and severe continental and mountainous climate of the Mongolian Plateau, the first significant human land use in Mongolia dates from the Bronze Age (3.5–4.0 kyr BP) when nomadic societies settled large ritual monuments (Allard et al., 2006). However, these archaeological findings are not sufficient for fully understanding the demography and land-use activities of this period. Late-Holocene Mongolian history is marked by a succession of nomadic cultures, including the famous scythes folks, before settlement of the Xiongnu empire. All of these different ethnic groups were pastoral and warlord societies. The impacts of multiple wars and livestock grazing on the landscapes are visible and noteworthy in different archives from the Mongolian Plateau (MP, Fernández-Giménez, 1999, 2006). According to Honeychurch and Amartuvshin (2007), the grazing steppe economy began around 4,000 cal yr BP in Mongolia and gradually rose from then on. Even if this period is marked by many important archaeological features in the current landscape, such as ritual and funeral remains, and especially the monumental Mongolian deer-stone and burials (Esin et al., 2017), habitats and workshops are much less represented. Since the Mongolian nomadic societies did not leave enough significant land-use archaeological remains, lake paleoenvironmental records represent the best alternative for understanding the past.

Table 1
Lake Ayrag dated samples.

Lab. ID	Depth (cm)	Thickness (cm)	Dry mass (g)	Type of material	C^{14} age (yr cal BP / 1σ)
Poz-110030	5	1	0.0882	Amaranthaceae seeds, charcoal	100.5 ± 0.31
Poz-110032	28	1	0.0060	Vegetation remains	980 ± 30
Poz-110033	62	1	0.0051	Vegetation remains	1960 ± 30
Poz-110034	76	1	0.0039	Vegetation remains, charcoal	2325 ± 35
Poz-38108	86.5	1.5	0.0031	Vegetation remains, charcoal	3660 ± 180

3. Material and methods

3.1. Coring and setting

Ayrag Nuur (Nuur means lake in Mongolian), in the Khangai mountains of central Mongolia (48°41′40.99″N; 101°25′44.89″E; 1,436 m a.s.l., Fig. 1.C), was cored during the Monaco-Mongolian joint archaeological expedition in the summer of 2009. During this period, the lake water depth was 80 cm. The lake is not affected by a structured hydrological network, even though it is located within the large Khanuii river basin. The Khanuii river is currently a meander river flowing on an alluvial terrace. The lake surface is approximately 1.7 km^2 (calculated from the GFCC Water Cover database, Townshend, 2016), although this fluctuates due to trampling from the numerous livestock using the lake for water. The current grazing maintains a lake edge covered by meadow vegetation and not sedge marsh. An 88 cm-long sediment core was retrieved from approximately the center of the lake using a boat and an interface corer (UWITEC). The core was subsequently sub-sampled every centimeter.

3.2. ^{14}C dating

The age scale is based on ^{14}C radio-dating methods. To avoid the influence of reservoir effects (Lowe, 1985) in this carbonate-rich environment, five vegetation macrorests were selected and radiocarbon dated at the Poznań Radiocarbon Laboratory for dating (table 1). The R module `Bacon v2.5.1` generated the age-model (Blaauw and Christen, 2011) displayed in Fig. 2 using an auto-regressive gamma process. Post-bomb dates were calibrated using the North Hemisphere zone 1 calibration curve (NH1, Reimer et al., 2004). The dates are displayed in calendar years BP.

3.3. Element and isotopic geochemistry

Magnetic susceptibility (MS) analyses and photography (Fig. 2) were performed on the Lake Ayrag sediment core in the *Chrono-Environnement* laboratory in Besançon, France; X-ray fluorescence analysis (XRF, Fig. 3) at *EDYTEM* in Chambéry using an XRF Core Scanner 3 (Jansen et al., 1992); and carbon and nitrogen elemental (EA) and bulk isotopic (EA-IRMS) analyses at *LGL-TPE* in Lyon using an Elementar Vario Micro Cube elemental analyser coupled with an Elementar Vision isotope ratio mass spectrometer (EA–IRMS, Fig. 4). Before analysis of total organic carbon (TOC), sediments were treated with HCl (1N) to remove carbonates that were potentially present. Total inorganic carbon (TIC) was deduced from mass loss due to carbonate removal. The resulting sediments were then freeze-dried and weighed into tin capsules (Elemental Microanalyses, 11.5×7mm) with a CPA26P Sartorius microbalance (2×10^{-6}g) before analysis.

TOC and $\delta^{13}C_{TOC}$ were measured on 4 to 8 μg of carbonate-free sediment. We separately analyzed non-acidified sediment by EA and EA–IRMS to measure the weight % of nitrogen, as detected by the EA Thermal Conductivity Detector (TCD), and δ^{15}N. The capsules were individually introduced into a combustion furnace (950°C) under an excess of oxygen. Copper oxide was used as an oxidation catalyst and He as the carrier gas. Reduction of N_xO_y to N_2 and removal of excess O_2 was achieved with reduced copper at 550°C. Water was removed using a phosphorous pentoxide chemical trap. N_2 and CO_2 were separated on a purge and trap desorption column. Finally, the ratio between TOC and wt%N_{total} was calculated and presented as C/N. A working standard, IVA sediment, was measured every ten samples to normalize the mass spectrometer signals. Each sample was analyzed three times, and mean values and a standard deviations were calculated.

3.4. GDGT extraction and analysis

The Lake Ayrag biomarker analyses were conducted on 43 samples. Glycerol dialkyl glycerol tetraethers (GDGTs) were extracted from these sediment samples using the laboratory protocol detailed in Dugerdil et al. (2021). In brief, 0.5 gram, freeze dried sediment samples were twice microwave extracted in a DCM:MeOH (3:1) solvent solution and filtered using SPE cartridges. Then a C_{46} GDGT was added as an internal standard (Huguet et al., 2006) and the polar molecular fraction was separated by SPE with elution in a DCM/MeOH (1:1) solution. Specific compounds were finally detected using high performance liquid chromatography coupled with mass spectrometry (HPLC-APCI-MS, Agilent 1200) at LGL-TPE and ENS de Lyon following the methods described in Hopmans et al. (2016) and Davtian et al. (2018). Treatment of the GDGT results was carried out following the two methods presented in Deng et al. (2016), Wang et al. (2016) and Yang et al. (2019): compounds were grouped by chemical structures as cycles or methyl groups into indexes (De Jonge et al., 2014a) or are expressed in fractional abundance [x_i] (results presented in Supplementary Fig. B2, following the formula of Sinninghe Damsté, 2016). All the index formulas used for Lake Ayrag GDGTs are presented in the supplementary information table in Dugerdil et al. (2021).

3.5. Pollen preparation and transfer functions

The Lake Ayrag pollen analyses were also conducted on 43 samples. The sediment samples were prepared according to standard protocol described by Faegri and Iversen (1989) at the Chrono-Environnement laboratory. All the residuals were concentrated in glycerol and mounted between slide and lamella. The pollen counts were conducted using a *Leica DM1000 LED* microscope with a 40× magnification lens. A calibrated concentration of *Lycopodium* spp. spores

were added to the Ayrag core sediments as an internal standard for calculation of pollen and NPP concentrations and influxes (Stockmarr, 1971). The total pollen count size was determined by the asymptotic behaviour of the rarefaction curve, plotted during counting using `PolSais 2.0`, a software developed in `Python 3.0` in Dugerdil et al. (2021). The count was stopped whenever the logarithmic regression fitting of the rarefaction curve reached a flat threshold (Birks et al., 1992). The average total count was generally in $n \in [400; 500]$ terrestrial grains for each slide. The pollen diagram was plotted in `R` with the `Rioja` package (Juggins and Juggins, 2019), with pollen as a fractional abundance ratio of Terrestrial Pollen count (%TP).

In arid environments, the paleo pollen signal is usually analyzed besides ratios between the major taxa (Herzschuh, 2007; Zhao et al., 2012). The ratios are semi-quantitative models for precipitation and temperature variation. The more common taxa used in these ratios are *Artemisia* spp. (Ar), Amaranthaceae (Am), Poaceae (Po), Cyperaceae (Cy) and *Thalictrum* spp. (Th). For this study we applied the Ar/Am, (El-Moslimany, 1990), Ar/Cy (Herzschuh et al., 2006), Ar/(Ar+Am), (Ar+Am)/Po, (Ar+Am)/(Po+Th) and (Ar+Am)/(Po+Th+Cy) ratios (Murad, 2012). We, thus, applied these ratios on the NMSDB in order to validate the reliability of the climate semi-quantitative reconstructions.

Then, as quantitative climate reconstructions, some transfer function methods were applied to the sequences using two different surface datasets (New Mongolian-Siberian Surface Data Base; NMSDB and the Cold Steppe Data Base; COSTDB, sample locations in Dugerdil et al. (2021, Supplementary information). Among the major transfer functions, and following the results presented in Dugerdil et al. (2021), we applied the Modern Analogue Technique (MAT, Overpeck et al., 1985; Guiot, 1990; Jackson and Williams, 2004), the Weighted Averaging Partial Least Squares regression (WAPLS; Ter Braak and Juggins, 1993; Ter Braak et al., 1993), and Boosted Regression Trees (BRT, Salonen et al., 2014; Li et al., 2015). More details about transfer functions, calibrations, and pollen-inferred climate reconstructions are given in (Dugerdil et al., 2021).

3.6. Calibration surface data set

A set of surface samples used as a local calibration for both pollen and GDGT climate models has been sampled from the Lake Baikal area in the southern part of the Mongolian Gobi desert, and is named the New Mongolian Siberian Surface Data Base (NMSDB, Fig. 1.A). The accurate location of each sample can be found in the supplementary information table from Dugerdil et al. (2021). A global Eurasian pollen database presented in Peyron et al. (2013, 2017) was sub-sampled with the *biomization* method (Prentice et al., 1996; Peyron et al., 1998) based on pollen–Plant Functional Type (Prentice et al., 1996; Harrison et al., 2010): only the Cold Steppe (COST) pollen samples have been kept as sub-dataset. The global calibration database for brGDGTs can be found in Dearing Crampton-Flood et al. (2020). These two global databases are compared with the local NMSDB.

3.7. Non-pollen palynomorph analysis

In parallel with pollen counts, two kinds of Non-Pollen Palynomorph (NPP) were analyzed: fungal spores and aquatic micro-fossils, such as micro-algae and spores, aquatic pollen or fossils of hydrophylous plants. These NPP underwent the same protocol as pollen (chemical, counting and plotting processes described in 3.5). The fungal spores are considered as a proxy for grazing and pasture activities (Cugny et al., 2010; Baker et al., 2013), wood decomposition (Cugny et al., 2010; Cugny, 2011) or wood burning markers (Van Geel, 1978; Bakker and Van Smeerdijk, 1982), vegetation change (Ghosh et al., 2017), and erosion (Anderson et al., 1984; Kolaczek et al., 2013). The algae *taxa* composition provides information about water level and the lake trophic system (Jankovská and Komárek, 2000). Identification of the Mongolian principal NPPs was driven by the keys supplied by Van Geel and Aptroot (2006), Cugny et al. (2010) and Murad (2012). The algae spectrum is expressed in the pollen diagram in fractional abundance (%TP + NPP) following eq. (1) :

$$f(NPP)_i = \frac{n_{NPP_i}}{\sum n_{NPP}} \times \sum n_{pollen} \times 100 \tag{1}$$

NPPs and algae in absolute values are expressed as influx (Fx) for each *taxon i*, calculated with concentration ($[NPP]_i$ in eq. 2) and ranked with the Sedimentary Accumulation Rate (SAR) and gamma-density of the core sediment (γD, eq. 3) as follows :

$$[NPP]_i = \frac{n_{NPP_i}}{n_{lycopodium_{counted}}} \times n_{lycopodium_{total}} \tag{2}$$

$$Fx(NPP_i) = [NPP]_i \times SAR \times \gamma D \tag{3}$$

For dung fungal spores, the number of spores counted for each sample was very low as compared to algae and pollen counts (10 to 25 times lower). Using the amount of spores divided by the NPP sum would have overwhelmed the spore signal, which is why the spores have only been presented in absolute concentration (number of counted grains reported to *Lycopodium* spp. amount). Moreover, the fungal spore signal marks an evolution in grazing impact, especially by its rising concentration and taxa diversity (Cugny, 2011; Baker et al., 2013). The within-community variations are less well understood. Finally, the algal NPPs are usually more concentrated than the pollen grains. The count limit for algae was 150 *Lycopodium* spp. spores counted, and 300 for the fungal NPPs (Etienne and Jouffroy-Bapicot, 2014). All counts were homogenized at the end

Table 2
Correspondence between major fungal spores and amoebae with their ecological indication.

Indicator	NPP type	NPP group	Reference(s)
Erosion markers	*Arcella* spp.	Testate amoebae	Miehe et al. (2009)
	Glomus spp.	Arbuscular mycorrhizal fungi	Anderson et al. (1984), Shumilovskikh et al. (2016), Shumilovskikh and van Geel (2020)
Dung fungal spores	*Arnium* spp.	Spore fungi	Cugny (2011), Shumilovskikh and van Geel (2020)
	Chaetomium spp.	Spore fungi	Shumilovskikh and van Geel (2020)
	Delitschia spp.	Spore fungi	Cugny (2011)
	Podospora spp.	Spore fungi	Cugny (2011), Van Geel (2002), Shumilovskikh and van Geel (2020)
	Sordaria spp.	Spore fungi	Cugny (2011), Van Geel (2002), Shumilovskikh and van Geel (2020)
	Sporormiella spp.	Spore fungi	Djamali et al. (2016), Cugny (2011), Shumilovskikh and van Geel (2020)
Parasitic spores	*Byssothecium circinans*	Spore fungi	Van Geel (1978), Van Geel and Andersen (1988),
	Endophramia spp.	Spore fungi	Cugny (2011)
	Kretzschmaria deusta	Spore fungi	Van Geel and Andersen (1988)
	Microthyrium spp.	Fruit body	Blackford and Innes (2006),
	Pleospora-type	Spore fungi	Cugny (2011)
	Thecaphora spp.	Spore ball of smut fungi	Miehe et al. (2009), Murad (2012), Shumilovskikh and van Geel (2020)
	Tilletia spp.	Spore ball of smut fungi	Cugny (2011), Murad (2012), Shumilovskikh and van Geel (2020)
Saprophytic spores	*Arthrinium* spp.	Spore fungi	Ellis and Ellis (1985), Cugny (2011) Van Geel and Aptroot (2006)
	Cercophora spp.	Spore fungi	Van Geel (2002), Montoya et al. (2010), Cugny (2011), Shumilovskikh and van Geel (2020)
	Coniochaetaceae - Xylariaceae type	Spore fungi	Cugny (2011) Murad (2012)
	Gelasinospora spp.	Spore fungi	Cugny (2011)
		fungi	Cugny (2011), Baker et al. (2013)
	Neurospora spp.	Spore fungi	Bakker and Van Smeerdijk (1982), Van Geel (1978)
	Trichocladium spp.	Spore fungi	Cugny et al. (2010), Cugny (2011)
Wetland markers	*Amphitrema flavum*	Testate amoebae	Van Geel (1978), Shumilovskikh and van Geel (2020)
	Caryospora spp.	Spore fungi	Murad (2012)
	Valsaria spp.	Spore fungi	Montoya et al. (2010), Cugny (2011)

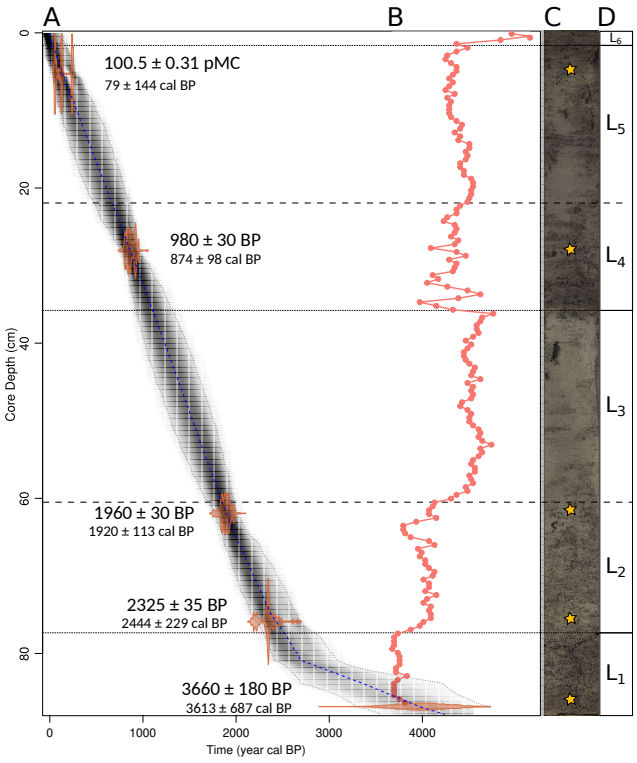

Figure 2: **A**: Age - depth model for the Lake Ayrag core performed by the BACON package (Blaauw and Christen, 2011) using the Markov chain model. The lithology boundary used in the model is displayed by a solid line (on the L_{1-2} boundary); **B**: magnetic susceptibility (10^{-5} SI); **C**: high-resolution picture of the core showing the different bulk lithologies. The date sampling quarters are shown by yellow stars. **D**: lithologic units in the core. The solid lines represent the most important boundaries visible on the picture C, the dashed lines represent the boundary visible only by magnetic susceptibility (A).

with the total sum of exotic marker grains.

Even if the NPP study especially insists on a link between spores and grazing, some fungal spores represent other environmental proxies such as for erosion, aquatic contributions, or forest burning activity (Cugny, 2011). In this former study, the author used surface samples and multivariate analyses to cluster three fungal spore assemblages: forest burning (Saprophytic spores), grazing, and overgrazing indicators (coprophilous spores). Here, we used this classification coupled with observations realized in other studies (Van Geel, 1978, 2002; Pals et al., 1980; Bakker and Van Smeerdijk, 1982; Anderson et al., 1984; Ellis and Ellis, 1985; Van Geel and Aptroot, 2006; Miehe et al., 2009; Montoya et al., 2010; Baker et al., 2013; Shumilovskikh and van Geel, 2020), some of which include Mongolian lakes (Murad, 2012). Then we gathered all of the identified fungal taxa into five different assemblages following the methods of Cugny et al. (2010) and Doyen and Etienne (2017). The correspondence between spore type and ecological type is presented in table (2).

3.8. Statistical methods

Statistical analyses were performed in R (version 4.0.3; R Core Team, 2013). A Principal Component Analysis (PCA) was performed on the XRF data using the FactoMineR package (Lê et al., 2008). The PCA permits determination of the axis explaining the most variance within samples. All plots were generated with the ggplot2 package (Wickham, 2016), or the Rioja package (Juggins and Juggins, 2019) for the stratigraphic plot and the pollen and the MS clustering using the CONISS analysis method applied to the %TP (Grimm, 1987). Where possible, uncertainties were estimated using diverse methods. For the Lake Ayrag GDGT signal, six replicated isotopic analysis were carried out for 5 samples equally distributed in the core sequence. On these replicated samples, the mean and the standard deviation were calculated, and the 95% uncertainty interval was calculated according to $P_{95\%} \in \left[\bar{x} - 1.86 \times \frac{\sigma_x}{\sqrt{6}}; \bar{x} + 1.86 \times \frac{\sigma_x}{\sqrt{6}}\right]$. The $P_{95\%}$ interval has been plotted for each GDGT index, and GDGT–climate inferred models extrapolated the standard deviation value for all the core samples to the closest replicate in the core sequence. Concerning the pollen-inferred climate values, the intervals have been determined with plus or minus the bootstrap value after cross-validation (Birks et al.,

2012). To facilitate interpretation of the climate reconstructions, smoothing lines and 95 % intervals have been added to the plots (Mann, 2004) using a loess regression method with span value varying with the number of sampling points along the cores.

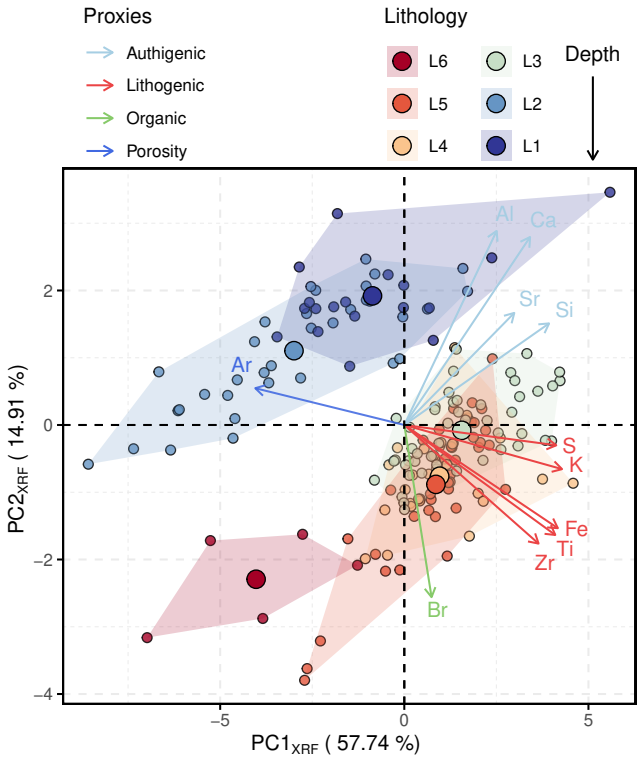

Figure 3: PCA analysis of selected XRF signals from Lake Ayrag. The 11 principal components are clustered by proxy: authigenic or lithogenic origin, sediment porosity, and organic matter. The samples are grouped by lithological units (Fig. 2.D). The centroid of each lithological unit is represented by large circles.

4. Results

4.1. Age-depth model and lithology

The understanding of the age-depth model for the Lake Ayrag core (Fig. 2.A) is supported by the MS signal (Fig. 2.B), particularly for locating with accuracy transition borders associated with shifts in sedimentation (clustered by CONISS analysis on the MS signal). These transitions are also visible in the sediment core itself (Fig. 2.C). These observations allow us to split the core into four major lithologies (Fig. 2.D): the bottom part (L_1, 80 to 88 cm) exhibits desiccation polygons and friable fragments; the lower-middle part (L_{2-3}, 35 cm to 80 cm) presents the same features but with fewer cracks and wetter sediment; the upper-middle (L_{4-5}, 5 to 35 cm) core consists of a clay and organic matter (OM) mixture; and the top of the core (L_6, 0 to 5 cm) is essentially the same but softer with not well indurated OM. The transition between these phases are smooth and continuous, and there is no evidence of any hiatus. The age-model is linear over the upper 80 centimeters with a mean sediment accumulation rate (SAR) of around 0.3mm.yr^{-1}, which is lower at the core bottom (SAR = 0.07mm.yr^{-1}). The oldest ^{14}C date (depth = 94.5 cm) has a greater uncertainty than the others, which could be an effect of the rock settlement dominating the lake sediments. However, algae counts show that there is already *Botryococcus* spp. and *Pediastrum boryanum* at the bottom of the core. Finally, to help the Markov-chain model of the Bacon module (Blaauw and Christen, 2011), a boundary at around 80 centimeters was set, representing the lithology shift (at the L_{1-2} boundary). The SAR variation (Fig. 2.A), which could be due to sediment compaction at the bottom of the core, has been taken into account. Following this age-depth model, the Lake Ayrag core covers from 3,900 cal yr BP to -20 cal yr BP.

4.2. XRF and bulk geochemistry

XRF signals display the 20 major chemical elements present in the core (Supplementary Fig. B1). All element variations follow the MS variations recorded along the core. To simplify interpretation of the chemical composition of the core, a PCA was performed on the 11 most abundant elements and is displayed in Fig. 3. The first component of the PCA, called here PC1$_{XRF}$, explains 57.74% of the elemental variation, while PC2$_{XRF}$ represents 14.91% of the variance, and PC3$_{XRF}$ around 10.59%. The first axis explains the opposition in argon composition on one hand, and the other mineral and organic elements on the other hand. Argon (Ar) is detained in the air gap inside the core, therefore the Ar signal is interpreted as a proxy for sediment porosity. The higher the Argon abundance, the less the core is compacted (Croudace and Rothwell, 2015). The top of the core (L_6) and the bottom (L_1 and L_2) have higher porosities. PC2$_{XRF}$ describes a dichotomy between two poles: one marked by the elements Zr, Fe, Ti, Ni, S and K, and another by Sr, Si, Ca and Al.

With regard to these observations (geochemistry of bulk elements, Fig. 4.C), the four main lithological divisions of the core derived from the high-quality image (Fig. 2.B) can be described by six more detailed units (Fig. 2.D). From 3,900 to 2,600 cal yr BP (L_1), the MS signal is low and steady. PC1$_{XRF}$ is dominant and decreasing, and all the other XRF elements are low. The organic proxies such as C/N and TOC are high. The system is marked by the transition from pieces of bedrock re-mobilized by the dead meander of the Khanuii river (resulting in high porosity) to recent lake sedimentation. Detrital erosion was almost absent and the lake was marked by an important OM influx as well as soil brGDGTs from the river catchment. The second stage, from 2,600 to 1,900 cal yr BP (L_2), suggests a well-established lake with the beginning of authigenic OM production (low C/N and high δ^{15}N). A first large increase in erosion (MS and PC2$_{XRF}$ rising) characterizes a transition to a weathering system from 1,900 to 1,100

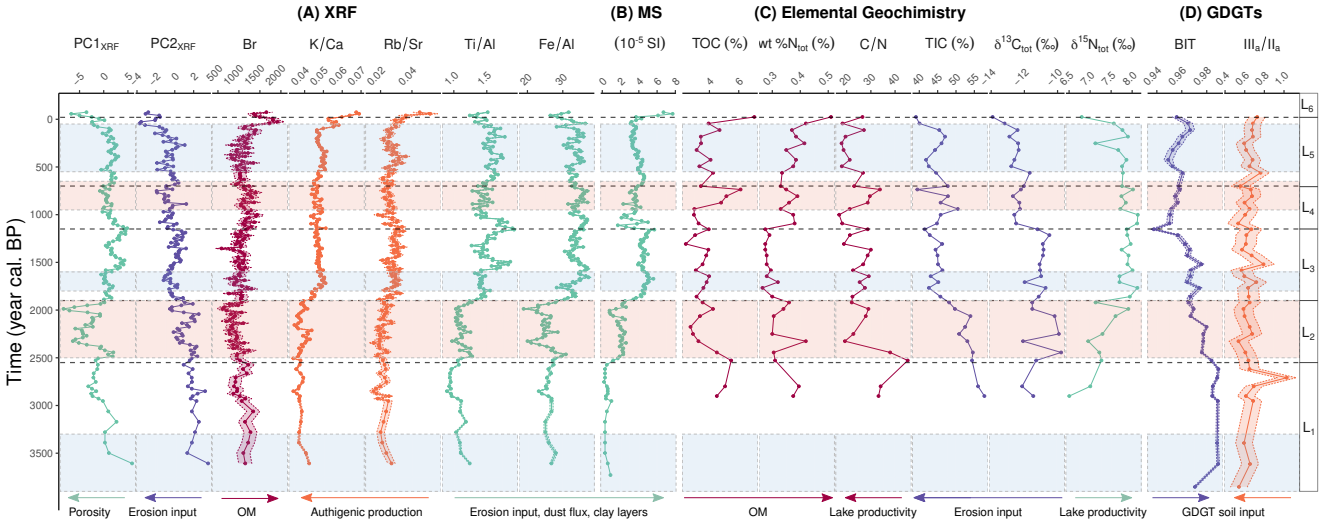

Figure 4: Geochemistry proxies applied to the Lake Ayrag sequence. **A**: selected XRF signals (PC_1 and PC_2 from Fig. 3, ratio of Potassium / Calcium, Rubidium / Strontium, Titanium / Aluminum, Iron / Aluminum); **B**: magnetic susceptibility; **C**: selected isotopes and element mass abundances (Total Organic Carbon (TOC), weight percentage of bulk Nitrogen ($w\%N_{tot}$), Total Inorganic Carbon (TIC), the ratio between TOC and $w\%N_{tot}$ (C/N), bulk $\delta^{13}C$, bulk $\delta^{15}N$); **D**: GDGT index for source origin (branched vs. isoprenoid tetraether (BIT) index and ratio III_a/II_a). Colors highlight the signals following the same trend: green curves show sediment compaction, and the clay and dust inputs provide nutrients for increasing lake productivity; purple curves decrease with lithogenic and ex-situ OM input, soil brGDGT, and algal production; purple curves show OM amount in the sediment; orange curves decrease with authigenic production.

cal yr BP (L_3), with a steady and elevated $PC2_{XRF}$, Fe/Al and Ti/Al. The fourth period, from 1,100 to 700 cal yr BP (L_4), is a parenthesis in the trend imprinted on the entire record. Rebounds in TOC, TIC, $wt\%N_{tot}$, and C/N suggest the influence of authigenic lake productivity, whereas the erosion signal (MS, Ti/Al) is tempered but not decreasing, with a $PC2_{XRF}$ still rising and a steady K/Ca and Fe/Al signal. The fifth period (L_5, 700 to 150 cal yr BP) is characterized by a return to the main trend (low TOC, C/N and high $\delta^{15}N$). Then the sixth unit (L_6) exhibits a peak in authigenic production (rapid rise in TOC and $w\%N_{tot}$) of organic matter, certainly linked to lake eutrophication and watershed erosion marked by peaks in MS, K/Ca and Rb/Sr.

The GDGT sediment concentrations for Lake Ayrag ($[brGDGT]_{tot} = 34.74 \pm 13.07\ ng.g^{-1}_{sed}$ and $[isoGDGT]_{tot} = 10.97 \pm 5.23\ ng.g^{-1}_{sed}$) are consistent with typical values in the literature (Yang et al., 2014). However, Ayrag GDGT concentrations are close to the minimal values when compared to some Chinese lakes (Wang et al., 2016; Cao et al., 2017). The cold-arid oligotrophic context of Lake Ayrag can explain these low GDGT concentrations. The fractional abundances also exhibit typical distributions (Supplementary Fig. B2): isoGDGTs are dominated by $GDGT_0$ and crenarcheol (these two compounds represent more than 80%); and brGDGTs by III'_a, II'_a and I_a (for a total of around 50%). The brGDGT fractional abundances from Lake Ayrag are dominated by pentamethylated (around 40-50%) and hexamethylated compounds (close to 30-40%, Supplementary Fig. B3). The signal is quite homogeneous throughout the last 4,000 years, and close to the lake top core and soil surface samples from global and Mongolian databases (Dearing Crampton-Flood et al., 2020; Martínez-Sosa et al., 2020; Dugerdil et al., 2021).

The Ayrag brGDGT record shows (Fig. 5) two ranges of amplitude over time: a major trend throughout the 3,900 cal yr BP sequence, and shorter amplitude variations during several centennial periods. Initially, MBT and MBT'_{5Me} (Fig. 5.A) suggest a temperature variation with a first limit after lake development (3,600–3,300 cal yr BP, L_1), followed by a second shorter step of increase from 2,800 to 2,300 cal yr BP (L_2), then a slow continuous decrease finishing with a third rebound (700 to 250 cal yr BP, L_5). This trend is quite similar for the Cyclisation of Branched Tetraether index (CBT and CBT_{5Me}), which trace pH variation, with a decrease over 3,900 cal yr BP (Fig. 5.B). The $mathrmCBT_{5Me}$ and MBT'_{5Me} indexes, which are more reliable for arid environments (De Jonge et al., 2014b; Dang et al., 2016), react more during the centennial-scale oscillations than the CBT and MBT indexes. Indeed, we can observe clear peaks during the MWP and RWP, and drops during the LIAand the DACP events.

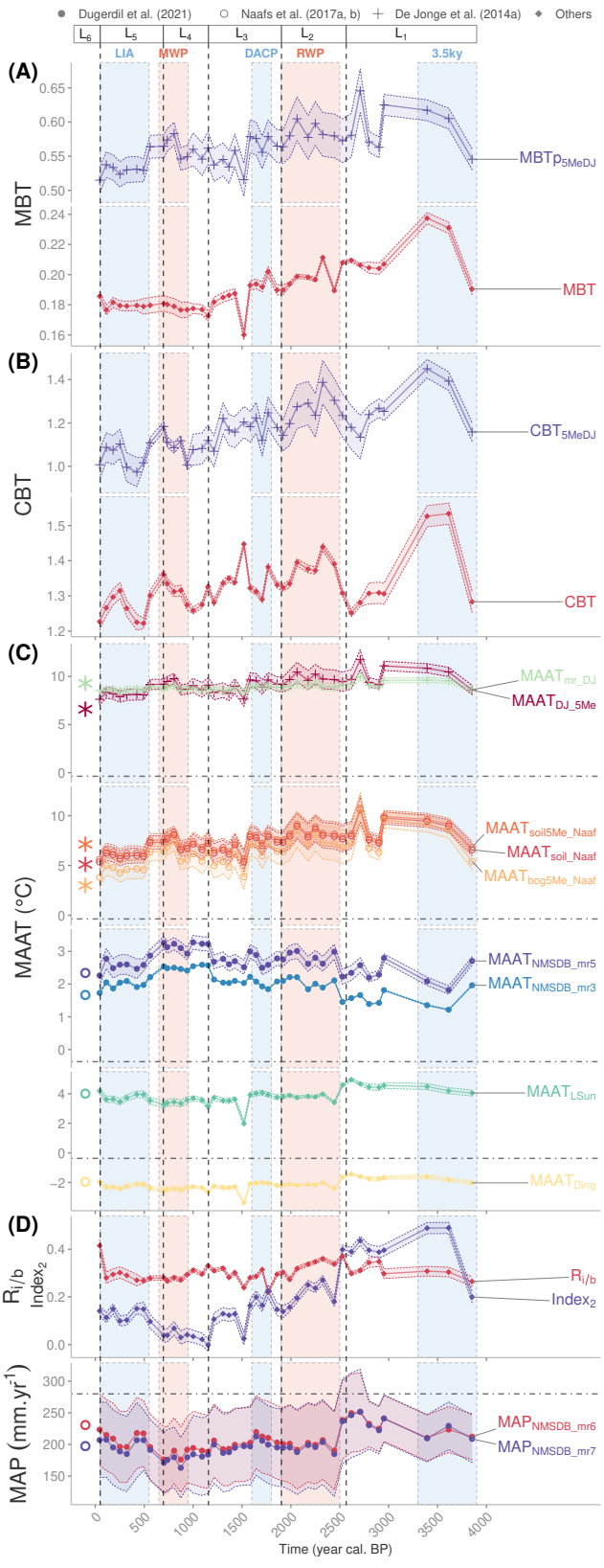

Figure 5: GDGT records for Lake Ayrag. From the top to the bottom; (**A**) MBT'_{5Me} and MBT indexes; (**B**) CBT and CBT_{5Me} indexes; (**C**) brGDGT–MAAT models calibrated from Sun et al. (2011), De Jonge et al. (2014b), Ding et al. (2015), Naafs et al. (2017a) and Dugerdil et al. (2021); (**D**) semi-quantitative precipitation indexes $R_{i/b}$ and $Index_2$ and MAP calibrations from Dugerdil et al. (2021). The symbol * indicates global calibrations and °the local ones. The dashed lines represent the actual MAAT and MAP for Lake Ayrag (*WorldClim2*, Fick and Hijmans, 2017). Following the ACA main paleoclimate studies, the warm (red frame) and cold (blue frame) periods highlighted are the 3.5 kyr event, RWP, DACP, MWP and LIA (Zhang et al., 2008; Chen et al., 2015b). The lithological units follow the MS record (Fig. 2.B).

These observations are confirmed by the brGDGT-inferred MAAT reconstructions (Fig. 5.C), which exhibit variations during the Late Holocene with centennial-scale oscillations. Using the Lake Ayrag top-core replicates compared with actual MAAT values (Dugerdil et al., 2021), we selected the best calibrations for brGDGT-inferred MAAT: soil (De Jonge et al., 2014b; Ding et al., 2015; Naafs et al., 2017a), peat (Naafs et al., 2017b), mixed (Dugerdil et al., 2021) and lake calibrations (Sun et al., 2011). Two major calibration groups appear: the local calibrations, with reduced climate amplitude during the last 3,900 years, and the global calibrations, with exaggerated amplitudes around more than 9 °C in temperature. Moreover, the local calibrations (from Sun et al., 2011; Ding et al., 2015; Dugerdil et al., 2021) better fit the best the actual surface values than the global ones (from De Jonge et al., 2014b; Naafs et al., 2017a). Even if the centennial-scale climate oscillations are well defined for each set of calibrations, the global MAAT trend shifts after 2,000 cal yr BP. The global calibration displays warmer conditions than the local calibration for the first part of the core (units L_{1-2}).

Concerning precipitation (Fig. 5.D), the $R_{i/b}$ index (a precipitation proxy according to Xie et al., 2012; Yang et al., 2014; Dang et al., 2016) follows a trend similar to that of $MAAT_{Lake-Sun}$, that is to say slightly rising from 3,950 to 2,500 cal yr BP (L_1, RWP beginning) and then slightly decreasing until 100 cal yr BP before a final abrupt change. This signal is even more marked in amplitude for CBT_{5Me} (soil pH, i.e soil moisture) and the $Index_2$. This index has in addition a last continuous rebounding from 1,100 cal yr BP until today. The late shift inferred by $Index_2$ could be interpreted as an anthropogenic impact (Wang et al., 2016), rising from 900 to 250 cal yr BP before an accelerated shift until today. However, it can also be linked to a MAP increase since the last driest period (L_4, MWP). Indeed, this trend is also the same as for the Mongolian locally calibrated brGDGT-inferred MAP from (Dugerdil et al., 2021). The seeming correlation between $Index_2$ and the MAP_{NMSDB} signal can indicate that the $Index_2$ is more linked to moisture than temperature in the Ayrag core.

4.3. Pollen signal

The complete (Supplementary fig. B4) and simplified pollen diagrams (Fig. 6.A), spanning a range of 3,900 cal yr BP, are continually dominated by Non-Arboreal Pollen (NAP). The NAP value runs from 80 to 90%. The major herbaceous taxa are *Artemisia* spp., Amaranthaceae, Poaceae and Cyperaceae. The 10 to 20% of Arboreal Pollen (AP) is composed in order of importance by *Pinus* spp., *Betula* spp., *Picea obovata* and *Larix sibirica*. The *Pinus sylvestris* and *P. sibirica* pollen grains were counted as separate types, but due to the large identification uncertainty (Robert Bagnell, 1975), we grouped them as *P. sylvestris* for the botanical survey and palynological analysis (Dugerdil et al., 2021).

The CONISS analysis helped us to define six majors zones in the pollen diagram. A first zone (U_1) is present at the very bottom of the core (3,900–3,700 cal yr BP), with Poaceae and *Artemisia* spp.. A second one (U_2) spans 3,700 to 2,500 cal yr BP and is widely dominated by *Artemisia* spp., while a third one (U_3) follows until 1,200 cal yr BP with an increasing share of Poaceae and a decreasing portion of *Artemisia* spp.. Then from 1,200 to 700 cal yr BP (U_4), Poaceae becomes broadly dominant, substituting for the *Artemisia* spp. part of the signal. Cyperaceae also increase continuously, with a peak at around 700 cal yr BP (U_5). The latest CONISS limit is set at around 150 cal yr BP (U_6), with an increase of *Artemisia* spp., a strong decline of Poaceae, and finally a mixed period with an increased diversity and higher abundance of AP. The pollen phases almost follow the lithological divisions, especially for U_4 to U_6 which match with L_4 to U_6. U_3 corresponds to L_2 plus L_3, and U_2 (except the first 200 years) matches with L_1.

The AP–NAP (Arboreal Pollen – Non Arboreal Pollen proportions do not shift significantly, but the small-scale variations are well anti-correlated with the Poaceae signal. The AP percentage decreases from 15 to 5 in the $U_2 - U_4$ units, with its lowest point on the $U_4 - U_5$ limit. Then it increases once again from 5% to almost 20%. Moreover, within the AP fraction, we see little composition shift; if the larches are steady, the units U_2, early U_3 and U_6 present a higher percentage of birch. Among the other trees, pines and spruces dominate the U_3 to U_5 units.

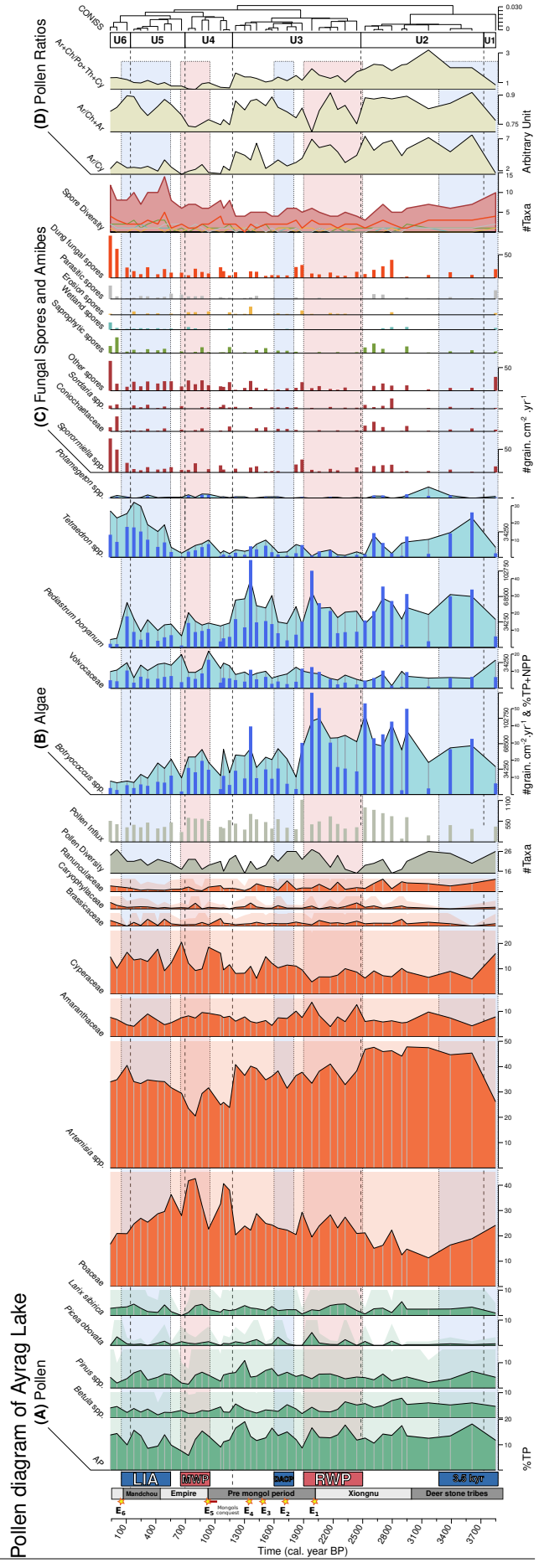

Figure 6: (**A**) Pollen, (**B**) algae and (**C**) fungal spore diagrams simplified. The pollen taxa are expressed in %TP, the NPP fractional abundances in %TP + NPP, and the influx in #grain.cm^{-2}.yr^{-1}. The Pollen Units U_2 to U_6 were determined with a CONISS analysis applied to the pollen fraction (%TP) only. The bars display influx, while curves represent fractional abundances. The diversity curves represent the number of different taxa counted for each slide whenever the rarefaction curve reached its asymptote. The spore diversity is clipped in type richness (Cugny et al., 2010) with the Saprophytic spores (green line), the Wetland markers (blue line), the Erosion markers (yellow line), the Parasitic spores (grey line) and the Dung fungal spores (orange line). The pollen ratios **(D)** were calculated following El-Moslimany (1990); Herzschuh et al. (2006) and Murad (2012). The major Mongolia invasion and cultural periods are noted by E_1, Ruanruan; E_2, Körtürks; E_3, Uyghurs; E_4, Kirghiz; E_5, Gengis Khan and E_6, the Mongolia independence from USSR. The major climate events are chronologically the 3.5 kyr events, the Roman Warm Period, the Dark Ages Cold Period, the Medieval Warm Period and the Little Ice Age. The period boundaries are derived from ACA paleoclimate studies.

The Ar/(Ar+Am) ratio suggests (Fig. 6.D) enhanced aridity when decreasing (El-Moslimany, 1990). However, this ratio applied on the NMSDB surface samples shows slightly better anti-correlation with T_{spr} than with precipitation ($R^2 = 0.63$, on Supplementary Fig. B5.A). Since MAP and T_{spr} appear to be anti-correlated in the NMSDB, this result is consistent. Thus, it points to two dry-warm periods at the beginning of U_3 (around 2,500 cal yr BP) and during U_4, while U_2, the end of U_3 and U_6 appear to have been wetter and cooler periods. Similar trends are observed for (Ar+Am)/(Po+Th+Cy), which shows a steady decrease from U_2 to U_5, then a slight increase top-ward (Murad, 2012). Here, this ratio points to slight and constant aridification B5.B). Finally, while the Ar/Cy ratio is usually considered as a T_{sum} indicator (Herzschuh et al., 2003), our results mainly suggest an aridification from U_2 to U_4 and finally a slight wetting trend during the last 200 cal yr BP. These semi-quantitative ratios can help us to determine the reliability of the transfer functions applied to pollen since they include only the major taxa.

4.4. NPP: algae and dung fungal communities

Throughout the Lake Ayrag core, algae influx is broadly higher than pollen and fungal spores influxes (Fig. 6.B). The dominant algae taxa counted are *Botryococcus* spp., *Pediastrum boryanum*, Volvocaceae, and *Tetraedron minimum*. Among the rare taxa are some Zygnemataceae as *Mougeotia* spp., *Zygnema* spp. and *Spirogyra* spp.. Few spores or pollen of wetland taxa as *Typha–Sparganium*-type and *Alisma* spp. were found. For the dung fungal spores (Supplementary fig. B6), the diversity is dominated by *Sporormiella* spp., *Glomus* spp., Coniochaetaceae, *Sordaria* spp., *Valsaria* spp., *Neurospora* spp., *Arnium* spp., *Kretzschmaria deusta* and *Distachia* spp.. A lot of unclassified spores were added to the Undetermined Spores category. A minority of identified spores were aggregated to the Other Fungal Spores category (Fig. 6.C). The spore diversity curve records only the determinant spores and not the true fungal diversity.

The algae community represents an important biomarker for lacustrine system variations and paleoenvironmental interpretations (Jankovská and Komárek, 2000; Aichner et al., 2012), even if it is a difficult proxy to interpret; Stivrins et al. (2018) demonstrates that algal remains on pollen slides are not a direct reflection of the actual algal biomass. Along the Lake Ayrag sequence, there is a distinct community succession within the lake ecological niche. First, during U_1 at the core bottom, the algae influx was very low. Then, as a first settler in U_2, the *Pediastrum boryanum-Tetraedron minimum* community appears. The *Botryococcus* spp. community takes over from them and dominates from the end of U_2 to the first part of U_3. The U_{3-4} transition, which is associated with the maximum algae influx, lacustrine authigenic OM productivity (Fig. 4.A and C), and DACP (Chen et al., 2015b), exhibits a co-dominance between *Botryococcus* spp. and a rebounded community of *P. boryanum*, reaching its peak during the upper part of the U_3 phase. The third community to colonize the lake was Volvocaceae–Zygnemataceae, with a high plateau in the U_4 and U_5 units, despite a short drop during the MWP. Finally, the *Tetraedron minimum* species took over the lake system for the two last U_5 and U_6 units, in association with few *Scenedesmus* spp. and aquatic pollen taxa such as *Potamogeton* spp.. These lacustrine communities are affected by climate and water body depth, as well as basin water influx (inorganic weathering and terrestrial OM influx, Aichner et al., 2012). Geochemical proxies (Fig. 4) associated with dung fungal spore inputs (Fig. 6.C) provide additional information for understanding the lacustrine system.

The dung fungal spore signal is marked by a general trend of increase in NPP production and spore diversity from 3,500 cal yr BP to the present (Fig. 6.C). They accurately follow the cluster zones provided by the pollen signal CONISS analysis. These two signals (NPP influx and spore diversity) shift together, with the first appearances around the U_{2-3} boundary, the first important steps after the U_{3-4} transition, and then the U_{4-5} boundary marks a second high step for NPPs. Finally, the last 100 cal yr BP exhibit an exponential increase of NPP influx and diversity, driven in part by a rise in *Sporormiella* spp. and *Sordaria* spp. spores. The Type Richness (TR) is used to determine which type of NPP contributes to the rising diversity patterns; Coprophilous spores (dung fungal spores, orange curve and histograms, Fig. 6.C) are already present throughout the core (especially at the lake development U_{1-2}), but they grow significantly around the U_{3-4} boundary and strongly increase after the U_{5-6} transition, explaining the trend in

the total diversity.

Saprophytic spores (green diversity curve and histograms, Fig. 6.C, Supplementary fig. B6) are mostly native to tree roots (Ellis and Ellis, 1985; Van Geel and Andersen, 1988). Some of them also require a wood burning phase to facilitate nutrition (Cugny et al., 2010). The Saprophytic signal in the core begins around the middle of U_2 (3,000 cal yr BP) and lasts until today with some discrete variations. This signal seems to suggest a rising pattern during the cold periods (DACP and LIA) and a decreasing one in the warm periods (RWP and MWP). Furthermore, the signal is anti-correlated with that of Coprophilous, except during the last WCP in which all the NPP influxes dramatically increase. Then the erosion markers are constituted of mycorrhiza fungi working in symbiosis with plant roots. Their presence in lake sediments indicates a weathering episode which tears them from the soil matrix (Kolaczek et al., 2013). In the Ayrag core, the erosion markers increase from the middle part of U_3, culminating during the U_4 phase and then declining in accord with the MS trends (Fig. 4.B). This increase in bare soil land-cover proportion could indicate semi-arid conditions in the watershed as well as a rising impact from grazing (assumption supported by the Dung fungal spore increasing signal). Finally, the two last spore assemblages are made of spores associated with plant-parasitism and wetland fungi generally living in peat or on the water table surface (Van Geel, 1972, 1978). In the Lake Ayrag sequence, they appear in the U_{4-5} units and do not decrease afterwards. This pattern is the same as for the algae *Tetraedron minimum*–Volvocaceae community, indicating an higher water table linked to wetter conditions.

4.5. Pollen-inferred climate reconstruction: MAT , BRT and WAPLS results

Temperature (MAAT, Fig. 7.A) and precipitation (MAP, Fig. 7.B) reconstructed values and associated statistical parameters (R^2, p-value and RMSE, Dugerdil et al., 2021) permit us to validate the reliability of the models. Especially, the transfer function reconstructions for Lake Ayrag follow similar trend than the Ar/(Ar+Am) ratio which as been shown to be the most representative semi-quantitative ratios (proxy of colder and wetter spring conditions, Supplementary Fig. B5.A). To select the most accurate model, it is appropriate to check the actual value fitting, the global amplitude for the time span, the comparison between reconstructions made using different proxies, and the correlation with already documented centennial-scale climate oscillations (Dugerdil et al., 2021). Following this method, only the $MAP_{WAPLS-COSTDB}$ is not considered accurate (wide amplitude, shift from the current value, and anti-correlated signals with other models). Based on the other reconstructions (this one excepted), the Lake Ayrag climate changes reconstructed for the Late Holocene period can be discussed.

On Fig. 7, similar climate trends appear for the different tests (regardless of the calibration data set or the model); the range of amplitude is small ($\Delta MAAT \in [-0.5; +0.5]°C$, Fig.7.A and $\Delta MAP \in [-50; +50] mm.yr^{-1}$, Fig.7.B). For the Late Holocene period, this range of amplitude is on the same order as for all the other Eurasian records controlled by the EASM influence (Liu et al., 2011; Lan et al., 2018). The regional trend is led by a slight cooling from the Holocene Optimum (around 5 kyr in northern China) to the LIA (Li et al., 2018). For Lake Ayrag, this is especially visible for the global calibrations, while the local calibrations are slightly flatter during the last 3,000 cal yr BP (i.e., the general trend is constant during the Late Holocene despite important periodic oscillations). For precipitation, the trend follows a slow aridification until the MWP with a steeper rebound towards today. It is in the same range of proportion ($\Delta MAP \in [-100; +100] mm.yr^{-1}$) as other Mongolian lakes (Huang et al., 2018b), driving towards a globally drier Mid to Late Holocene (Klinge and Sauer, 2019) period. Following the MAAT global vs. local calibrations, the MAP locally calibrated models show flatter precipitation variation than the global ones do. The transfer function method choice slightly modifies the reconstruction results: the BRT presents higher amplitude variation through time than the MAT and the WAPLS ones. The BRT anomaly between current climate and reconstructed climate parameters is also slightly wider than the MAT and the WAPLS ones. However, for both MAAT and MAP, and for all the MAT, BRT and WAPLS models, all the climatic Eurasian periods are very well defined: a generally temperate-dry 3.5 kyr event, the RWP was warm-dry, the DACP followed a slightly cooler and wetter phase, the MWP was warm-dry again, and the LIA was colder and wetter.

5. Discussion

5.1. Proxy interpretation and model calibration assessment

All of the Lake Ayrag proxies contain biases and diverse ecological interpretations, as is the case for the majority of multi-proxy studies (Aichner et al., 2012; Murad, 2012; Unkelbach et al., 2019, 2020).

5.1.1. Isotopic and organic biomarker responses to environmental changes

The $\delta^{13}C_{TOC}$ and C/N variations through time (Fig. 8.A) suggest a shift from a system dominated by C_3 plants toward a system mixed between C_3 plants and algae (Leary O., 1988). Furthermore, and even if $\delta^{15}N_{tot}$ is more complex to interpret from a paleoenvironmental point of view (Last and Smol, 2001), Fig. 8.B highlights the same trend for $\delta^{15}N_{tot}$ and $\delta^{13}C_{TOC}$. In units U_2 and U_3, the source was likely a C_4/C_3 blend, but very soon afterwards the system was overprinted by a C_3 signature. The influence of C_4 plants, characterized by a $\delta^{13}C_{TOC}$ between -15 and -10 ‰ and a $\delta^{15}N_{tot}$ between 2 and 5 ‰, remains almost null through the Late Holocene. The Lake Ayrag $\delta^{13}C_{TOC}$

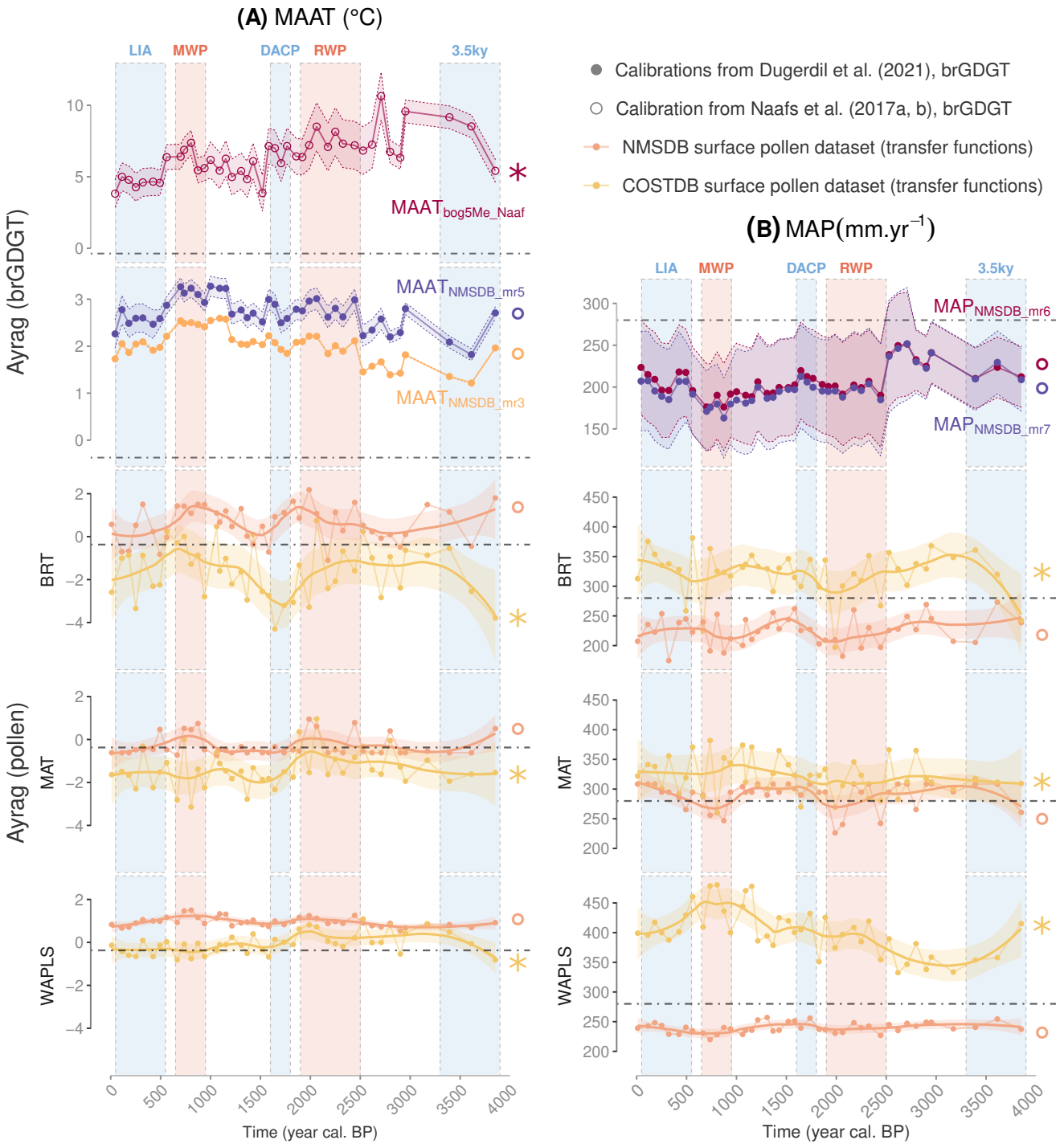

Figure 7: Lake Ayrag air annual temperature (MAAT, **A**) and annual precipitation (MAP, **B**) inferred from brGDGT data (upper panels), pollen data (MAT approach, BRT and WAPLS transfer functions). For the brGDGT models, the empty circles represent global calibration from (Naafs et al., 2017a,b), while solid dots display Mongolian local calibrations (in blue and orange) from (Dugerdil et al., 2021). The shaded area is calculated from the variance between replicated samples. For pollen, the local calibrated models (NMSDB) and the Eurasian steppes models (COSTDB) are also presented in (Dugerdil et al., 2021). The large line is a loess smoothed curve and the shaded area is the 95% confidence interval for this model. The symbol * indicate global calibrations and °the local ones. The blue rectangles represent cold events (from left to right the Little Ice age, Dark Age Cold Period, and 3.5 kyr event) and the red ones correspond to warm periods (the Medieval Warm Period and the Roman Warm Period) following the Chen et al. (2015b) and Zhang et al. (2008) Central Asian reviews.

values oscillate around -25‰ with a few spikes to -20‰ which seems to suggest that the vegetation was dominated by C_3 plants without high variation throughout the core. It is generally known that C_4 plants are characteristic of steppe environments and C_3 plants are more representative of a forest environment (Still et al., 2003). Interpreted in this way, the Ayrag $\delta^{13}C_{TOC}$ signal seems contradictory with the pollen AP/NAP signal. However, according to Pyankov et al. (2000) the families dominating the open landscape in Mongolia like Poaceae, Asteraceae and Amaranthaceae include very few C_4 plants. In this study, only 25 C_4 species are accounted for in the Poaceae family, representing 10% of Poaceae species. Moreover, the *Artemisia* spp. from Mongolia, which dominate the pollen diagram along the core (Fig. 6.A), are also C_3 plants (Pyankov et al., 2000). If the $\delta^{13}C_{TOC}$ signal is representative of only 10% of the main steppe family, this bias has to be taken into account for paleoenvironmental interpretations. Conversely, 45% of the Amaranthaceae species of Mongolia are C_4 plants (Pyankov et al., 2000), therefore a distinct increase in $\delta^{13}C$ could be interpreted as a rise in desert vegetation associated with a drier climate. The bulk geochemistry helps us to conclude that the steppe percentage of the total vegetation cover was stable throughout the Late Holocene, but the vegetation assemblage within the grassland formation shifts consistently with the pollen signal (especially along a Poaceae vs. *Artemisia* spp. gradient shown on Fig. 6.A).

Concerning GDGT origins, the trend suggests increasing authigenic production (biogenic inorganic matter and algal OM) through time. The BIT index stays flat (value above 0.94) over time, indicating that GDGT production was predominantly brGDGTs coming from the watershed and not from the lake itself (Hopmans et al., 2016). Moreover, the III_a/II_a ratio shifts (0.4 to 0.8 from L_2 to L_6, Fig. 4). This ratio, which is more distinctive for GDGT input than the BIT index (Xiao et al., 2016), increases moderately, suggesting a slight rise in lake archaeal production throughout the Late Holocene, and especially during the last 200 cal yr BP when Lake Ayrag eutrophication occurs.

5.1.2. *Lithogenic fluxes and authigenic production in Lake Ayrag*

The Fe, Ti, Rb, S, K and Zr elements belong to the lithogenic and allogenic classes of the mineral elements (Schwanghart et al., 2008; Murad, 2012), whereas Ca, Si and Sr represent authigenic lake production (Schwanghart et al., 2008). Iron in particular is a marker of dust influx (Kylander et al., 2011) or clay rich layers (Cuven et al., 2011). S could be linked to Redox conditions (Sluijs et al., 2008) or even evaporite concentration (Burn and Palmer, 2014), as well as Mn (Supplementary Fig. B1).

Silica production is often dominated by biogenic production (Olsen et al., 2010; Liu et al., 2013) as realized by diatoms, radiolarians and siliceous sponges within lakes.

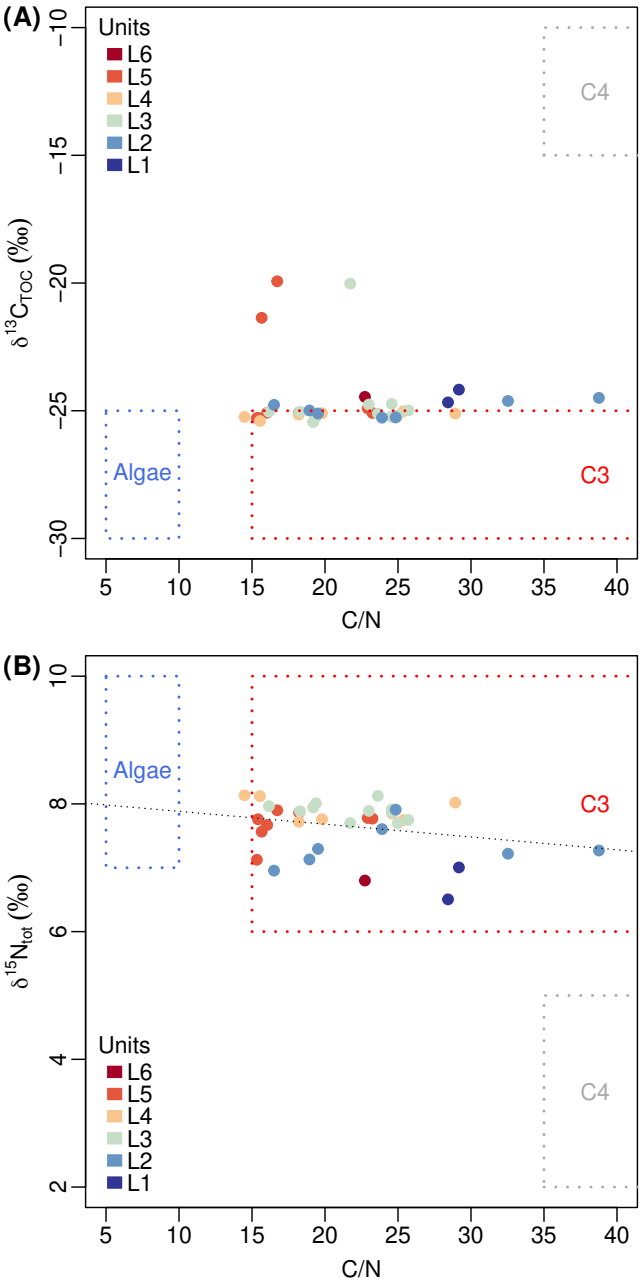

Figure 8: Trend of the Lake Ayrag shift during the Late Holocene from a lacustrine end member to basin influence, as interpreted from the C/N versus $\delta^{13}C_{TOC}$ ratio (**A**), and the C/N versus $\delta^{15}N$ ratio (**B**). The boxes represent the major end members for organic matter input based on C/N, (Zhao et al., 2015), $\delta^{13}C_{TOC}$ (Last and Smol, 2001) and $\delta^{15}N$ (Aranibar et al., 2008) values.

But in some contexts Si can be detrital, as for biogenic silica contained in phytoliths or as abiotic silica produced by the weathering of silicate minerals such as quartz (Olsen et al., 2010). In the Khangai range, which is largely made of volcanic rocks, the rivers are enriched in diluted silicates coming from the plutonic granite plumes of the batholith (Yarmolyuk et al., 2008, 2019). These silicates are eroded by the underground waters warmed by a strong geothermal

influx (Oyuntsetseg, 2014) in the range. Hence, $PC2_{XRF}$ shows the variation between the lake production system ($PC2_{XRF} > 0$) and a foreign erosion input. Following Schwanghart et al. (2008) the lake production is also associated with the TIC signal. The TIC influx can come from both detrital sources (Cohen, 2003) and plankton shells such as ostracods (Lara et al., 2012) or gastropods, bivalves and mollusks (Cohen, 2003). It is notable on Fig. 4 that the TIC signal (a carbonate proxy) is correlated with $PC2_{XRF}$ and anti-correlated with K/Ca and Rb/Sr (erosion proxies, Fig. 4). It suggests that, for the Ayrag core, the TIC is lake-produced (as are all the purple signals shown on Fig. 4). For the OM concentration proxies, the cross-plot displayed in Supplementary Fig. B7.A confirms that the Br signal roughly follows that of TOC and C/N ($R^2 = 0.38$ and $p - value <= 0.005$).

Finally, the element Aluminum has the strongest resistance to weathering (Goldschmidt, 1937), which is why it is used as a standard for XRF normalization of the weathering elements such as Fe and Ti (Fig. 4.A, Löwemark et al., 2011). These signals (green curves in Fig. 4) are also correlated with $\delta^{15}N_{tot}$, which is representative of the lake OM productivity (Teranes and Bernasconi, 2000) ($R^2 = 0.54$ and $p - value <= 0.005$ on Supplementary Fig. B7). We can see an effect of nutrient influx enhanced by dust inputs on increasing lake algae production. These records are anti-correlated with C/N, $wt\%N_{tot}$ (decreases when algae production increases), and the BIT index (decreases when lacustrine archaeal brGDGT production increases).

From a general point of view, the whole core is marked by an increasing tendency towards basin weathering, which delivers more and more mineral elements to the sediments (MS, $PC2_{XRF}$, Ti/Al, Fe/Al from Fig. 4.A and B). Conversely, increasing lacustrine organic matter production is characterized by decreasing TIC, C/N, $\delta^{13}C_{tot}$ and $\delta^{15}N_{tot}$, shifting towards algal productivity (Fig. 4.C, Aranibar et al., 2008). In terms of OM abundance, we observe three phases: high OM content certainly coming from the watershed (L_1), low OM in a context of authigenic production (L_{2-3}), and a rebound of the OM from well developed lake productivity (L_{4-6}).

5.1.3. *Climate reconstruction: global vs. local calibrations*

Limits also exist for the different climate reconstruction methods and calibration data sets (Birks et al., 2010; Salonen et al., 2019; Kaufman et al., 2020; Chevalier et al., 2020). Each method is based on different ecological and statistical concepts; the role of the modern pollen data set used to calibrate the models is also important, but this point is unfortunately rarely tested. Especially, during the Late Holocene, the human impact on pollen signal can biased climate reconstructions (Herzschuh et al., 2010). This motivates an independent multi-proxy method to validate the climate reconstruction reliability: the brGDGT-inferred models can validate the accuracy of the human-impacted pollen-inferred climate reconstruction. On the other hand, the pollen is less sensitive to soil pH and composition than the brGDGT fractional abundances. Moreover, the climate reconstruction also depends on the method selected and on the size of the training calibration-set.

First, concerning the brGDGT–inferred (Fig. 5.C and D) and the pollen–inferred (Fig. 7) climate reconstructions, it appears that all the models follow same trends but they still present variability. For the brGDGTs, $MAAT_{NMSDB-mr3}$ and $MAP_{NMSDB-mr6}$ appear to be the best models because they closely match the current MAAT, the uncertainties are very low in terms of the mean variations through time (small error bars on Fig. 7.A), the amplitude is coherent with known Late Holocene trends (Zheng et al., 2018; Gao et al., 2019; Zhang et al., 2021), the principal oscillations follow the 3.5 kyr event, RWP, DACP, MWP and LIA (Zhang et al., 2008; Yao et al., 2017; Lu et al., 2019; Aichner et al., 2019), and the signal correlates with the pollen–inferred MAAT and MAP values (Fig. 7.A). $MAAT_{NMSDB-mr5}$ and $MAP_{NMSDB-mr7}$ are slightly less accurate.

Second, for pollen–inferred climate reconstructions, the local calibration (NMSDB) is almost always better than the global one (COSTDB): surface climate reconstruction closer to the current climate parameter and smaller amplitude variation through time (Fig. 7.A). The best fitting methods are from the MAT and BRT approaches since the tendencies are very similar to brGDGT–inferred climate (centennial-scale oscillations and Late Holocene stead cooling). Because the MAT and BRT are based on different statistical analyses and yield similar results, we can conclude on the reliability of the pollen-inferred climate reconstruction at Ayrag. By the way, if the selection of a best reconstruction in the particular case of Lake Ayrag is needed, the MAT-NMSDB model for both MAAT and MAP is selected because of its medium amplitude range, slight cooling, well-marked centennial oscillations and accurate anomaly against current climate parameters.

Finally, after the method and the calibration set selection, we aim to validate the reliability of the multi-climate parameter reconstruction. The question is: can we reconstruct independently several climate parameters from the same brGDGT or pollen spectra ? In Salonen et al. (2019), it has been shown that it is possible to reconstruct two or more climate parameters from the same pollen spectra if some conditions are respected. First the climate parameters have to be as less as possible correlated with each other and secondly they have to be relevant to explain the vegetation distribution. In the particular case of Mongolia and following Wesche et al. (2016), it appears that temperature seasonality and winter precipitations are the two most important factors controlling the steppe environment distribution in Eurasia. In the Mongolian Plateau

(MP), the current main precipitation period appears in summer (Dulamsuren et al., 2005; Angerer et al., 2008). According to Salonen et al. (2019) reconstructing P_{sum} and temperature seasonality could be relevant as well, but in Dugerdil et al. (2021) we choose to focus on mean annual precipitation and temperature because of better statistical results and because MAAT and MAP are more commonly used in paleoclimate studies. Finally, since most of precipitation occurs in summer (MAP $\simeq P_{sum}$), MAP and summer precipitation yield similar reconstructions. Moreover these parameters are also relevant in vegetation distribution. About the second mandatory condition presented in Salonen et al. (2019), the independence between the current MAAT and MAP has to be checked. In Mongolia, even if a light correlation between MAAT and MAP is observed, it does not stand while adding independent samples from Siberia ($R^2 = 0.35$, Supplementary information, Fig. S5; Dugerdil et al., 2021).

5.2. Forcing mixed influences on Lake Ayrag proxy records

5.2.1. Trophic variation in Lake Ayrag

In Lake Ayrag, the abrupt and well-marked shifts in algal community succession are the most reliable indicators of lake dynamics (Last et al., 2001; Last and Smol, 2001). The co-variation between algae and lake productivity markers suggest a great influence of algal authigenic productivity on organic biomarker signals (Coffinet, 2015; Buckles et al., 2016). Lithological processes (marked by MS, XRF and bulk geochemistry) are also important in shallow Lake Ayrag. In addition, the watershed dynamics characterized by soil structure, erosion systems and rock composition are also determinant (De Jonge et al., 2014b,a; Yang et al., 2014; Xiao et al., 2016).

From 3,900 to 3,400 cal yr BP (3.5 kyr event, U_1 to the beginning of U_2), Lake Ayrag remained in a development process (algae influx of *Tetraedron* spp. increasing in Fig. 6.B and lacustrine-brGDGT rising production in Fig. 4.D). Then, the period from 3,400 to 2,500 cal yr BP (second part of U_2) was marked by a *Botryococcus* spp. optimum, suggesting that the lake system was fully installed. Moreover, this algae community dominated by *Botryococcus* spp. characterizes an early eutrophic phase linked to the pioneer ecology of the lake (Djamali et al., 2016). After 2,500 cal yr BP (RWP, U_3), the lake sediment exhibits a lower porosity ($PCA1_{XRF}$ Fig. 4.A), higher SAR and smaller desiccation cracks in the lithology (Fig. 2.C). The erosion system in the basin also generated an elevated dust influx and thus a rise of redox conditions, as shown by the higher K, MS and $PCA2_{XRF}$ values, as well as a rise in S, Mn and Fe. All of these variations appear to be associated with a warm-dry RWP. The Br, TOC and $wt\%N_{tot}$ values drop, suggesting a much lower OM proportion in the lake, while C/N implies a higher in-situ lake productivity. The OM was diluted by higher erosion inputs. Algal productivity reached its maximum, associated with a shift in the dominant communities: *Botryococcus* spp. and *Tetraedron minimum* decreased, and were progressively replaced by Volvocaceae and *Pediastrum boryanum*, indicating nutrient and erosion influxes from the watershed (Patterson et al., 2002). This explains the increasing authigenic productivity (C/N minimum and $\delta^{15}N_{tot}$ maximum, Fig. 4.C).

Around 1,200 cal yr BP (U_{3-4}), the transition to the MWP was very steep and marked by abrupt and high amplitude proxy oscillations: especially for MS, $PCA2_{XRF}$ and the TIC/TOC ratio. For the MWP (1,200–700 cal yr BP, U_4), the CBT index is related to the pH of the soil catchment but also of the lake (De Jonge et al., 2014a). The acidification of Lake Ayrag seems to have been constant from 3,500 cal yr BP to 2,700, then from 2,400 to the present (especially in U_3). Such acidification is very often correlated with a drought event (Leyden et al., 2016). This trend is consistent with the $MAP_{mr-NMSDB}$ model and the MAT, BRT and WAPLS pollen reconstructions (Fig. 7.B). With regard to the lake system, we observe meso to eutrophic nutrient conditions; a Volvocaceae maximum (Chen et al., 2003; Kramer et al., 2010), *Tetraedron* spp. reduction, and Br, TOC, TIC, C/N and $\delta^{15}N_{tot}$ suggest a peak in OM concentration originating from lacustrine productivity. The second part of the U_4 unit is clearly imprinted by the MWP optimum, which lasted from 950 to 650 cal yr BP according to Chen et al. (2015b). These time boundaries fit with the Ayrag erosion markers; $wt\%N_{Tot}$ increases first, followed by rises in TOC and C/N in the upper part of U_4. Even XRF_{PCA2} suggests stronger erosion inputs, which may due to bare soil wind erosion during an arid period (Felauer et al., 2012) associated with enhanced pastoralism pressure (Miehe et al., 2009). The flat Ti/Al and Fe/Al records are interpreted as a dilution effect; erosion was enhanced, but so was lacustrine productivity (warmer and more eutrophic lake conditions), which is why the signal stays steady.

Between 700 and 150 cal yr BP (LIA, U_5), the TOC and C/N signals remained low because of the cold temperatures (due to lower in-situ lake production) and the dilution effect of terrigenous influx (MS, $PCA2_{XRF}$ and $R_{i/b}$), themselves driven by a new rise in MAP (Fig. 7.B). Thus, the algal community was largely dominated by *Tetraedron minimum* in association at the lake's edge with a few *Potamogeton* spp. and *Scenedesmus* spp. (these taxa are expressed in the *Other algae* curve, Fig. 6.B). This community is characteristic of eutrophic lake conditions (Jankovská and Komárek, 2000). Many examples in the literature attribute the link between *Tetraedron minimum* and *Pediastrum boryanum* communities to elevated human pollution in cool/cold Alpine lakes such as Bichelsee, Burgäschisee, Unterer and Chatzensee (Lotter et al., 1997; Jankovská and Komárek, 2000). After 150 cal yr BP (U_6), the organic geochemistry proxies exhibit the same pattern; TOC and $wt\%N_{tot}$ rose, indicating an increase in OM productivity still predominantly of lacustrine origin (C/N still decreasing).

Conversely, δ^{15}N only exhibits a late decrease. This isotopic ratio is supposed to be related to lake productivity (Teranes and Bernasconi, 2000), however a δ^{15}N decrease could also indicate the appearance of nitrogen fixers (Brenner et al., 1999; Talbot and Lĕrdal, 2000). Here, this decrease could be linked to the synchronized development of the *Tetraedron minimum*–Volvocaceae lacustrine ecosystem.

5.2.2. *Human impacts and Mongolian civilization history*

Human impacts are also a major factor that could affect almost all of the proxies (pollen, NPP, vegetation and geochemical makers; Miehe et al., 2007, 2014; Doyen and Etienne, 2017), including a potential bias in pollen-based transfer functions (Herzschuh et al., 2010), especially during the Late Holocene (Klinge and Sauer, 2019). Since the pollen signal from Lake Ayrag does not seem to be strongly human-impacted (very low and steady abundances of pastoral and settlement *indicator-species* following Gaillard (2007) and Miehe et al. (2014) such as *Stellera chamaejasme*, *Plantago lanceolata*, *Rumex acetosella* and *Urtica urens/dioica*-type, on Fig. B4), the Mongolian human impact history will be mainly discussed based upon the NPPs results. The fungal spores are essentially the more reliable indicator for over grazing and human land use (Baker et al., 2013; Etienne and Jouffroy-Bapicot, 2014; Doyen and Etienne, 2017). The harsh and isolated Arkhangai environment represents a case study for the understanding of human pastoralism history and its influence on environmental proxies such as NPP. Broadly, pastoralism around Ayrag exhibited three distinct shifts: a first development during the Deer stone - Khirigsuur, Slab grave and Xiongnu periods (3,000 to 2,000 cal yr BP) (Honeychurch and Amartuvshin, 2007; Savelyev and Jeong, 2020), followed by a collapse associated with Mongolian society instability (Zhang et al., 2021). The second pastoralism phase started at the appearance of the Mongol Empire (around 900 cal yr BP, Fernández-Giménez, 2006) and exponentially increased since then (Wesche et al., 2016).

More precisely, it appears that NPP influx and diversity were already high since the beginning of the record (U_2), especially undetermined and parasitic spores but also dung fungal spores. This signal could be interpreted as grazing of large wild animals (Baker et al., 2013) or the footprint of a pre-pastoral *Deer Stone tribes* society (Allard et al., 2006). From 3,700 to 2,500 cal yr BP (U_2), the diversity richness in fungal spores remained high and the dung fungal spore influx rose (Fig. 6.C). This dung input can explain the beginning of lake eutrophication as led by grazing (Fig.4.C). During this period the Xiongnu human nomadic societies were still not well developed and pastoralism stayed extensive (Allard et al., 2006), even if the stretches of fresh water were attractive (Fernández-Giménez, 2006). The coprophilous spores could have been produced by wild animals (Johnson, 2009; Feranec et al., 2011) still numerous on the MP. The Xiongnu development (3,000 cal yr BP, second part of U_2) saw a great and rising impact of pastoralism.

Then, between 2,500 and 1,900 cal yr BP (RWP, U_3), the NPP signal shows a drop in spore diversity and influx. This pastoralism decrease could be linked to the Mongolian society instability during this period (wars and empire shift effects, Zhang et al., 2021). This climate transition would have maintained the RWP perturbation in pastoralism systems of the declining Xiongnu society and the replacing Uyghurs society (Honeychurch and Amartuvshin, 2007), in association with the low coprophilous and high Saprophytic spore influxes (1,900–1,400 cal yr BP). Worse pasture management may have driven the decrease of coprophilous spores and left space for shrub land or forest development favoring the Saprophytic Spores, the NAP. Moreover, the political instability and wars associated with repeated Mongolian conquests could have driven a higher fire frequency, which could explain the rise in Saprophytic fungi (Cugny, 2011; Van Geel and Andersen, 1988). Analysis of complementary fire proxies such as charcoal (Umbanhowar Jr et al., 2009; Rudaya et al., 2020), tree rings (Hessl et al., 2012) or levoglucosan (Bhattarai et al., 2019) could be used to clarify this assumption. Finally, this situation changed abruptly around 1,150 cal yr BP. The MWP period (950–650 cal yr BP, U_4) was also marked by the strongest political instability ever in Mongolian history. The effects of anthropic actions on climate and the inverse are inter-correlated (Zhang et al., 2021), which is why we cannot exclude the anthropic assumption to explain the major shifts occurring during the MWP. The wars led to steppe fires, livestock abandonment and other effects (Zhang et al., 2021).

Pastoral pressure begin a renewed impact from 700 to 150 cal yr BP (LIA, U_5), with landscapes affected by human societies; coprophilous diversity and influx were steady, pollen diversity rose, and Poaceae meadows were replaced by *Artemisia* spp. steppe, which could have been a consequence of overgrazing. This pasture over-pressure led to the development of a hyper-eutrophic lake system optimum for the Volvocaceae–*Tedredron minimum* algal community, aggregated to the aquatic fungi community. During the end of the LIA and the WCP (U_6), the lake system followed the same trend as for the previous period (U_5 unit). The eutrophisation of Lake Ayrag was also correlated with high fungal spore influx and diversity, suggesting a large amount of livestock dung in the watershed. The NPP rise was enhanced by *Sporormiella* spp., attesting to an over-grazed open-land system in the area (Djamali et al., 2016), linked to other Sordariaceae spores (Van Geel, 2002). The *others taxa* column in the simplified pollen diagram (Fig. 6.A) includes some pastoral indicator-species (shown in Fig. B4). They slightly follow the same trend, similarly to the pollen diversity curve . This also induces an anthropic impact on vegetation cover.

5.2.3. Arkhangai vegetation changes

The Mongolian landscapes are partly overprinted by the grazing pressure from Mongolian semi-nomadic society (Saizen et al., 2010). Vegetation changes are strongly correlated with climate and anthropic impacts (Kramer et al., 2010; Tian et al., 2014; Dendievel et al., 2019a,b). Moreover, there are also some feedbacks (Birks et al., 1998; Telford and Birks, 2005; Ma et al., 2008; Herzschuh et al., 2010) and taphonomic biases (Lebreton et al., 2010) that can influence the archives. Pollen composition and diversity represent the most reliable proxies in this case, even if the sediment organic geochemistry can also aid in interpretation. However, in the Arkhangai forest-steppe ecotone (Erdos et al., 2018), a modern vegetation-pollen rain calibration is necessary to more accurately understand the former vegetation cover representation (Ma et al., 2008; Cheng et al., 2020). Throughout the Late Holocene, the steppe-forest ecotone surrounding Lake Ayrag seems to have suffered from the slight aridification of the climate. The steppe and meadow herbaceous communities were more sensitive and resilient to centennial-scale climate oscillations.

More precisely, from 3,900 to 2,500 cal yr BP (3.5 kyr event, U_{1-2}), the vegetation surrounding Lake Ayrag was dominated by steppe plants such as *Artemisia* spp., Poaceae, Cyperaceae and other herbs, and a few forest taxa such as *Larix sibirica*, *Pinus* spp. and *Betula* spp., certainly transported from the whole hydrological basin. The biome was characterized by a very characteristic forest-steppe ecotone controlled by high steppe *Artemisia* spp.. However, at the basin scale, some forest patches were present (AP peak on Fig 6.A and Saprophytic spores peaks on Fig. 6.C). Then, during the RWP and even more so during the DACP (2,500–1,200 cal yr BP, U_3), we observe a first strong drop in the watershed in the *Artemisia* spp. community, which was replaced mainly by Poaceae but also by some Amaranthaceae and Cyperaceae. In the forest-steppe ecotone, the birches were replaced by a *Pinus* spp./*Picea obovata* community more tolerant to climate instability. Even if the MAP changes are not clearly interpretable, it appears with a high likelihood that MAAT was rising.

The vegetation from the U_{3-4} transition around 1,200 cal yr BP was particularly unstable; Poaceae steppes alternated with a *Artemisia* spp.–Cyperaceae forest-steppe ecotone. Until this time, the percentage of Cyperaceae was low in the vegetation cover, but from 1,200 cal yr BP (U_4) to the current time (WCP, U_6), the Cyperaceae signal became more pronounced. The major question about Cyperaceae pollen type is whether this signal represents a local lake shore Cyperaceae wetland community or a regional alpine meadow *Koeleria* spp.–*Carex* spp. community. Several results invite us to validate the second assumption. First, the present lake shore is not at all covered by semi-aquatic tussocks; there are a few short *Carex* spp., but not more than the meadow species common in Central Asian high-altitude meadows (Herzschuh et al., 2006; Ma et al., 2008). This type of semi aquatic vegetation exists in Mongolia, but it is above all associated with not well developed peat or pond systems. However, Lake Ayrag seems to have been stable since 2,600 cal yr BP. Furthermore, the lake edge *Carex* spp. are very often associated with a mycorrhizal fungi called Gaeumannomyces (Van Geel et al., 1983) or other aquatic pollen such as *Typha* spp. or *Alisma* spp., which leave some remains observable as pollen and NPP paleo signals (Pals et al., 1980). In this study, throughout the Holocene the records of Cyperaceae pollen type and Gaeumannomyces NPP imply that the Cyperaceae pollen signal is local to the lake basin. According to Bennett and Willis (2002), this approach is accurate for determining the origin of Cyperaceae inputs. In Lake Ayrag, MWP vegetation (950–650 cal yr BP, U_4) was thus dominated by Cyperaceae and Poaceae meadows. This high-altitude ecosystem could have resulted from both a slight drought event (erosion spores and amoebae, Fig. 6.C) and a rise in pasture pressure (coprophilous spore values remain high in Fig. 6.C). The U_4 unit exhibits two separate phases in the proxy trends. For the oldest part of U_4 (1,200–1,100 cal yr BP), the vegetation changes with a predominance of Poaceae, the algal community shows a slight rebound of *Botryococcus* spp. / *Pediastrum boryanum*, and a rise in spore influx and richness and an anticipated drop in MS and $\delta^{13}C_{Tot}$ are observable. These trends could be due to a local microclimatic process showing an early effect of the MWP in the Arkhangai area.

From 700 cal yr BP (U_5) to the top of the core, the vegetation was clearly impacted by human societies. The coprophilous diversity and influx were steady, pollen diversity rose, and Poaceae steppe was replaced by *Artemisia* spp. steppe mixed with Cyperaceae alpine meadow, which could have been consequences of overgrazing and/or a rise in precipitation. This assumption is also supported by the slight increases in AP, Saprophytic spore influx and *Larix sibirica* (an under-represented pollen type, Ma et al., 2008; Dugerdil et al., 2021). The CWP (from 150 cal yr BP, U_6) drove the Lake Ayrag surrounding vegetation to the current steppe-forest mixed with alpine meadow ecosystem.

5.2.4. Mongolian Plateau Late Holocene climate shifts

Our results on the Lake Ayrag sequence confirm that the long scale cooling and drying trend observed was controlled by an EASM response to orbital forcing, while the rapid events (3.5 kyr events, RWP, DACP, MWP and LIA) were controlled by Monsoon Oscillations. For the latest CWP, the anthropogenic influence on climate is also marked in the Lake Ayrag proxies. Our coupled GDGT–pollen approach acts to buffer climate reconstruction uncertainties. These models allow discussion of the ACA Late Holocene climate system shifts.

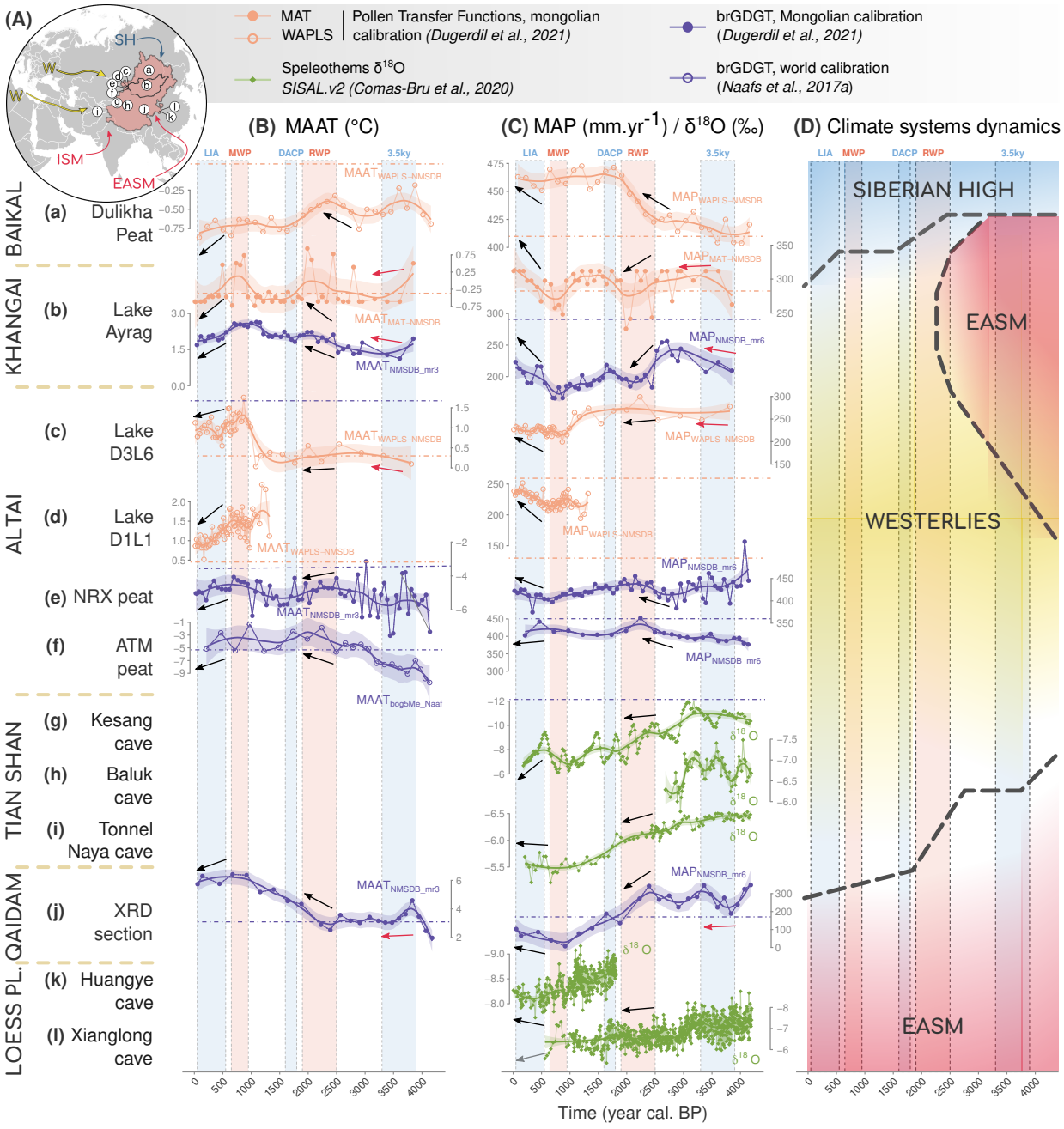

Figure 9: Synthesis of Lake Ayrag climate reconstructed changes during the Late Holocene, among other available climate reconstructions **(A)** based on pollen, brGDGTs and δ^{18}O speleothems. The MAAT **(B)**, MAP **(C)** and a diagram of the climate systems influencing each ACA record **(D)** are displayed. The past records are, from top to bottom (north–south transect): **(a)** Dulikha peat (pollen WAPLS, Bezrukova et al., 2005; Binney, 2017), **(b)** Lake Ayrag (pollen MAT and brGDGT from this study), **(c)** Lake D3L6 and **(d)** Lake D1L1 (pollen WAPLS, Unkelbach et al., 2019, 2020), **(e)** NRX peat (brGDGT, Rao et al., 2020), **(f)** ATM peat (brGDGT, Wu et al., 2020), **(g)** Kesang, **(h)** Baluk, **(i)** Tonnel'Naya caves (δ^{18}O SISAL.v2, Comas-Bru et al., 2020), **(j)** XRD section (brGDGT, Sun et al., 2019), **(k)** Huangye and **(l)** Xianglong caves (δ^{18}O, SISAL.v2).

At 3,700 cal yr BP (U_2 beginning), the forested patches were composed of a birch vegetation cover higher than today, indicating a slightly higher humidity (also marked by wetland spores) and cool climate (*Tetraedron* spp. peak and high pollen ratios). The precipitation reconstructed by $MAP_{mr-Mongolia}$ suggests a wetter climate than today, explaining the low influx of mineral dust from the southern drier area of the Mongolian Plateau

(weak terrigenous influx, Fig. 4.A and B). The MAT and BRT pollen-inferred MAP values also indicate a slightly wetter climate than today in accordance with the Central Asian mid Holocene wet conditions at this period (Fig. 9.A, Chen et al., 2008, 2010, 2015b; Lu et al., 2019). Between 3,700 and 2,500 cal yr BP (3.5 kyr event, U_2), the elevated lake productivity could have been enhanced by the favorable warm air temperature (Fig. 7). The locally calibrated MAAT models (brGDGT – $MAAT_{NMSDB-mr3}$ and Pollen – $MAAT_{NMSDB}$) display a secular warming trend until 2,500 cal yr BP (U_{2-3} boundary), while the globally calibrated models such as the MAAT–GDGT inferred by MBT / CBT (Sun et al., 2011; De Jonge et al., 2014a; Naafs et al., 2017a) or the transfer function $MAAT_{WAPLS-COST}$ model highlight merely a Late Holocene light cooling affecting all of central Asia (Fig. 9.B, Klinge and Sauer, 2019). In the first part of U_3 (2,500–1,900 cal yr BP), the lake seems to have beome warmer (drop in *Tetraedron minimum*, rise of Amaranthaceae) and mesotrophic. This period matches with the East Asian Monsoon Oscillation associated with the Roman Warm Period (RWP, 2500–1900 cal yr BP ; Zhang et al., 2008; Chen et al., 2009). The Volvocaceae community (which is only present in ACA lakes) emerged during this enhanced mesotrophic warm period (Chen et al., 2003; Kramer et al., 2010; Murad, 2012), and it slowly reduced during the following Dark Ages Cold Period (DACP, 1,800–1,600 cal yr BP, Aichner et al., 2019). Before the DACP, all the models (Fig. 5) and pollen ratios (Fig. 6.D) were affected by the RWP from about 2,500–2,000 cal yr BP. This trend was interrupted at first by an abrupt climate inversion at 1,900 to 1,800 cal yr BP; weathering rose dramatically ($R_{i/b}$, MS, Fe/Al) and MAAT dropped 0.5°C, while the MAP seems to have rebounded (all models in Fig. 7 and the Ar/(Ar+Am) ratio in Fig. 6 suggest wetter and cooler conditions). All these variations could reflect a DACP characterized in the Arkhangai by a relatively humid period such as for other central Asian sites (Fig. 9.C, Chen et al., 2010, 2015b). The upper part of U_3 (1,700–1,200 cal yr BP) seems to have been cooler and drier than today (erosion increases in Fig. 4 and climate reconstruction in Fig. 7). This could have been a prolongation of the DACP or simply a long transition before the warming of the MWP observed in U_4 (1,200–700 cal yr BP). Both the pollen and brGDGT MAAT reconstructions marked a 1 °C warmer period associated with drier conditions in U_4. The relationship between MAAT and MAP during the MWP is a major issue for the understanding of Monsoon Oscillations (Chen et al., 2015b). ACA was characterized by warm and dry conditions during the MWP (under Westerlies control), while Eastern China underwent warm and wet conditions. Mongolia, although located to the north of the modern summer monsoon limit (Haoran and Weihong, 2007), is on the outskirts of this system, and thus the question is still debated (An et al., 2008; Klinge and Sauer, 2019).

The MWP was followed by the LIA cold period. As for the MWP, the MAAT / MAP relationship during the LIA is determinant for Monsoon Oscillation understanding. According to Chen et al. (2010, 2015b), who review lake changes from the northern part of the modern Asian summer monsoon limit, there is an anti-correlation between MAAT and MAP during the LIA at these sites. Their synthesis confirms our results for Lake Ayrag during this period: a steady and long cooling trend associated with wet conditions during almost all of the 700–150 cal yr BP (U_5) period. Then, after 150 cal yr BP, the U_6 unit begins at the end of the LIA. The CONISS analysis sets the boundary at this smooth inflection point corresponding to the gradual transition between a cold, wet LIA and the beginning of the Warm Current Period. The lake system follows the same trend as the U_5 unit. The low sampling resolution in the upper core (due to the age-depth model) does not permit observation of the exponential human impact on climate change during the CWP, such as for other Mongolian studies (Tian et al., 2013, 2014; Lan et al., 2018; Unkelbach et al., 2019, 2020).

5.3. Late Holocene climate synthesis for northern ACA

5.3.1. Current climate system interactions

The Lake Ayrag multi-proxy climate reconstructions provide an accurate and reliable archive for understanding the central Asian climate cell variations through time. However, to interpret past climate changes with reliability, it is necessary to well understand the current climate system dominating the MP. The question is to determine which system is currently dominating the central part of the MP (Arkhangai). This is still an open question involving many possibilities: the MP under a Westerlies influence (Herzschuh, 2006), under an EAWM influence (Wang and Feng, 2013), the MP locked only by SH with water vapor evaporative recycling (Piao et al., 2018), under an EASM/Westerlies mix (Gunin et al., 1999; Tian et al., 2013; Chen et al., 2019), or even under the EASM associated with weak EASM events (Zhang, 2021). The geographical and mountainous setting associated with the main atmospheric air mass movement in ACA suggest that the Westerlies are presently dominating MP circulation (Ning et al., 2019). However, the major share of MP precipitation occurs in summer time (Dulamsuren et al., 2005; Angerer et al., 2008; Wesche et al., 2016; Unkelbach et al., 2019, 2020).

The present climate dynamics for Lake Ayrag inferred from *Worlclim2* (Fick and Hijmans, 2017) suggest that the main share of annual precipitation occurs during summer time, consonantly with the *CRUTS.v4* surrounding weather station data (Harris et al., 2020). This is generally the same for the whole MP (Dulamsuren et al., 2005; Klinge and Sauer, 2019). This suggests that Lake Ayrag, within the MP, is controlled by a mix between the SH and westerlies influences. Moreover, the climate variations of the most recent climate period (CWP) for the MP cores (Ayrag, D3L6 and D1L1 in Fig. 9) seem to follow a warmer-drier trend. This trend is more readily observable in the *CRUTS.v4* climate time series for the MP (Harris et al., 2020). Here, the MP be-

came warmer-drier since the beginning of the 20th Century. This is the same for the *CRUTS.v4* MAAT and MAP from the Baikal area (close to the Dulikha sequence, Fig. 9) and the zone under EASM influence. Conversely, the WDCR (Fig. 1.A, Chen et al., 2019) is getting warmer-wetter. These observations validate the weak EASM period described by Zhang (2021) and the assumption of a current SH / EASM mixed influence for Lake Ayrag. However, this assumption could have changed throughout time.

5.3.2. *Late Holocene ACA and MP climate system variations*

Once the current climate system interactions are defined, we investigate how to determine which climate system controlled the Lake Ayrag recorded climate proxies through time. There are different approaches for that: (1) reconstruction of the paleo P_{sum} or P_{win} through time (Li et al., 2020a), although it is not always easy to obtain robust seasonal climate parameters without quantitative climate reconstructions since they are biased by weather station data availability in ACA; (2) checking the amount of precipitation with rising MAP under monsoon control (Chen et al., 2015a, 2016); (3) focus on the MAAT / MAP phased or "out-of-phase" response: westerlies un-phased (warm/dry and cold/wet periods), monsoon phased (warm/wet and cold/dry periods, Chen et al., 2015b, 2019). However, this method has to be mitigated by the reliability of two climate reconstructions made on the same pollen or brGDGT spectra (Salonen et al., 2019).

To apply these approaches on the MP and ACA, some climate reconstructions inferred from available brGDGT and pollen records have been performed here and the results are compared with the Ayrag signal (Fig. 9): Dulikha peat (Bezrukova et al., 2005; Binney, 2017), Lake D3L6 and Lake D1L1 (Unkelbach et al., 2019, 2020), NRX peat (Rao et al., 2020), ATM peat (Wu et al., 2020) and XRD section (Sun et al., 2019). The $\delta^{18}O$ speleothem studies from *SISAL.v2* (Comas-Bru et al., 2020) available in ACA have also been used as an independent climate proxy (Kesang, Baluk, Tonnel'Naya caves, Huangye and Xianglong caves, Fig. 1.A). The Lake Ayrag MAP and MAAT vary with a high amplitude during the Late Holocene (more than for other sites, Fig. 9 a, f, g, h, i, k and l). This is also the case for other Westerlies/EASM transitional zone records, which seem to be particularly sensitive to large-scale climate change (9 c, d and e; Tian et al., 2013). In Lake Ayrag pollen and brGDGT climate reconstructions, regardless of the calibration method used, the wettest time period appears to be during the LIA (Fig. 9.B in accordance with other Mongolia sequences, Tian et al., 2013). The MWP and RWP (two warm periods) were drier than the LIA, DACP and the 3.5 kyr cooling event. For the first 3,000 cal yr BP, the MAAT / MAP models are "out-of-phase"; the wet periods were the coolest and the dry periods were the warmest (black arrows in Fig. 9). This response is particularly similar to some other Transitional Zone sites (D1L1 (c), D3L6 (d) NRX (e) and ATM (f) in Fig. 9). This assumption allows inclusion of Lake Ayrag into the Westerlies-dominated system since 3,000 cal yr BP. The Dulikha peat also exhibits an "out-of-phase" MAAT/MAP relationship (a in Fig. 9), but the global Late Holocene trend is towards a constant cooling with increasing moisture. However, between 3,900 and 3,000 cal yr BP, the Lake Ayrag MAAT/MAP signal is not as clearly "out-of-phase" as it was during the last 3,000 cal yr BP (red arrows in Fig. 9). This shift could be due to a former EASM stronger influence on the southern part of the MP. This climate system co-domination through time is schematized in Fig. 9.D.

On a larger geographical scale, the mid-latitude Asian sites allow visualization of the Late Holocene Monsoon Oscillation. In Fig. 9.B, the global temperature trend shows a northern cooling (Zhang et al., 2021) and a southern warming from the Altai (Rao et al., 2020), Tian-Shan (Huang et al., 2015), Qaidam basin (Sun et al., 2019), and the Loess Plateau (Gao et al., 2019) to the south-eastern Tibetan Plateau (Ning et al., 2019). For moisture as well, a gradient appears in between northern increasingly wet climate and the central/southern Chinese Late Holocene aridification (Ji et al., 2005; Klinge and Sauer, 2019; Zhang, 2021). Lake Ayrag occupies a northern position in this asynchronous Holocene Optimum north-south gradient. At the centennial oscillation scale as well, the ACA sites (red arrows in Fig. 9 for Ayrag, D3L6 and XRD sections) show a common trend of quasi-flattened MAAT/MAP between 4,000–3,500 cal yr BP, interpreted as a stronger EASM influence in the Mid Holocene (Zhang, 2021). This deeper EASM incursion toward continental Asia suggests a weaker EASM at the Mid Holocene than at present (An, 2000; Gao et al., 2019). The weak EASM was possibly driven by warmer Pacific sea surface temperatures and/or stronger Tibetan and Mongolian Plateau snow cover (Liu and Yanai, 2002; Ding and Chan, 2005) at the Mid Holocene. Following the current climate mode studies and especially the connection between ITCZ variations and EASM weakness (Wen et al., 2005; Li and Zhou, 2012), this present ACA paleo record study validates the Mid Holocene ITCZ northward migration proposed by Wanner and Brönnimann (2012).

6. Conclusions

The Lake Ayrag multi-proxy records and other MP and ACA sequences allow a better understanding of environmental, climatic and anthropic histories from Mongolia during the Late Holocene. More particularly, it appears that:

1. The elemental and isotopic signals in Lake Ayrag sediments appear necessary to accurately determine the local history of the lacustrine system. Mainly, in Lake Ayrag it appears that the arid periods enhance lithogenous watershed erosion inputs into the lake,

which leads to algal blooms by nutrient delivery. After that, the authigenic organic matter productivity increases.

2. Furthermore, this coupled multi-proxy study (NPPs, OM history and pollen) allows reconstruction of pastoralism's impact on the fragile steppe-forest ecotone through time. It appears that this ecotone is particularly sensitive to grazing, since it is possible to detect livestock impact from 3,000 cal yr BP with the Xiongnu settlement (Allard et al., 2006), and overgrazing consequences on vegetation and lake eutrophication since 500 cal yr BP associated with the Soviet administration in Mongolia.
3. Lake Ayrag represents the first coupled brGDGT–pollen analysis performed on the same core in ACA.
4. Concerning climate, the local calibrations for pollen and brGDGTs presented and discussed in detail in Dugerdil et al. (2021) provide a more accurate and reliable climate reconstruction for Lake Ayrag than do the global calibrations. Even if the current complex climate system control for the Mongolian Plateau is still under debate (Westerlies, SH and EASM co-domination), it appears that Lake Ayrag remained under Westerlies domination since 3,000 cal yr BP following a Westerlies/EASM teleconnection between 4,000 and 3,000 cal yr BP (Chen et al., 2015b, 2019).
5. The paleo records from the Westerlies/EASM transitional zone and especially the Lake Ayrag sequence are very sensitive to Late Holocene centennial-scale oscillations (fast response and high climate amplitude), which invites us to carefully look into this area's response to current climate warming.
6. Finally, Lake Ayrag, among other sites in ACA, shows that the Late Holocene temperature and precipitation optimum asynchronous pattern describes a Mongolian Plateau–south-eastern Chinese coastal area gradient (following An, 2000; Gao et al., 2019): cooler and wetter in the SH-dominated area, a slight warming and aridification in ACA, and an abrupt warming and aridification in the monsoonal system. As proposed by Chen et al. (2015b), this gradient is due to a link between monsoon variations and the El Niño Southern Oscillation (ENSO). The ACA aridification during the Late Holocene was associated with a southward ITCZ migration (Wanner and Brönnimann, 2012). An approach of climate reconstruction interpolated maps throughout the Late Holocene in ACA could help the prediction of future regional climate change patterns in vulnerable continental Asian drylands.

Declaration of competing interests

The authors declare that they have no known competing financial interests or personal relationships that could have influenced the work reported in this paper.

Acknowledgments

This research has been supported by the French Centre National de la Recherche Scientifique (CNRS) and the ISEM team DECG. Lucas Dugerdil's salary has been supported by the Ecole Normale Supérieure de Lyon. For the analytical work completed at LGLTPE-ENS de Lyon and the paper registration fees, this research was funded by Institut Universitaire de France funds to Guillemette Ménot.

We also thank two anonymous reviewers, as well as the editor, for constructive comments that helped to improve the manuscript. This is an ISEM contribution number XXXX. We are grateful to all the direct and indirect contributors to the global surface pollen dataset, the pollen and brGDGT past record available in open access data, Marc Dugerdil for the help with Python fixing, Salomé Ansanay-Alex for her spectrometer expertise and *La Tendresse* and *Le BIB* for their support.

Appendix A

Supplementary data to this article can be found online at

References

Ahrens, C.D., Henson, R., 2021. Meteorology Today: An Introduction to Weather, Climate, and the Environment. Cengage learning.

Aichner, B., Feakins, S.J., Lee, J.E., Herzschuh, U., Liu, X., 2019. High-resolution leaf wax carbon and hydrogen isotopic record of the late holocene paleoclimate in arid central asia. Climate of the past .

Aichner, B., Herzschuh, U., Wilkes, H., Schulz, H.M., Wang, Y., Plessen, B., Mischke, S., Diekmann, B., Zhang, C., 2012. Ecological development of lake donggi cona, north-eastern tibetan plateau, since the late glacial on basis of organic geochemical proxies and non-pollen palynomorphs. Palaeogeography, Palaeoclimatology, Palaeoecology 313, 140–149. 00040.

Aizen, E.M., Aizen, V.B., Melack, J.M., Nakamura, T., Ohta, T., 2001. Precipitation and atmospheric circulation patterns at mid-latitudes of Asia. International Journal of Climatology 21, 535–556. doi:10.1002/joc.626.

Allard, F., Erdenebaatar, D., Houle, J.L., 2006. Recent archaeological research in the khanuy river valley, central mongolia, in: Beyond the Steppe and the Sown: Proceedings of the 2002 University of Chicago Conference on Eurasian Archaeology, Brill Academic Publishers Leiden and Boston. p. 202–224.

An, C.B., Chen, F.H., Barton, L., 2008. Holocene environmental changes in mongolia: A review. Global and Planetary Change .

An, Z., 2000. The history and variability of the east asian paleomonsoon climate. Quaternary Science Reviews 19, 171–187. doi:10/bj3tw7.

Anderson, R.S., Homola, R.L., Davis, R.B., Jacobson Jr, G.L., 1984. Fossil remains of the mycorrhizal fungal Glomus fasciculatum complex in postglacial lake sediments from Maine. Canadian Journal of Botany 62, 2325–2328. doi:10.1139/b84-316.

Angerer, J., Han, G., Fujisaki, I., Havstad, K., 2008. Climate change and ecosystems of Asia with emphasis on Inner Mongolia and Mongolia. Rangelands 30, 46–51.

Aranibar, J.N., Anderson, I.C., Epstein, H.E., Feral, C.J.W., Swap, R.J., Ramontsho, J., Macko, S.A., 2008. Nitrogen isotope composition of soils, c3 and c4 plants along land use gradients in southern africa. Journal of Arid Environments 72, 326–337.

Baker, A.G., Bhagwat, S.A., Willis, K.J., 2013. Do dung fungal spores make a good proxy for past distribution of large herbivores? Quaternary Science Reviews 62, 21–31. 00101.

Bakker, M., Van Smeerdijk, D.G., 1982. A palaeoecological study of a late holocene section from "het ilperveld", western netherlands. Review of palaeobotany and palynology 36, 95–163.

Barnosky, A.D., Hadly, E.A., Gonzalez, P., Head, J., Polly, P.D., Lawing, A.M., Eronen, J.T., Ackerly, D.D., Alex, K., Biber, E., 2017. Merging paleobiology with conservation biology to guide the future of terrestrial ecosystems. Science doi:10.1126/science.aah4787.

Bennett, K.D., Willis, K.J., 2002. Pollen. Springer. p. 5–26.

Berger, J.F., Lespez, L., Kuzucuoğlu, C., Glais, A., Hourani, F., Barra, A., Guilaine, J., Paolo, B., 2016. Interactions between climate change and human activities during the early to mid-holocene in the eastern mediterranean basins. Climate of the Past 12. doi:10/gcc454.

Bezrukova, E.V., Abzaeva, A.A., Letunova, P.P., Kulagina, N.V., Vershinin, K.E., Belov, A.V., Orlova, L.A., Danko, L.V., Krapivina, S.M., 2005. Post-glacial history of Siberian spruce (Picea obovata) in the Lake Baikal area and the significance of this species as a paleo-environmental indicator. Quaternary International 136, 47–57. doi:10.1016/j.quaint.2004.11.007.

Bhattarai, H., Saikawa, E., Wan, X., Zhu, H., Ram, K., Gao, S., Kang, S., Zhang, Q., Zhang, Y., Wu, G., 2019. Levoglucosan as a tracer of biomass burning: Recent progress and perspectives. Atmospheric research .

Binney, H., 2017. Vegetation of eurasia from the last glacial maximum to the present: the pollen data. URL: https://eprints.soton.ac.uk/403426/.

Birks, H, H., Line, J., 1992. The use of rarefaction analysis for estimating palynological richness from quaternary pollen–analytical data. The Holocene 2, 1–10.

Birks, H.J.B., Frey, D.G., Deevey, E.S., 1998. Numerical tools in palaeolimnology-progress, potentialities, and problems. Journal of paleolimnology 20, 307–332.

Birks, H.J.B., Heiri, O., Seppä, H., Bjune, A.E., 2010. Strengths and weaknesses of quantitative climate reconstructions based on late-quaternary. The Open Ecology Journal 3.

Birks, H.J.B., Lotter, A.F., Juggins, S., Smol, J.P. (Eds.), 2012. Tracking Environmental Change Using Lake Sediments. Volume 5 : Data Handling and Numerical Techniques. volume 5 of *Developments in Paleoenvironmental Research*. Springer Netherlands, Dordrecht. doi:10.1007/978-94-007-2745-8.

Blaauw, M., Christen, J.A., 2011. Flexible paleoclimate age-depth models using an autoregressive gamma process. Bayesian analysis 6, 457–474. 01050.

Blackford, J.J., Innes, J.B., 2006. Linking current environments and processes to fungal spore assemblages: surface npm data from woodland environments. Review of Palaeobotany and Palynology 141, 179–187. doi:10.1016/j.revpalbo.2006.03.010.

Brenner, M., Whitmore, T.J., Curtis, J.H., Hodell, D.A., Schelske, C.L., 1999. Stable isotope (δ13C and δ15N) signatures of sedimented organic matter as indicators of historic lake trophic state. Journal of Paleolimnology 22, 205–221. doi:10.1023/a:1008078222806.

Buckles, L.K., Verschuren, D., Weijers, J.W., Cocquyt, C., Blaauw, M., Sinninghe Damsté, J.S., 2016. Interannual and (multi-)decadal variability in the sedimentary bit index of lake challa, east africa, over the past 2200 years: assessment of the precipitation proxy. Climate of the Past 12, 1243–1262. doi:10.5194/cp-12-1243-2016.

Burn, M.J., Palmer, S.E., 2014. Solar forcing of Caribbean drought events during the last millennium: Solar forcing of Caribbean drought events. Journal of Quaternary Science 29, 827–836. doi:10.1002/jqs.2660.

Cao, J., Rao, Z., Jia, G., Xu, Q., Chen, F., 2017. A 15 ka ph record from an alpine lake in north china derived from the cyclization ratio index of aquatic brgdgts and its paleoclimatic significance. Organic Geochemistry 109, 31–46. doi:10/gbhs34.

Cao, X.y., Herzschuh, U., Telford, R.J., Ni, J., 2014. A modern pollen–climate dataset from china and mongolia: Assessing its potential for climate reconstruction. Review of Palaeobotany and Palynology 211, 87–96. doi:10/gg976p.

Carter, V.A., Chiverrell, R.C., Clear, J.L., Kuosmanen, N., Moravcová, A., Svoboda, M., Svobodová-Svitavská, H., van Leeuwen, J.F., van der Knaap, W.O., Kuneš, P., 2018. Quantitative palynology informing conservation ecology in the bohemian/bavarian forests of central europe. Frontiers in plant science 8, 2268. doi:10/gfs2zf. 00003.

Chang, C.P. (Ed.), 2004. East Asian Monsoon. Number v. 2 in World Scientific Series on Meteorology of East Asia, World Scientific, Hackensack, NJ.

Chen, F., Chen, J., Huang, W., Chen, S., Huang, X., Jin, L., Jia, J., Zhang, X., An, C., Zhang, J., 2019. Westerlies Asia and monsoonal Asia: Spatiotemporal differences in climate change and possible mechanisms on decadal to sub-orbital timescales. Earth-Science Reviews 192, 337–354. doi:10.1016/j.earscirev.2019.03.005.

Chen, F., Holmes, J., Wünnemann, B., Yu, Z., 2009. Holocene climate variability in arid asia: Nature and mechanisms. Quaternary International 194, 1–5. 00013.

Chen, F., Wu, W., Holmes, J.A., Madsen, D.B., Zhu, Y., Jin, M., Oviatt, C.G., 2003. A mid-holocene drought interval as evidenced by lake desiccation in the alashan plateau, inner mongolia china. Chinese Science Bulletin 48, 1401.

Chen, F., Xu, Q., Chen, J., Birks, H.J.B., Liu, J., Zhang, S., Jin, L., An, C., Telford, R.J., Cao, X., 2015a. East Asian summer monsoon precipitation variability since the last deglaciation. Scientific reports 5, 1–11.

Chen, F., Yu, Z., Yang, M., Ito, E., Wang, S., Madsen, D.B., Huang, X., Zhao, Y., Sato, T., John B. Birks, H., et al., 2008. Holocene moisture evolution in arid central asia and its out-of-phase relationship with asian monsoon history. Quaternary Science Reviews 27, 351–364. doi:10.1016/j.quascirev.2007.10.017.

Chen, F.H., Chen, J.H., Holmes, J., Boomer, I., Austin, P., Gates, J.B., Wang, N.L., Brooks, S.J., Zhang, J.W., 2010. Moisture changes over the last millennium in arid central asia: a review, synthesis and comparison with monsoon region. Quaternary Science Reviews 29, 1055–1068. doi:10.1016/j.quascirev.2010.01.005.

Chen, J., Chen, F., Feng, S., Huang, W., Liu, J., Zhou, A., 2015b. Hydroclimatic changes in china and surroundings during the medieval climate anomaly and little ice age: spatial patterns and possible mechanisms. Quaternary Science Reviews 107, 98–111.

Chen, J., Rao, Z., Liu, J., Huang, W., Feng, S., Dong, G., Hu, Y., Xu, Q., Chen, F., 2016. On the timing of the East Asian summer monsoon maximum during the Holocene—Does the speleothem oxygen isotope record reflect monsoon rainfall variability? Science China Earth Sciences 59, 2328–2338. doi:10.1007/s11430-015-5500-5.

Cheng, Y., Liu, H., Dong, Z., Duan, K., Wang, H., Han, Y., 2020. East Asian summer monsoon and topography co-determine the Holocene migration of forest-steppe ecotone in northern China. Global and Planetary Change 187, 103135. doi:10.1016/j.gloplacha.2020.103135.

Chevalier, M., Davis, B.A., Heiri, O., Seppä, H., Chase, B.M., Gajewski, K., Lacourse, T., Telford, R.J., Finsinger, W., Guiot, J., 2020. Pollen-based climate reconstruction techniques for late Quaternary studies. Earth-Science Reviews , 103384doi:10.1016/j.earscirev.2020.103384.

Coffinet, S., 2015. Validation and application of lipid biomarkers to reconstruct past environmental changes in East Africa. Ph.D. thesis. Paris 6. 00001.

Cohen, A.S., 2003. Paleolimnology: the history and evolution of lake systems. Oxford University Press.

Comas-Bru, L., Rehfeld, K., Roesch, C., Amirnezhad-Mozhdehi, S., Harrison, S.P., Atsawawaranunt, K., Ahmad, S.M., Ait Brahim, Y., Baker, A., Bosomworth, M., Breitenbach, S.F.M., Burstyn, Y., Columbu, A., Deininger, M., Demény, A., Dixon, B., Fohlmeister, J., Hatvani, I.G., Hu, J., Kaushal, N., Kern, Z., Labuhn, I., Lechleitner, F.A., Lorrey, A., Martrat, B., Novello, V.F., Oster, J., Pérez-Mejías, C., Scholz, D., Scroxton, N., Sinha, N., Ward, B.M., Warken, S., Zhang, H., the SISAL members, 2020. SISALv2: A Comprehensive Speleothem Isotope Database with Multiple Age-Depth Models. Preprint. Geosciences – Palaeooceanography, Palaeoclimatology. doi:10.5194/essd-2020-39.

Croudace, I.W., Rindby, A., Rothwell, R.G., 2006. ITRAX: Description and evaluation of a new multi-function X-ray core scanner. Geological Society, London, Special Publications 267, 51–63. doi:10.1144/GSL.SP.2006.267.01.04.

Croudace, I.W., Rothwell, R.G., 2015. Micro-XRF Studies of Sediment Cores: Applications of a non-destructive tool for the environmental sci-

ences. volume 17. Springer.

Cugny, C., 2011. The use of non-pollen palynomorphs for reconstructing the history of pastoral activities in the Pyrenees, from modern datasets to reconstruction of the past. Ph.D. thesis. Université Toulouse le Mirail, Toulouse II.

Cugny, C., Mazier, F., Galop, D., 2010. Modern and fossil non-pollen palynomorphs from the basque mountains (western pyrenees, france): the use of coprophilous fungi to reconstruct pastoral activity. Vegetation History and Archaeobotany 19, 391–408. 00165.

Cuven, S., Francus, P., Lamoureux, S., 2011. Mid to Late Holocene hydroclimatic and geochemical records from the varved sediments of East Lake, Cape Bounty, Canadian High Arctic. Quaternary Science Reviews 30, 2651–2665. doi:10.1016/j.quascirev.2011.05.019.

Dang, X., Yang, H., Naafs, B.D.A., Pancost, R.D., Xie, S., 2016. Evidence of moisture control on the methylation of branched glycerol dialkyl glycerol tetraethers in semi-arid and arid soils. Geochimica et Cosmochimica Acta 189, 24–36. doi:10/f8xv6b.

Davis, B.A.S., Chevalier, M., Sommer, P., Carter, V.A., Finsinger, W., Mauri, A., Phelps, L.N., Zanon, M., Abegglen, R., Åkesson, C.M., Alba-Sánchez, F., Anderson, R.S., Antipina, T.G., Atanassova, J.R., Beer, R., Belyanina, N.I., Blyakharchuk, T.A., Borisova, O.K., Bozilova, E., Bukreeva, G., Bunting, M.J., Clò, E., Colombaroli, D., Combourieu-Nebout, N., Desprat, S., Di Rita, F., Djamali, M., Edwards, K.J., Fall, P.L., Feurdean, A., Fletcher, W., Florenzano, A., Furlanetto, G., Gaceur, E., Galimov, A.T., Gałka, M., García-Moreiras, I., Giesecke, T., Grindean, R., Guido, M.A., Gvozdeva, I.G., Herzschuh, U., Hjelle, K.L., Ivanov, S., Jahns, S., Jankovska, V., Jiménez-Moreno, G., Karpińska-Kołaczek, M., Kitaba, I., Kołaczek, P., Lapteva, E.G., Latałowa, M., Lebreton, V., Leroy, S., Leydet, M., Lopatina, D.A., López-Sáez, J.A., Lotter, A.F., Magri, D., Marinova, E., Matthias, I., Mavridou, A., Mercuri, A.M., Mesa-Fernández, J.M., Mikishin, Y.A., Milecka, K., Montanari, C., Morales-Molino, C., Mrotzek, A., Muñoz Sobrino, C., Naidina, O.D., Nakagawa, T., Nielsen, A.B., Novenko, E.Y., Panajiotidis, S., Panova, N.K., Papadopoulou, M., Pardoe, H.S., Pędziszewska, A., Petrenko, T.I., Ramos-Román, M.J., Ravazzi, C., Rösch, M., Ryabogina, N., Sabariego Ruiz, S., Salonen, J.S., Sapelko, T.V., Schofield, J.E., Seppä, H., Shumilovskikh, L., Stivrins, N., Stojakowits, P., Svobodova Svitavska, H., Święta-Musznicka, J., Tantau, I., Tinner, W., Tobolski, K., Tonkov, S., Tsakiridou, M., Valsecchi, V., Zanina, O.G., Zimny, M., 2020. The Eurasian Modern Pollen Database (EMPD), version 2. Earth System Science Data 12, 2423–2445. doi:10.5194/essd-12-2423-2020.

Davtian, N., Bard, E., Ménot, G., Fagault, Y., 2018. The importance of mass accuracy in selected ion monitoring analysis of branched and isoprenoid tetraethers. Organic geochemistry 118, 58–62.

Davtian, N., Ménot, G., Bard, E., Poulenard, J., Podwojewski, P., 2016. Consideration of soil types for the calibration of molecular proxies for soil ph and temperature using global soil datasets and vietnamese soil profiles. Organic Geochemistry 101, 140–153.

De Jonge, C., Hopmans, E.C., Zell, C.I., Kim, J.H., Schouten, S., Sinninghe Damsté, J.S., 2014a. Occurrence and abundance of 6-methyl branched glycerol dialkyl glycerol tetraethers in soils: Implications for palaeoclimate reconstruction. Geochimica et Cosmochimica Acta 141, 97–112.

De Jonge, C., Stadnitskaia, A., Hopmans, E.C., Cherkashov, G., Fedotov, A., Sinninghe Damsté, J.S., 2014b. In situ produced branched glycerol dialkyl glycerol tetraethers in suspended particulate matter from the yenisei river, eastern siberia. Geochimica et Cosmochimica Acta 125, 476–491.

Dearing Crampton-Flood, E., Tierney, J.E., Peterse, F., Kirkels, F.M.S.A., Sinninghe Damsté, J.S., 2020. BayMBT: A Bayesian calibration model for branched glycerol dialkyl glycerol tetraethers in soils and peats. Geochimica et Cosmochimica Acta 268, 142–159. doi:10/gg9758.

deMenocal, P.B., Stringer, C., 2016. Human migration: Climate and the peopling of the world. Nature doi:10/b657.

Dendievel, A.M., Dietre, B., Cubizolle, H., Hajdas, I., Kofler, W., Oberlin, C., Haas, J.N., 2019a. Holocene paleoecological changes and agro-pastoral impact on the la narce du béage mire (massif central, france). The Holocene 29, 992–1010. doi:10.1177/0959683619831416.

Dendievel, A.M., Serieyssol, K., Dietre, B., Cubizolle, H., Quiquerez, A., Haas, J.N., 2019b. Late-glacial and early holocene environmental changes affecting the shallow lake basin of la narce du béage (ardèche, massif central, france). Quaternary International , S1040618219307505doi:10.1016/j.quaint.2019.09.014.

Deng, L., Jia, G., Jin, C., Li, S., 2016. Warm season bias of branched gdgt temperature estimates causes underestimation of altitudinal lapse rate. Organic Geochemistry 96, 11–17.

Dimiceli, C., Carroll, M., Sohlberg, R., Kim, D.H., Kelly, M., Townshend, J.R.G., 2015. MOD44B MODIS/Terra vegetation continuous fields yearly L3 global 250m SIN grid V006 [data set]. NASA EOSDIS land processes DAAC.

Dinerstein, E., Olson, D., Joshi, A., Vynne, C., Burgess, N.D., Wikramanayake, E., Hahn, N., Palminteri, S., Hedao, P., Noss, R., et al., 2017. An ecoregion-based approach to protecting half the terrestrial realm. BioScience 67, 534–545. doi:10/gbh29s.

Ding, S., Xu, Y., Wang, Y., He, Y., Hou, J., Chen, L., He, J.S., 2015. Distribution of branched glycerol dialkyl glycerol tetraethers in surface soils of the qinghai–tibetan plateau: implications of brgdgts-based proxies in cold and dry regions. Biogeosciences 12, 3141–3151.

Ding, Y., Chan, J.C., 2005. The east asian summer monsoon: an overview. Meteorology and Atmospheric Physics 89, 117–142. doi:10.1007/s00703-005-0125-z.

Djamali, M., Jones, M.D., Migliore, J., Balatti, S., Fader, M., Contreras, D., Gondet, S., Hosseini, Z., Lahijani, H., Naderi, A., 2016. Olive cultivation in the heart of the persian achaemenid empire: new insights into agricultural practices and environmental changes reflected in a late holocene pollen record from lake parishan, sw iran. Vegetation History and Archaeobotany 25, 255–269.

Doyen, E., Etienne, D., 2017. Ecological and human land-use indicator value of fungal spore morphotypes and assemblages. Vegetation History and Archaeobotany 26, 357–367. doi:10.1007/s00334-016-0599-2.

Dugerdil, L., Joannin, S., Peyron, O., Jouffroy-Bapicot, I., Vannière, B., Bazartseren, B., Unkelbach, J., Behling, H., Ménot, G., 2021. Climate reconstructions based on gdgt and pollen surface datasets from mongolia and siberia: calibrations and applicability to extremely cold-dry environments over the late holocene. Climate of the Past , 1–39.

Dulamsuren, C., Hauck, M., Mühlenberg, M., 2005. Vegetation at the taiga forest—steppe borderline in the western Khentey Mountains, northern Mongolia, in: Annales Botanici Fennici, JSTOR. pp. 411–426.

El-Moslimany, A.P., 1990. Ecological significance of common nonarboreal pollen: examples from drylands of the middle east. Review of Palaeobotany and Palynology 64, 343–350.

Ellis, M.B., Ellis, J.P., 1985. Microfungi on Land Plants. An Identification Handbook. Croom Helm Ltd.

Erdos, L., Ambarlı, D., Anenkhonov, O.A., Bátori, Z., Cserhalmi, D., Kiss, M., Kröel-Dulay, G., Liu, H., Magnes, M., Molnár, Z., 2018. The edge of two worlds: A new review and synthesis on eurasian forest-steppes. Applied Vegetation Science 21, 345–362. doi:10/ggspn6.

Esin, Y.N., Magail, J., Yeruul-Erdene, C., Gantulga, J., 2017. Paint on deer stones of mongolia. ARCHAEOLOGY ETHNOLOGY AND ANTHROPOLOGY OF EURASIA 45, 79–89.

Etienne, D., Jouffroy-Bapicot, I., 2014. Optimal counting limit for fungal spore abundance estimation using sporormiella as a case study. Vegetation history and archaeobotany 23, 743–749. 00020.

Faegri, K., Iversen, J., 1989. 1989: Textbook of pollen analysis . chichester: John wiley. .

Felauer, T., Schlütz, F., Murad, W., Mischke, S., Lehmkuhl, F., 2012. Late quaternary climate and landscape evolution in arid central asia: A multi-proxy study of lake archive bayan tohomin nuur¢, gobi desert, southern mongolia. Journal of Asian Earth Sciences 48, 125–135.

Feng, Z.D., Ma, Y., Zhang, H., Narantsetsega, T., Zhang, X., 2013. Holocene climate variations retrieved from Gun Nuur lake-sediment core in the northern Mongolian Plateau. The Holocene 23, 1721–1730. doi:10.1177/0959683613505337.

Feranec, R.S., Miller, N.G., Lothrop, J.C., Graham, R.W., 2011. The Sporormiella proxy and end-Pleistocene megafaunal extinction: A per-

spective. Quaternary International 245, 333–338. doi:10.1016/j.quaint.2011.06.004.

Fernández-Giménez, M.E., 1999. Sustaining the steppes: a geographical history of pastoral land use in mongolia. Geographical Review 89, 315–342.

Fernández-Giménez, M.E., 2006. Land use and land tenure in mongolia: A brief history and current issues. USDA Forest Service Proceedings .

Fick, S.E., Hijmans, R.J., 2017. Worldclim 2: new 1-km spatial resolution climate surfaces for global land areas: New climate surfaces for global land areas. International Journal of Climatology 37, 4302–4315.

Free, C.M., Jensen, O.P., Mendsaikhan, B., 2015. A mixed-method approach for quantifying illegal fishing and its impact on an endangered fish species. PloS one 10, e0143960.

Gaillard, M.J., 2007. POLLEN METHODS AND STUDIES | Archaeological Applications, in: Elias, S.A. (Ed.), Encyclopedia of Quaternary Science. Elsevier, Oxford, pp. 2570–2595. doi:10.1016/B0-44-452747-8/00214-3.

Gaillard, M.J., Birks, H.J.B., Emanuelsson, U., Berglund, B.E., 1992. Modern pollen/land-use relationships as an aid in the reconstruction of past land-uses and cultural landscapes: an example from south sweden. Vegetation history and archaeobotany 1, 3–17. 00158.

Gao, F., Jia, J., Xia, D., Lu, C., Lu, H., Wang, Y., Liu, H., Ma, Y., Li, K., 2019. Asynchronous holocene climate optimum across midlatitude asia. Palaeogeography, palaeoclimatology, palaeoecology 518, 206–214. doi:10.1016/j.palaeo.2019.01.012.

Gauthier, E., Jouffroy-Bapicot, I., 2021. Detecting human impacts: Non-Pollen Palynomorphs as proxies for human impact on the environment. Geological Society, London, Special Publications 511.

Ghosh, R., Paruya, D.K., Acharya, K., Ghorai, N., Bera, S., 2017. How reliable are non-pollen palynomorphs in tracing vegetation changes and grazing activities? study from the darjeeling himalaya, india. Palaeogeography, Palaeoclimatology, Palaeoecology 475, 23–40. 00003.

Goldschmidt, V.M., 1937. The principles of distribution of chemical elements in minerals and rocks. the seventh hugo müller lecture, delivered before the chemical society on march 17th, 1937. Journal of the Chemical Society (Resumed) 0, 655–673.

Gong, D.Y., Ho, C.H., 2002. The Siberian High and climate change over middle to high latitude Asia. Theoretical and Applied Climatology 72, 1–9. doi:10.1007/s007040200008.

Gong, D.Y., Wang, S.W., Zhu, J.H., 2001. East Asian winter monsoon and Arctic oscillation. Geophysical Research Letters 28, 2073–2076.

Grimm, E.C., 1987. CONISS: A FORTRAN 77 program for stratigraphically constrained cluster analysis by the method of incremental sum of squares. Computers & geosciences 13, 13–35. doi:10.1016/0098-3004(87)90022-7.

d'Alpoim Guedes, J., Bocinsky, R.K., 2018. Climate change stimulated agricultural innovation and exchange across Asia. Science advances 4, eaar4491.

Guiot, J., 1990. Methodology of the last climatic cycle reconstruction in france from pollen data. Palaeogeography, Palaeoclimatology, Palaeoecology 80, 49–69.

Gunin, P.D., Vostokova, E.A., Dorofeyuk, N.I., Tarasov, P.E., Black, C.C., 1999. Vegetation Dynamics of Mongolia. Springer Netherlands, Dordrecht. doi:10.1007/978-94-015-9143-0.

Gupta, A.K., 2004. Origin of agriculture and domestication of plants and animals linked to early Holocene climate amelioration. CURRENT SCIENCE-BANGALORE- 87, 54–59.

Hao, R., Yu, D., 2018. Optimization schemes for grassland ecosystem services under climate change. Ecological Indicators 85, 1158–1169. doi:10/gdmqmv.

Haoran, H., Weihong, Q., 2007. Identifying the northernmost summer monsoon location in east asia. Progress in Natural Science 17, 812–820.

Harris, I., Osborn, T.J., Jones, P., Lister, D., 2020. Version 4 of the cru ts monthly high-resolution gridded multivariate climate dataset. Scientific data 7, 1–18. doi:10.1038/s41597-020-0453-3.

Harrison, S.P., Prentice, I.C., Barboni, D., Kohfeld, K.E., Ni, J., Sutra, J.P., 2010. Ecophysiological and bioclimatic foundations for a global plant functional classification. Journal of vegetation Science 21, 300–317. doi:10.1111/j.1654-1103.2009.01144.x.

He, Y., Hou, J., Wang, M., Li, X., Liang, J., Xie, S., Jin, Y., 2020. Temperature variation on the central tibetan plateau revealed by glycerol dialkyl glycerol tetraethers from the sediment record of lake linggo co since the last deglaciation. Frontiers in Earth Science 8. URL: https://www.frontiersin.org/articles/10.3389/feart.2020.574206/full, doi:10/gg975s.

Herzschuh, U., 2006. Palaeo-moisture evolution in monsoonal central asia during the last 50,000 years. Quaternary Science Reviews 25, 163–178. doi:10.1016/j.quascirev.2005.02.006.

Herzschuh, U., 2007. Reliability of pollen ratios for environmental reconstructions on the tibetan plateau. Journal of Biogeography 34, 1265–1273. doi:10.1111/j.1365-2699.2006.01680.x.

Herzschuh, U., Birks, H.J.B., Mischke, S., Zhang, C., Böhner, J., 2010. A modern pollen–climate calibration set based on lake sediments from the Tibetan Plateau and its application to a Late Quaternary pollen record from the Qilian Mountains. Journal of Biogeography 37, 752–766. doi:10/bdxvnw.

Herzschuh, U., Kürschner, H., Ma, Y., 2003. The surface pollen and relative pollen production of the desert vegetation of the alashan plateau, western inner mongolia. Chinese Science Bulletin 48, 1488–1493.

Herzschuh, U., Tarasov, P., Wünnemann, B., Hartmann, K., 2004. Holocene vegetation and climate of the alashan plateau, nw china, reconstructed from pollen data. Palaeogeography, Palaeoclimatology, Palaeoecology 211, 1–17.

Herzschuh, U., Winter, K., Wünnemann, B., Li, S., 2006. A general cooling trend on the central tibetan plateau throughout the holocene recorded by the lake zigetang pollen spectra. Quaternary International 154, 113–121.

Hessl, A.E., Ariya, U., Brown, P., Byambasuren, O., Green, T., Jacoby, G., Sutherland, E.K., Nachin, B., Maxwell, R.S., Pederson, N., 2012. Reconstructing fire history in central mongolia from tree-rings. International Journal of Wildland Fire 21, 86–92.

Honeychurch, W., 2010. Pastoral nomadic voices: a mongolian archaeology for the future. World Archaeology 42, 405–417.

Honeychurch, W., Amartuvshin, C., 2007. Hinterlands, urban centers, and mobile settings: the" new" old world archaeology from the eurasian steppe. Asian perspectives , 36–64.

Hopmans, E.C., Schouten, S., Damsté, J.S.S., 2016. The effect of improved chromatography on gdgt-based palaeoproxies. Organic Geochemistry 93, 1–6.

Hopmans, E.C., Weijers, J.W., Schefus s, E., Herfort, L., Damsté, J.S.S., Schouten, S., 2004. A novel proxy for terrestrial organic matter in sediments based on branched and isoprenoid tetraether lipids. Earth and Planetary Science Letters 224, 107–116.

Hou, K., Qian, H., Zhang, Q., Lin, T., Chen, Y., Zhang, Y., Qu, W., 2020. Influence of quaternary paleoclimate change on the permeability of the loess–paleosol sequence in the loess plateau, northern china. Earth Surface Processes and Landforms 45, 862–876. doi:10.1002/esp.4779.

Huang, J., Yu, H., Guan, X., Wang, G., Guo, R., 2016. Accelerated dryland expansion under climate change. Nature Climate Change 6, 166–171. doi:10/gbn62d.

Huang, X., Chen, X., Du, X., 2018a. Modern pollen assemblages from human-influenced vegetation in northwestern China and their relationship with vegetation and climate. Vegetation History and Archaeobotany 27, 767–780. doi:10.1007/s00334-018-0672-0.

Huang, X., Peng, W., Rudaya, N., Grimm, E.C., Chen, X., Cao, X., Zhang, J., Pan, X., Liu, S., Chen, C., et al., 2018b. Holocene vegetation and climate dynamics in the altai mountains and surrounding areas. Geophysical Research Letters URL: http://doi.wiley.com/10.1029/2018GL078028, doi:10/gdqdqk.

Huang, X.z., Chen, C.z., Jia, W.n., An, C.b., Zhou, A.f., Zhang, J.w., Jin, M., Xia, D.s., Chen, F.h., Grimm, E.C., 2015. Vegetation and climate history reconstructed from an alpine lake in central Tienshan Mountains since 8.5ka BP. Palaeogeography, Palaeoclimatology, Palaeoecology 432, 36–48. doi:10/f7h3zc.

Huguet, C., Hopmans, E.C., Febo-Ayala, W., Thompson, D.H., Sinninghe Damste, J.S., Schouten, S., 2006. An improved method to determine the absolute abundance of glycerol dibiphytanyl glycerol tetraether

lipids. Organic Geochemistry 37, 1036–1041. 00301.

Jackson, S.T., Williams, J.W., 2004. Modern analogs in quaternary paleoecology: here today, gone yesterday, gone tomorrow? Annual Review of Earth and Planetary Sciences 32.

Jankovská, V., Komárek, J., 2000. Indicative value ofpediastrum and other coccal green algae in palaeoecology. Folia Geobotanica 35, 59–82. 00219.

Jansen, J., Van der Gast, S., Kostner, B., Vaars, A., 1992. Cortex, an xrf-scanner for chemical analyses of sediment cores. GEOMAR Reports 15.

Ji, J., Shen, J., Balsam, W., Chen, J., Liu, L., Liu, X., 2005. Asian monsoon oscillations in the northeastern qinghai–tibet plateau since the late glacial as interpreted from visible reflectance of qinghai lake sediments. Earth and Planetary Science Letters 233, 61–70.

Johnson, C.N., 2009. Ecological consequences of Late Quaternary extinctions of megafauna. Proceedings of the Royal Society B: Biological Sciences 276, 2509–2519. doi:10.1098/rspb.2008.1921.

JPL, N., 2014. ASTER Global Emissivity Dataset, 100-meter, HDF5. doi:10.5067/COMMUNITY/ASTER_GED/AG100.003.

Juggins, S., Juggins, M.S., 2019. Package 'rioja'. RCRAN .

Kaufman, D., McKay, N., Routson, C., Erb, M., Davis, B., Heiri, O., Jaccard, S., Tierney, J., Dätwyler, C., Axford, Y., Brussel, T., Cartapanis, O., Chase, B., Dawson, A., de Vernal, A., Engels, S., Jonkers, L., Marsicek, J., Moffa-Sánchez, P., Morrill, C., Orsi, A., Rehfeld, K., Saunders, K., Sommer, P.S., Thomas, E., Tonello, M., Tóth, M., Vachula, R., Andreev, A., Bertrand, S., Biskaborn, B., Bringué, M., Brooks, S., Caniupán, M., Chevalier, M., Cwynar, L., Emile-Geay, J., Fegyveresi, J., Feurdean, A., Finsinger, W., Fortin, M.C., Foster, L., Fox, M., Gajewski, K., Grosjean, M., Hausmann, S., Heinrichs, M., Holmes, N., Ilyashuk, B., Ilyashuk, E., Juggins, S., Khider, D., Koinig, K., Langdon, P., Larocque-Tobler, I., Li, J., Lotter, A., Luoto, T., Mackay, A., Magyari, E., Malevich, S., Mark, B., Massaferro, J., Montade, V., Nazarova, L., Novenko, E., Pařil, P., Pearson, E., Peros, M., Pienitz, R., Płóciennik, M., Porinchu, D., Potito, A., Rees, A., Reinemann, S., Roberts, S., Rolland, N., Salonen, S., Self, A., Seppä, H., Shala, S., St-Jacques, J.M., Stenni, B., Syrykh, L., Tarrats, P., Taylor, K., van den Bos, V., Velle, G., Wahl, E., Walker, I., Wilmshurst, J., Zhang, E., Zhilich, S., 2020. A global database of Holocene paleotemperature records. Scientific Data 7, 115. doi:10/gg975z.

Kehl, M., 2009. Quaternary climate change in iran – the state of knowledge. ERDKUNDE 63, 1–17. doi:10/dzqv6r.

Klinge, M., Dulamsuren, C., Erasmi, S., Karger, D.N., Hauck, M., 2018. Climate effects on vegetation vitality at the treeline of boreal forests of mongolia. Biogeosciences 15, 1319–1333. doi:10/gc63k4. 00003.

Klinge, M., Sauer, D., 2019. Spatial pattern of late glacial and holocene climatic and environmental development in western mongolia - a critical review and synthesis. Quaternary Science Reviews 210, 26–50. 00000.

Kolaczek, P., Zubek, S., Blaszkowski, J., Mleczko, P., Margielewski, W., 2013. Erosion or plant succession—how to interpret the presence of arbuscular mycorrhizal fungi (glomeromycota) spores in pollen profiles collected from mires. Review of Palaeobotany and Palynology 189, 29–37. 00000.

Kramer, A., Herzschuh, U., Mischke, S., Zhang, C., 2010. Late quaternary environmental history of the south-eastern tibetan plateau inferred from the lake naleng non-pollen palynomorph record. Vegetation History and Archaeobotany 19, 453–468.

Kylander, M.E., Ampel, L., Wohlfarth, B., Veres, D., 2011. High-resolution X-ray fluorescence core scanning analysis of Les Echets (France) sedimentary sequence: new insights from chemical proxies. Journal of Quaternary Science 26, 109–117. doi:10.1002/jqs.1438.

Labban, A.H., Mashat, A.W.S., Awad, A.M., 2021. The variability of the Siberian high ridge over the Middle East. International Journal of Climatology 41, 104–130. doi:10.1002/joc.6611.

Lan, J., Xu, H., Sheng, E., Yu, K., Wu, H., Zhou, K., Yan, D., Ye, Y., Wang, T., 2018. Climate changes reconstructed from a glacial lake in high central asia over the past two millennia. Quaternary International 487, 43–53.

Lara, C.M.C., Roy, P., Miranda, M.M.C., Carreño, A.L., Lakshumanan, C., 2012. Lacustrine ostracodes from the chihuahuan desert of mexico and inferred late quaternary paleoecological conditions. Revista Mexicana de Ciencias Geológicas 29, 422–431.

Last, W.M., Smol, J.P., 2001. Tracking Environmental Change Using Lake Sediments. Volume 2: Physical and Geochemical Methods. Kluwer Academic.

Last, W.M., Smol, J.P., Birks, H.J.B., 2001. Tracking Environmental Change Using Lake Sediments. Volume 3: Terrestrial, algal, and siliceous indicators. Kluwer Academic. 00050.

Lê, S., Josse, J., Husson, F., 2008. FactoMineR: An R package for multivariate analysis. Journal of statistical software 25, 1–18. doi:10.18637/jss.v025.i01.

Leary O., M.H., 1988. Carbon isotopes in photosynthesis. Bioscience 38, 328–336.

Lebreton, V., Messager, E., Marquer, L., Renault-Miskovsky, J., 2010. A neotaphonomic experiment in pollen oxidation and its implications for archaeopalynology. Review of Palaeobotany and Palynology 162, 29–38.

Lehmkuhl, F., Grunert, J., Hülle, D., Batkhishig, O., Stauch, G., 2018. Paleolakes in the gobi region of southern mongolia. Quaternary Science Reviews 179, 1–23. doi:10.1016/j.quascirev.2017.10.035.

Lehmkuhl, F., Hilgers, A., Fries, S., Hülle, D., Schlütz, F., Shumilovskikh, L., Felauer, T., Protze, J., 2011. Holocene geomorphological processes and soil development as indicator for environmental change around karakorum, upper orkhon valley (central mongolia). Catena 87, 31–44.

Leyden, E., Cook, F., Hamilton, B., Zammit, B., Barnett, L., Lush, A.M., Stone, D., Mosley, L., 2016. Near shore groundwater acidification during and after a hydrological drought in the lower lakes, south australia. Journal of contaminant hydrology 189, 44–57.

Li, J., Wang, N., Dodson, J., Yan, H., Zhang, X., Jia, P.W., Seppä, H., 2020a. Holocene negative coupling of summer temperature and moisture availability over southeastern arid Central Asia. Climate Dynamics , 1–22.

Li, J., Xu, Q., Zheng, Z., Lu, H., Luo, Y., Li, Y., Li, C., Seppä, H., 2015. Assessing the Importance of Climate Variables for the Spatial Distribution of Modern Pollen Data in China. Quaternary Research 83, 287–297. doi:10.1016/j.yqres.2014.12.002.

Li, J.F., Xie, G., Yang, J., Ferguson, D.K., Liu, X.D., Liu, H., Wang, Y.F., 2020b. Asian Summer Monsoon changes the pollen flow on the Tibetan Plateau. Earth-Science Reviews 202, 103114. doi:10.1016/j.earscirev.2020.103114.

Li, J.X., Chen, Y.N., Xu, C.C., Li, Z., 2019. Evaluation and analysis of ecological security in arid areas of central asia based on the emergy ecological footprint (eef) model. Journal of Cleaner Production 235, 664–677. doi:10.1016/j.jclepro.2019.07.005.

Li, Q., Wu, H., Yu, Y., Sun, A., Luo, Y., 2018. Quantifying regional vegetation changes in china during three contrasting temperature intervals since the last glacial maximum. Journal of Asian Earth Sciences doi:10.1016/j.jseaes.2018.10.013. 00000.

Li, R., Lv, F., Yang, L., Liu, F., Liu, R., Dong, G., 2020c. Spatial–Temporal Variation of Cropping Patterns in Relation to Climate Change in Neolithic China. Atmosphere 11, 677. doi:10.3390/atmos11070677.

Li, X., Zhou, W., 2012. Quasi-4-yr coupling between El Niño–Southern Oscillation and water vapor transport over East Asia–WNP. Journal of climate 25, 5879–5891. doi:10.1175/JCLI-D-11-00433.1.

Liu, J., Chen, F., Chen, J., Xia, D., Xu, Q., Wang, Z., Li, Y., 2011. Humid medieval warm period recorded by magnetic characteristics of sediments from gonghai lake, shanxi, north china. Chinese Science Bulletin 56, 2464–2474.

Liu, X., Colman, S.M., Brown, E.T., Minor, E.C., Li, H., 2013. Estimation of carbonate, total organic carbon, and biogenic silica content by ftir and xrf techniques in lacustrine sediments. Journal of Paleolimnology 50, 387–398. doi:10.1007/s10933-013-9733-7.

Liu, X., Yanai, M., 2002. Influence of Eurasian spring snow cover on Asian summer rainfall. International Journal of Climatology: A Journal of the Royal Meteorological Society 22, 1075–1089. doi:10.1002/joc.784.

Liu, Z., Henderson, A.C.G., Huang, Y., 2006. Alkenone-based reconstruction of late-holocene surface temperature and salinity changes in lake qinghai, china. Geophysical Research Letters 33.

Lotter, A.F., Birks, H.J.B., Hofmann, W., Marchetto, A., 1997. Modern diatom, cladocera, chironomid, and chrysophyte cyst assemblages as quantitative indicators for the reconstruction of past environmental conditions in the alps. i. climate. Journal of Paleolimnology 18, 395–420.

Lowe, J., 1985. Handbook of holocene palaeoecology and palaeohydrology. Quaternary Science Reviews 4, xv–xviii. 00000.

Lu, F., Ma, C., Zhu, C., Lu, H., Zhang, X., Huang, K., Guo, T., Li, K., Li, L., Li, B., 2019. Variability of east asian summer monsoon precipitation during the holocene and possible forcing mechanisms. Climate Dynamics 52, 969–989.

Lu, H., Wu, N., Liu, K.b., Zhu, L., Yang, X., Yao, T., Wang, L., Li, Q., Liu, X., Shen, C., Li, X., Tong, G., Jiang, H., 2011. Modern pollen distributions in Qinghai-Tibetan Plateau and the development of transfer functions for reconstructing Holocene environmental changes. Quaternary Science Reviews 30, 947–966. doi:10.1016/j.quascirev.2011.01.008.

Löwemark, L., Chen, H.F., Yang, T.N., Kylander, M., Yu, E.F., Hsu, Y.W., Lee, T.Q., Song, S.R., Jarvis, S., 2011. Normalizing xrf-scanner data: A cautionary note on the interpretation of high-resolution records from organic-rich lakes. Journal of Asian Earth Sciences 40, 1250–1256. 00156.

Ma, Y., Liu, K.b., Feng, Z., Sang, Y., Wang, W., Sun, A., 2008. A survey of modern pollen and vegetation along a south–north transect in mongolia. Journal of Biogeography 35, 1512–1532.

Magny, M., 2019. Aux Racines de l'anthropocène: Une Crise Écologique Reflet d'une Crise de l'homme. Éditions le Bord de l'eau.

Mann, M.E., 2004. On smoothing potentially non-stationary climate time series. Geophysical Research Letters 31. doi:10.1029/2004GL019569.

Martin, C., Ménot, G., Thouveny, N., Davtian, N., Andrieu-Ponel, V., Reille, M., Bard, E., 2019. Impact of human activities and vegetation changes on the tetraether sources in lake st front (massif central, france). Organic Geochemistry 135, 38–52. doi:10/gf35hn.

Martínez-Sosa, P., Tierney, J.E., Meredith, L.K., 2020. Controlled lacustrine microcosms show a brGDGT response to environmental perturbations. Organic Geochemistry 145, 104041. doi:10/ggvt59.

Mathis, M., Sorrel, P., Klotz, S., Huang, X., Oberhänsli, H., 2014. Regional vegetation patterns at lake Son Kul reveal Holocene climatic variability in central Tien Shan (Kyrgyzstan, Central Asia). Quaternary Science Reviews 89, 169–185. doi:10.1016/j.quascirev.2014.01.023.

Miehe, G., Miehe, S., Böhner, J., Kaiser, K., Hensen, I., Madsen, D., Liu, J., Opgenoorth, L., 2014. How old is the human footprint in the world's largest alpine ecosystem? a review of multiproxy records from the tibetan plateau from the ecologists' viewpoint. Quaternary Science Reviews 86, 190–209. doi:10/f5vcsn.

Miehe, G., Miehe, S., Kaiser, K., Reudenbach, C., Behrendes, L., Duo, L., Schlütz, F., 2009. How old is pastoralism in tibet? an ecological approach to the making of a tibetan landscape. Palaeogeography, Palaeoclimatology, Palaeoecology 276, 130–147. doi:10.1016/j.palaeo.2009.03.005.

Miehe, G., Schlütz, F., Miehe, S., Opgenoorth, L., Cermak, J., Samiya, R., Jäger, E.J., Wesche, K., 2007. Mountain forest islands and holocene environmental changes in central asia: a case study from the southern gobi altay, mongolia. Palaeogeography, Palaeoclimatology, Palaeoecology 250, 150–166. doi:10/ffrbms.

Montoya, E., Rull, V., van Geel, B., 2010. Non-pollen palynomorphs from surface sediments along an altitudinal transect of the venezuelan andes. Palaeogeography, Palaeoclimatology, Palaeoecology 297, 169–183. doi:10.1016/j.palaeo.2010.07.026.

Murad, W., 2012. Late Quaternary vegetation history and climate change in the Gobi Desert, South Mongolia. Ph.D. thesis. Göttingen centre for biodiversity and ecology.

Naafs, B., Gallego-Sala, A., Inglis, G., Pancost, R., 2017a. Refining the global branched glycerol dialkyl glycerol tetraether (brgdgt) soil temperature calibration. Organic Geochemistry 106, 48–56.

Naafs, B.D.A., Inglis, G.N., Zheng, Y., Amesbury, M.J., Biester, H., Bindler, R., Blewett, J., Burrows, M.A., Del Castillo Torres, D., Chambers, F.M., 2017b. Introducing global peat-specific temperature and pH calibrations based on brGDGT bacterial lipids. Geochimica et Cosmochimica Acta 208, 285–301. doi:10/f99n9b.

Naafs, B.D.A., McCormick, D., Inglis, G.N., Pancost, R.D., 2018. Archaeal and bacterial h-gdgts are abundant in peat and their relative abundance is positively correlated with temperature. Geochimica et Cosmochimica Acta 227, 156–170. 00004.

Ning, D., Zhang, E., Shulmeister, J., Chang, J., Sun, W., Ni, Z., 2019. Holocene mean annual air temperature (MAAT) reconstruction based on branched glycerol dialkyl glycerol tetraethers from Lake Ximenglongtan, southwestern China. Organic Geochemistry doi:10/ggw626.

Nunez, S., Alkemade, R., Kok, K., Leemans, R., 2020. Potential biodiversity change in central asian grasslands: scenarios for the impact of climate and land-use change. Regional Environmental Change 20, 39. doi:10.1007/s10113-020-01619-4.

Olsen, J., Björck, S., Leng, M.J., Gudmundsdóttir, E.R., Odgaard, B.V., Lutz, C.M., Kendrick, C.P., Andersen, T.J., Seidenkrantz, M.S., 2010. Lacustrine evidence of holocene environmental change from three faroese lakes: a multiproxy xrf and stable isotope study. Quaternary Science Reviews 29, 2764–2780.

Overpeck, J.T., Webb, T., Prentice, I.C., 1985. Quantitative interpretation of fossil pollen spectra: dissimilarity coefficients and the method of modern analogs. Quaternary Research 23, 87–108.

Oyuntsetseg, D., 2014. Isotopic and geochemical study of geothermal fluids in Mongolia for geothermal exploration. Ph.D. thesis. Department of Environmental Biology and Chemistry, University of Toyama.

Pals, J.P., Van Geel, B., Delfos, A., 1980. Paleoecological studies in the klokkeweel bog near hoogkarspel (prov. of noord-holland). Review of Palaeobotany and Palynology 30, 371–418.

Park, C.E., Jeong, S.J., Joshi, M., Osborn, T.J., Ho, C.H., Piao, S., Chen, D., Liu, J., Yang, H., Park, H., et al., 2018. Keeping global warming within 1.5 c constrains emergence of aridification. Nature Climate Change 8, 70–74. doi:10/gcpzd3.

Patterson, R.T., Dalby, A., Kumar, A., Henderson, L.A., Boudreau, R.E., 2002. Arcellaceans (thecamoebians) as indicators of land-use change: settlement history of the swan lake area, ontario as a case study. Journal of Paleolimnology 28, 297–316. doi:10.1023/A:1021621622090.

Peyron, O., Combourieu-Nebout, N., Brayshaw, D., Goring, S., Andrieu-Ponel, V., Desprat, S., Fletcher, W., Gambin, B., Ioakim, C., Joannin, S., et al., 2017. Precipitation changes in the mediterranean basin during the holocene from terrestrial and marine pollen records: a model–data comparison. Climate of the Past 13, 249–265. doi:https://doi.org/10.5194/cp-13-249-2017.

Peyron, O., Guiot, J., Cheddadi, R., Tarasov, P., Reille, M., de Beaulieu, J.L., Bottema, S., Andrieu, V., 1998. Climatic reconstruction in europe for 18,000 yr bp from pollen data. Quaternary research 49, 183–196.

Peyron, O., Magny, M., Goring, S., Joannin, S., De Beaulieu, J.L., Brugiapaglia, E., Sadori, L., Garfi, G., Kouli, K., Ioakim, C., 2013. Contrasting patterns of climatic changes during the holocene across the italian peninsula reconstructed from pollen data. Climate of the Past 9, 1233–1252.

Pfeiffer, M., Dulamsuren, C., Jäschke, Y., Wesche, K., 2018. Grasslands of china and mongolia: spatial extent, land use and conservation. CRC Press .

Piao, J., Chen, W., Zhang, Q., Hu, P., 2018. Comparison of moisture transport between siberia and northeast asia on annual and interannual time scales. Journal of Climate 31, 7645–7660. doi:10.1175/JCLI-D-17-0763.1.

Prentice, C., Guiot, J., Huntley, B., Jolly, D., Cheddadi, R., 1996. Reconstructing biomes from palaeoecological data: a general method and its application to european pollen data at 0 and 6 ka. Climate Dynamics 12, 185–194.

Prentice, I.C., 1985. Pollen representation, source area, and basin size: toward a unified theory of pollen analysis. Quaternary Research 23, 76–86.

Pyankov, V.I., Gunin, P.D., Tsoog, S., Black, C.C., 2000. C 4 plants in the vegetation of mongolia: their natural occurrence and geographical distribution in relation to climate. Oecologia 123, 15–31.

R Core Team, t., 2013. R: A language and environment for statistical computing .

Rao, Z., Guo, H., Cao, J., Shi, F., Jia, G., Li, Y., Chen, F., 2020. Consistent long-term Holocene warming trend at different elevations in the Altai

Mountains in arid central Asia. Journal of Quaternary Science 35, 1036–1045. doi:10.1002/jqs.3254.

Reimer, P.J., Brown, T.A., Reimer, R.W., 2004. Discussion: Reporting and calibration of post-bomb 14C data. Radiocarbon 46, 1299–1304. doi:10.1017/S0033822200033154.

Robert Bagnell, C., 1975. Species distinction among pollen grains of abies, picea, and pinus in the rocky mountain area (a scanning electron microscope study). Review of Palaeobotany and Palynology 19, 203–220. doi:10.1016/0034-6667(75)90041-X.

Roberts, N., Eastwood, W.J., Kuzucuoğlu, C., Fiorentino, G., Caracuta, V., 2011. Climatic, vegetation and cultural change in the eastern Mediterranean during the mid-Holocene environmental transition. The Holocene 21, 147–162. doi:10/c88bvv.

Rudaya, N., Li, H.C., 2013. A new approach for reconstruction of the holocene climate in the mongolian altai: The high-resolution d13c records of toc and pollen complexes in hoton-nur lake sediments. Journal of Asian Earth Sciences 69, 185–195. doi:10/gg976x.

Rudaya, N., Sergey, K., Michał, S., Xianyong, C., Snezhana, Z., 2020. Postglacial history of the Steppe Altai: Climate, fire and plant diversity. Quaternary Science Reviews 249, 106616. doi:10.1016/j.quascirev.2020.106616.

Rudaya, N.A., Tarasov, P.E., Dorofeyuk, N.I., Kalugin, I.A., Andreev, A.A., Diekmann, B., Daryin, A.V., 2008. Environmental changes in the mongolian altai during the holocene. Archaeology, Ethnology and Anthropology of Eurasia 36, 2–14. doi:10/dk7m57. 00017.

Saizen, I., Maekawa, A., Yamamura, N., 2010. Spatial analysis of time-series changes in livestock distribution by detection of local spatial associations in mongolia. Applied Geography 30, 639–649.

Salonen, J.S., Korpela, M., Williams, J.W., Luoto, M., 2019. Machine-learning based reconstructions of primary and secondary climate variables from North American and European fossil pollen data. Scientific reports 9, 1–13. doi:10/gg978t.

Salonen, J.S., Luoto, M., Alenius, T., Heikkilä, M., Seppä, H., Telford, R.J., Birks, H.J.B., 2014. Reconstructing palaeoclimatic variables from fossil pollen using boosted regression trees: Comparison and synthesis with other quantitative reconstruction methods. Quaternary Science Reviews 88, 69–81. doi:10/f5xsdd.

Savelyev, A., Jeong, C., 2020. Early nomads of the Eastern Steppe and their tentative connections in the West. Evolutionary Human Sciences 2. doi:10.1017/ehs.2020.18.

Schlütz, F., Dulamsuren, C., Wieckowska, M., Mühlenberg, M., Hauck, M., 2008. Late Holocene vegetation history suggests natural origin of steppes in the northern Mongolian mountain taiga. Palaeogeography, Palaeoclimatology, Palaeoecology 261, 203–217. doi:10.1016/j.palaeo.2007.12.012.

Schwanghart, W., Schütt, B., Walther, M., 2008. Holocene climate evolution of the ugii nuur basin, mongolia. Advances in atmospheric sciences 25, 986–998.

Sharkhuu, A., Sharkhuu, N., Etzelmüller, B., Heggem, E.S.F., Nelson, F.E., Shiklomanov, N.I., Goulden, C.E., Brown, J., 2007. Permafrost monitoring in the hovsgol mountain region, mongolia. Journal of Geophysical Research: Earth Surface 112.

Sharkhuu, N., 2003. Recent changes in the permafrost of mongolia, in: Proceedings of the 8th International Conference on Permafrost, 21-25 July 2003, Zurich, Switzerland, AA Balkema, Lisse, the Netherlands. p. 1029–1034.

Sherwood, S., Fu, Q., 2014. A drier future? Science 343, 737–739. doi:10/gc3fmd.

Shukurov, K.A., Mokhov, I.I., 2017. Potential sources of precipitation in Lake Baikal basin, in: 23rd International Symposium on Atmospheric and Ocean Optics: Atmospheric Physics, International Society for Optics and Photonics. p. 104663T.

Shumilovskikh, L.S., van Geel, B., 2020. Non-pollen palynomorphs. Springer International Publishing. p. 65–94. doi:10.1007/978-3-030-42622-4-4. citation Key: Shumilovskikh2020.

Shumilovskikh, L.S., Seeliger, M., Feuser, S., Novenko, E., Schlütz, F., Pint, A., Pirson, F., Brückner, H., 2016. The harbour of elaia: A palynological archive for human environmental interactions during the last 7500 years. Quaternary Science Reviews 149, 167–187. doi:10.1016/j.quascirev.2016.07.014.

Sinninghe Damsté, J.S., 2016. Spatial heterogeneity of sources of branched tetraethers in shelf systems: The geochemistry of tetraethers in the berau river delta (kalimantan, indonesia). Geochimica et Cosmochimica Acta 186, 13–31.

Sluijs, A., Röhl, U., Schouten, S., Brumsack, H.J., Sangiorgi, F., Damsté, J.S.S., Brinkhuis, H., 2008. Arctic late Paleocene–early Eocene paleoenvironments with special emphasis on the Paleocene-Eocene thermal maximum (Lomonosov Ridge, Integrated Ocean Drilling Program Expedition 302). Paleoceanography 23. doi:10.1029/2007pa001495.

Still, C.J., Berry, J.A., Collatz, G.J., DeFries, R.S., 2003. Global distribution of c3 and c4 vegetation: carbon cycle implications. Global Biogeochemical Cycles 17, 6–1.

Stivrins, N., Soininen, J., Tõnno, I., Freiberg, R., Veski, S., Kisand, V., 2018. Towards understanding the abundance of non-pollen palynomorphs: A comparison of fossil algae, algal pigments and sedaDNA from temperate lake sediments. Review of Palaeobotany and Palynology 249, 9–15. doi:10.1016/j.revpalbo.2017.11.001.

Stockmarr, J.A., 1971. Tabletes with spores used in absolute pollen analysis. Pollen spores 13, 615–621.

Sun, Q., Chu, G., Liu, M., Xie, M., Li, S., Ling, Y., Wang, X., Shi, L., Jia, G., Lü, H., 2011. Distributions and temperature dependence of branched glycerol dialkyl glycerol tetraethers in recent lacustrine sediments from china and nepal. Journal of Geophysical Research: Biogeosciences 116.

Sun, W., Zhao, S., Pei, H., Yang, H., 2019. The coupled evolution of mid- to late holocene temperature and moisture in the southeast qaidam basin. Chemical Geology 528, 119282. doi:10.1016/j.chemgeo.2019.119282.

Sun, Y., Xu, Q., Zhang, S., Li, Y., Li, M., Li, Y., Wang, T., Zhang, X., Wang, Y., Huang, R., Hao, J., Zheng, Z., Zhou, Z., 2020. A novel procedure for quantitative regional paleoclimatic reconstruction using surface pollen assemblages. Quaternary Science Reviews 240, 106385. doi:10.1016/j.quascirev.2020.106385.

Talbot, M.R., Lērdal, T., 2000. The late pleistocene-holocene palaeolimnology of lake victoria, east africa, based upon elemental and isotopic analyses of sedimentary organic matter. Journal of Paleolimnology 23, 141–164.

Telford, R.J., Birks, H.J.B., 2005. The secret assumption of transfer functions: Problems with spatial autocorrelation in evaluating model performance. Quaternary Science Reviews 24, 2173–2179. doi:10/fs8tgx.

Ter Braak, C.J., Juggins, S., 1993. Weighted averaging partial least squares regression (wa-pls): an improved method for reconstructing environmental variables from species assemblages, in: Twelfth International Diatom Symposium, Springer. p. 485–502.

Ter Braak, C.J.F., Juggins, S., Birks, H.J.B., Van der Voet, H., 1993. Weighted averaging partial least squares regression (WA-PLS): definition and comparison with other methods for species-environment calibration. Elsevier. chapter 25. p. 525–560.

Teranes, J.L., Bernasconi, S.M., 2000. The record of nitrate utilization and productivity limitation provided by $\delta 15n$ values in lake organic matter—a study of sediment trap and core sediments from baldeggersee, switzerland. Limnology and Oceanography 45, 801–813.

Tian, F., Herzschuh, U., Dallmeyer, A., Xu, Q., Mischke, S., Biskaborn, B.K., 2013. Environmental variability in the monsoon–westerlies transition zone during the last 1200 years: Lake sediment analyses from central Mongolia and supra–regional synthesis. Quaternary Science Reviews 73, 31–47.

Tian, F., Herzschuh, U., Mischke, S., Schlütz, F., 2014. What drives the recent intensified vegetation degradation in mongolia–climate change or human activity? The Holocene 24, 1206–1215.

Townshend, J., 2016. Global Forest Cover Change (GFCC) Water Cover 2000 Global 30 m V001. doi:10.5067/MEASURES/GFCC/GFCC30WC.001.

Umbanhowar Jr, C.E., Shinneman, A.L., Tserenkhand, G., Hammon, E.R., Lor, P., Nail, K., 2009. Regional fire history based on charcoal analysis of sediments from nine lakes in western mongolia. The Holocene 19, 611–624.

Unkelbach, J., Kashima, K., Enters, D., Dulamsuren, C., Punsalpaamuu, G., Behling, H., 2019. Late holocene (meghalayan) palaeoenvironmen-

tal evolution inferred from multi-proxy-studies of lacustrine sediments from the dayan nuur region of mongolia. Palaeogeography, Palaeoclimatology, Palaeoecology 530, 1–14. doi:10.1016/j.palaeo.2019.05.021.

Unkelbach, J., Kashima, K., Punsalpaamuu, G., Shumilovskikh, L., Behling, H., 2020. Decadal high-resolution multi-proxy analysis to reconstruct natural and human-induced environmental changes over the last 1350 cal. yr bp in the altai tavan bogd national park, western mongolia. The Holocene , 0959683620908662doi:10/gg9776.

Van Geel, B., 1972. Palynology of a section from the raised peat bog 'wietmarscher moor ', with special reference to fungal remains. Acta Botanica Neerlandica 21, 261–284. doi:10/gftpsw. 00074.

Van Geel, B., 1978. A palaeoecological study of holocene peat bog sections in germany and the netherlands, based on the analysis of pollen, spores and macro-and microscopic remains of fungi, algae, cormophytes and animals. Review of palaeobotany and palynology 25, 1–120. doi:10/bjct43. 00670.

Van Geel, B., 2002. Non-pollen palynomorphs. Springer. p. 99–119.

Van Geel, B., Andersen, S.T., 1988. Fossil ascopores of the parasitic fungus ustulina deusta in eemian deposits in denmark. Review of Palaeobotany and Palynology 56, 89–93.

Van Geel, B., Aptroot, A., 2006. Fossil ascomycetes in quaternary deposits. Nova Hedwigia 82, 313–329.

Van Geel, B., Hallewas, D.P., Pals, J.P., 1983. A late holocene deposit under the westfriese zeedijk near enkhuizen (prov. of noord-holland, the netherlands): palaeoecological and archaeological aspects. Review of Palaeobotany and Palynology 38, 269–335.

Vozhehova, R., Lykhovyd, P., Biliaieva, I., 2020. Aridity assessment and forecast for kherson oblast (ukraine) at the climate change. EurAsian Journal of BioSciences 14.

Wang, H., Liu, W., Lu, H., 2016. Appraisal of branched glycerol dialkyl glycerol tetraether-based indices for north china. Organic Geochemistry 98, 118–130.

Wang, M., Yang, H., Zheng, Z., Tian, L., 2020. Altitudinal climatic index changes in subtropical China indicated from branched glycerol dialkyl glycerol tetraethers proxies. Chemical Geology , 119579doi:10/gg977b.

Wang, W., Feng, Z., 2013. Holocene moisture evolution across the mongolian plateau and its surrounding areas: A synthesis of climatic records. Earth-Science Reviews 122, 38–57.

Wang, W., Liu, L., Li, Y., Niu, Z., He, J., Ma, Y., Mensing, S.A., 2019. Pollen reconstruction and vegetation dynamics of the middle Holocene maximum summer monsoon in northern China. Palaeogeography, Palaeoclimatology, Palaeoecology 528, 204–217. doi:10.1016/j.palaeo.2019.05.023.

Wang, W., Ma, Y., Feng, Z., Meng, H., Sang, Y., Zhai, X., 2009. Vegetation and climate changes during the last 8660 cal. a BP in central Mongolia, based on a high-resolution pollen record from Lake Ugii Nuur. Chinese Science Bulletin 54, 1579–1589.

Wang, W., Ma, Y., Feng, Z., Narantsetseg, T., Liu, K.B., Zhai, X., 2011. A prolonged dry mid-holocene climate revealed by pollen and diatom records from lake ugii nuur in central mongolia. Quaternary International 229, 74–83. doi:10.1016/j.quaint.2010.06.005.

Wang, Y., Liu, X., Herzschuh, U., 2010. Asynchronous evolution of the indian and east asian summer monsoon indicated by holocene moisture patterns in monsoonal central asia. Earth-Science Reviews 103, 135–153.

Wanner, H., Brönnimann, S., 2012. Is there a global Holocene climate mode? PAGES news 20, 44–45. doi:10.22498/pages.20.1.44.

Warner, T.T., 2004. Desert Meteorology. Cambridge University Press, Cambridge; New York.

Wen, R., Xiao, J., Ma, Y., Feng, Z., Li, Y., Xu, Q., 2013. Pollen–climate transfer functions intended for temperate eastern asia. Quaternary International 311, 3–11.

Wen, Z., Chan, J.C.L., Chongyin, L., 2005. South China Sea summer monsoon onset in relation to the off-equatorial ITCZ. Advances in Atmospheric Sciences 22, 665–676. doi:10.1007/BF02918710.

Weng, C., Hooghiemstra, H., Duivenvoorden, J.F., 2006. Challenges in estimating past plant diversity from fossil pollen data: Statistical assessment, problems, and possible solutions. Diversity and Distributions 12, 310–318. doi:10/b6w9t4.

Wesche, K., Ambarlı, D., Kamp, J., Török, P., Treiber, J., Dengler, J., 2016. The palaearctic steppe biome: a new synthesis. Biodiversity and conservation 25, 2197–2231.

Wickham, H., 2016. ggplot2: elegant graphics for data analysis. Springer.

Windley, B.F., Allen, M.B., 1993. Mongolian plateau: Evidence for a late Cenozoic mantle plume under central Asia. Geology 21, 295–298. doi:10.1130/0091-7613(1993)021<0295:MPEFAL>2.3.CO;2.

Wolff, C., Plessen, B., Dudashvilli, A.S., Breitenbach, S.F., Cheng, H., Edwards, L.R., Strecker, M.R., 2017. Precipitation evolution of Central Asia during the last 5000 years. The Holocene 27, 142–154. doi:10/f9mbfh.

Wu, B., Wang, J., 2002. Possible impacts of winter Arctic Oscillation on Siberian high, the East Asian winter monsoon and sea–ice extent. Advances in Atmospheric Sciences 19, 297–320. doi:10.1007/s00376-002-0024-x.

Wu, D., Cao, J., Jia, G., Guo, H., Shi, F., Zhang, X., Rao, Z., 2020. Peat brgdgts-based holocene temperature history of the altai mountains in arid central asia. Palaeogeography, Palaeoclimatology, Palaeoecology 538, 109464. doi:10.1016/j.palaeo.2019.109464.

Xiao, W., Wang, Y., Zhou, S., Hu, L., Yang, H., Xu, Y., 2016. Ubiquitous production of branched glycerol dialkyl glycerol tetraethers (brgdgts) in global marine environments: a new source indicator for brgdgts. Biogeosciences 13, 5883–5894.

Xie, S., Pancost, R.D., Chen, L., Evershed, R.P., Yang, H., Zhang, K., Huang, J., Xu, Y., 2012. Microbial lipid records of highly alkaline deposits and enhanced aridity associated with significant uplift of the tibetan plateau in the late miocene. Geology 40, 291–294. 00080.

Yang, H., Pancost, R.D., Dang, X., Zhou, X., Evershed, R.P., Xiao, G., Tang, C., Gao, L., Guo, Z., Xie, S., 2014. Correlations between microbial tetraether lipids and environmental variables in chinese soils: Optimizing the paleo-reconstructions in semi-arid and arid regions. Geochimica et Cosmochimica Acta 126, 49–69.

Yang, H., Xiao, W., Słowakiewicz, M., Ding, W., Ayari, A., Dang, X., Pei, H., 2019. Depth-dependent variation of archaeal ether lipids along soil and peat profiles from southern china: Implications for the use of isoprenoidal gdgts as environmental tracers. Organic Geochemistry 128, 42–56. 00000.

Yao, F., Ma, C., Zhu, C., Li, J., Chen, G., Tang, L., Huang, M., Jia, T., Xu, J., 2017. Holocene climate change in the western part of Taihu Lake region, East China. Palaeogeography, Palaeoclimatology, Palaeoecology 485, 963–973. doi:10.1016/j.palaeo.2017.08.022.

Yarmolyuk, V.V., Kozlovsky, A.M., Travin, A.V., Kirnozova, T.I., Fugzan, M.M., Kozakov, I.K., Plotkina, Y.V., Eenjin, G., Oyunchimeg, T., Sviridova, O.E., 2019. Duration and geodynamic nature of giant Central Asian Batholiths: Geological and geochronological studies of the Khangai Batholith. Stratigraphy and Geological Correlation 27, 73–94. doi:10.1134/S0869593819010088.

Yarmolyuk, V.V., Kudryashova, E.A., Kozlovsky, A.M., Lebedev, V.A., 2008. Late Cenozoic volcanism of Khangai (Central Mongolia): Evidence for recent orogeny in Central Asia, in: Doklady Earth Sciences, Springer Nature BV. p. 1032. doi:10.1134/S1028334X08070064.

Zang, J., Lei, Y., Yang, H., 2018. Distribution of glycerol ethers in turpan soils: implications for use of gdgt-based proxies in hot and dry regions. Frontiers of Earth Science 12, 862–876. doi:10/gfb6xq. 00000.

Zhang, C., Zhao, C., Zhou, A., Zhang, H., Liu, W., Feng, X., Sun, X., Yan, T., Leng, C., Shen, J., et al., 2021. Quantification of temperature and precipitation changes in northern china during the "5000-year" chinese history. Quaternary Science Reviews 255, 106819. doi:10.1016/j.quascirev.2021.106819.

Zhang, P., Cheng, H., Edwards, R.L., Chen, F., Wang, Y., Yang, X., Liu, J., Tan, M., Wang, X., Liu, J., 2008. A test of climate, sun, and culture relationships from an 1810-year chinese cave record. science 322, 940–942.

Zhang, X., 2021. Penetration of monsoonal water vapour into arid central Asia during the Holocene: An isotopic perspective. Quaternary Science Reviews 251, 106713. doi:10.1016/j.quascirev.2020.106713.

Zhao, Y., Liu, H., Li, F., Huang, X., Sun, J., Zhao, W., Herzschuh, U., Tang,

Y., 2012. Application and limitations of the artemisia/chenopodiaceae pollen ratio in arid and semi-arid china. The Holocene 22, 1385–1392.

Zhao, Y., Wu, F., Fang, X., Yang, Y., 2015. Topsoil c/n ratios in the qilian mountains area: Implications for the use of subaqueous sediment c/n ratios in paleo-environmental reconstructions to indicate organic sources. Palaeogeography, Palaeoclimatology, Palaeoecology 426, 1–9.

Zheng, Y., Pancost, R.D., Naafs, B.D.A., Li, Q., Liu, Z., Yang, H., 2018. Transition from a warm and dry to a cold and wet climate in ne china across the holocene. Earth and Planetary Science Letters 493, 36–46. doi:10.1016/j.epsl.2018.04.019.

Zheng, Y., Yu, G., Wang, S.M., Xue, B., Zhuo, D.Q., Zeng, X.M., Liu, H.Q., 2004. Simulation of paleoclimate over east asia at six ka bp and twenty one ka bp by a regional climate model. Climate Dynamics 23, 513–529. 00002.

Zheng, Z., Wei, J., Huang, K., Xu, Q., Lu, H., Tarasov, P., Luo, C., Beaudouin, C., Deng, Y., Pan, A., Zheng, Y., Luo, Y., Nakagawa, T., Li, C., Yang, S., Peng, H., Cheddadi, R., 2014. East Asian pollen database: Modern pollen distribution and its quantitative relationship with vegetation and climate. Journal of Biogeography 41, 1819–1832. doi:10/gg976k.